DUPLICATE

METEOROLOGICAL OFFICE

Forecasting Research

Forecasting Research Division
Technical Report No. 127

IMPACT OF A NEW GRAVITY WAVE DRAG SCHEME AND OROGRAPHIC ROUGHNESS IN THE UNIFIED MODEL. I. GLOBAL MODEL TESTS

by

S.F. Milton, C. Wilson, R.A. Stratton, O. Hammon and F. Rawlins

OCTOBER 1994

ORGS UKMO F
National Meteorological Library
FitzRoy Road, Exeter, Devon. EX1 3PB

Meteorological Office
London Road
Bracknell
Berkshire
RG12 2SZ
United Kingdom

Forecasting Research
Technical Report No. 127

IMPACT OF A NEW GRAVITY WAVE DRAG SCHEME AND OROGRAPHIC ROUGHNESS IN THE UNIFIED MODEL. I. GLOBAL MODEL TESTS

by
S.F. Milton, C. Wilson, R.A. Stratton ,O. Hammon and F.Rawlins.

OCTOBER 1994
©Crown copyright 1994

Forecasting Research Division
Meteorological Office
London Road
Bracknell
Berkshire RG12 2SZ
England

N.B. This paper has not been published. Permission to quote from it must be obtained from the above Met. Office Division.

1. INTRODUCTION

Diagnostic studies with the global Unified model (UM) have suggested that a possible source of the westerly bias in the Northern Hemisphere (NH) mid-latitudes may be a lack of parametrized drag in the troposphere (Milton, 1994). Current drag/dissipation mechanisms operating in the UM include (i) a parametrization of orographic gravity wave drag (GWD), (ii) turbulent mixing within the boundary layer, (iii) horizontal diffusion and (iv) vertical diffusion in the tropics. Research conducted in the last decade has suggested that a number of physical mechanisms operating in the atmosphere are currently unaccounted for in our parametrizations of subgridscale orographic effects.

Observational evidence and modelling studies (Peltier and Clark, 1979) of mountain waves suggests that considerable drag is applied in the lower troposphere above orography in situations when the Froude number (Fr = U/Nh) approaches unity from above and low level wave breaking and non-linear resonant trapping of gravity waves occurs. These flow configurations often display a fast moving current on the lee side of the mountain (downslope windstorm), a stagnant region above associated with the wave breaking and a 'hydraulic jump' in the streamlines downstream. Such flows are often referred to as "high drag states" as they can lead to a fivefold increase in the surface drag compared to estimates given by linear theory. Such effects are currently ignored in the parametrization of subgridscale orographic gravity waves in the U.K. Meteorological Office UM, although several other centres have attempted to account for such low level wave breaking effects in their gravity wave drag parametrizations (for a review see Kim and Arakawa, 1994). Further aspects of orographically induced gravity waves not accounted for in most large-scale models include trapped lee waves which are often observed in satellite imagery downstream of mountains and are known to exert an appreciable drag on the atmosphere (Bretherton, 1969).

In addition recent research has suggested that "form drag", which occurs as a consequence of normal pressure forces due to turbulent flow over bluff bodies (e.g turbulent flow over low hills), may lead to a surface drag comparable with that resulting from gravity waves. Mason (1985) and Wood and Mason (1993) have suggested that form drag due to subgridscale orography can be parametrized in large scale numerical models via an effective roughness length for momentum which includes the effects of orography. Roughness lengths in the global and LAM configurations of the UM only account for vegetative roughness at the present time.

Work is currently underway at the U.K. Meteorological Office to develop new parameterization schemes which incorporate the above mechanisms of subgridscale orographic forcing into the UM. These include;

(i) A new gravity wave drag scheme based upon ideas suggested by Shutts (1990).

(ii) A representation of orographic roughness in the boundary layer formulation.

This paper describes preliminary results from both 5 day forecasts and climate integrations of the global UM run with various versions of the new gravity wave drag scheme and the orographic roughness. Section 2 reviews the diagnostic evidence for increasing the parametrized drag in the UM. The two new parametrisations are briefly described in section 3 and the experiments are outlined in section 4. The body of results are given in section 5, and those solely interested in the impacts should turn to this section. Conclusions and recommendations are drawn in section 6.

Part II of this paper describes results from a parallel trial of the new parametrizations run during October and November 1994.

2. EVIDENCE FOR APPLYING MORE DRAG IN THE UM.

2.1 Systematic Errors

The monthly mean T+72 systematic errors (SE) in zonally averaged zonal wind from December 1993 (Fig. 1), show the UM has a westerly SE of order 1 m/s in mid-latitudes at 40°N-60°N and 45°S-60°S in the troposphere and an easterly SE over the poles, tropical boundary layer and tropical stratosphere. In general the SE pattern in the troposphere is such that both westerly and easterly flows are too strong in the model forecasts compared to analyses (Fig. 1(a)), consistent with too little drag acting upon the model atmosphere. Similar westerly SE occur in the global UM climate integrations. A comparison of climate integrations run at operational resolution (0.83 x 1.25, L19) and climate resolution (2.5 x 3.75,L19) also show that the westerly SE increases with increasing horizontal resolution.

2.2 Initial Momentum Balance

Following Klinker and Sardesmukh (1992) a technique has been applied to the operational forecast version of global UM which attempts to diagnose momentum and thermally forced SE sources. This involves running very short-range forecasts (two-timesteps) from the four operational analyses available per day, and determining the complete monthly-mean thermal and momentum budgets using the increments from each model routine (dynamics and parameterizations). The residual in this budget is a measure of the systematic "initial tendency error" in the model and Klinker and Sardesmukh showed that it bore a strong resemblance to 6-hour and medium-range monthly mean SE. This suggests that errors in model forcing are evident even after one timestep of integration, which means we can examine the contribution of individual model routines to the budget residual and form hypotheses on *possible* error sources, which can be tested using more direct experiments (e.g. altering model formulation).

The zonally averaged momentum budget residual for zonal wind during December 1993 (Fig. 2 plotted on model levels) bears a strong resemblance to the T+72 SE (Fig. 1), with westerly tendencies in midlatitudes and easterly tendencies in the tropical boundary layer and over the poles. Diagnostics from individual model routines show that this initial imbalance in the model's momentum budget arises from the parametrized forcing being smaller than that required to balance the dynamical tendencies. Although difficult to prove conclusively, comparisons with the ECMWF model which has better initial momentum balance suggest that it is the parametrized forcing which is underestimated. The residual westerly tendencies at 40°N are also located over the major mountain ranges (Milton, 1994), which is again suggestive that the *subgridcale orographic* forcing may be underdone.

The difference between UKMO and ECMWF momentum flux parametrizations is illustrated by the tendencies due to the respective gravity wave drag schemes (Fig. 3). In the operational UM GWD scheme most of the gravity wave drag is applied in the model stratosphere above the jet (see Milton (1994) for details of the calculations). The existence of westerly SE in the troposphere and easterly SE in the stratosphere in mid-latitudes in the UM (Fig. 1), is consistent with the application of too much gravity wave drag in the stratosphere and too little in the troposphere. A similar conclusion was reached in the original momentum budget study of Klinker and Sardesmukh (1987) with the ECMWF model. Subsequently, changes were made to the ECMWF GWD parametrization to;

(i) Add an additional gravity wave stress term due to high drag states which is non-zero when the Froude number is less than one.

(ii) Set the vertical profile of gravity wave stress so that 70% of the stress diagnosed at the surface is applied in the lower troposphere.

Figure 3(b) shows that these changes result in more drag being applied at low levels in the ECMWF model, which has a beneficial impact on the forecasts (Miller, 1989).

3. THE NEW PARAMETRIZATIONS.

3.1 Gravity Wave Drag

The proposed changes to the gravity wave drag scheme (Shutts,1990), seek to include a number of low level wave breaking mechanisms and correct some obvious defects of the original scheme of Palmer, Shutts and Swinbank (1986). As with all gravity wave drag schemes the problem is to determine (i) the surface gravity wave stress and (ii) the vertical profile of the gravity wave stress. The new features include;

(i) *Anisotropy in the orography and a new expression for surface stress*

The current gravity wave drag scheme assumes that the surface stress due to gravity waves lies in the same direction as the surface wind. In reality a wind incident upon a ridge at an oblique angle implies a drag acting at right angles to the axis of a ridge. The fourier transform spectrum of the sub-gridscale orographic height is used to derive a new expression for the surface stress. In the zonal direction this new gravity wave surface stress is given by

$$\tau_x(s) = K^{-1}\rho\frac{U^3}{N}\left[\frac{\sigma_{xx}}{\sigma}\cos\chi+\frac{\sigma_{xy}}{\sigma}\sin\chi\right]h_1h_2$$

where σ_{xx} and σ_{xy} are the squared orographic gradients and account for the anisotropy of the orography within a model gridbox (see section 3.3), χ is the direction of the surface wind with respect to the zonal direction, σ is the variance of the subgridscale orography, and K^{-1} is a constant. The term h_1h_2 depends upon the *inverse* Froude number and gives 3 possible regimes;

(a) Linear regime (Fr>1) where $h_1h_2 \approx N^2\sigma/U^2$ and the surface stress is proportional to U. This is similar to the expression used in the current operational scheme.
(b) Intermediate regime where $h_1h_2 \approx N\sigma^{1/2}/U$ and the surface stress is proportional U^2
(c) High drag regime (Fr< 1) where $h_1h_2=1$ and the surface stress is proportional to U^3.

(ii) *High drag states.*

In the new scheme a 'high drag state' is encountered if $N\sigma^{1/2}/U < \alpha$, where α is a tuneable constant of the order 0.3 to 0.4. A simple model of the high drag state (Smith, 1985) is used to determine the depth of the hydraulic jump layer (Ho).The stress is assumed to decrease linearly between the surface and Ho to some predetermined factor of the surface stress.

(iii) *Trapped Lee waves.*

Trapped lee wave trains occur when the Scorer parameter

$$l^2 = \frac{N^2}{U^2} - \frac{1}{U^2}\frac{\partial^2 U}{\partial z^2}$$

decreases rapidly with height. The analysis of Bretherton (1969) has been used to develop a simple two-layer model which predicts the occurrence, wavelength, amplitude structure, and drag of trapped lee waves.

(iv) *Partial internal reflection of gravity waves*
The new scheme accounts for the partial internal reflection of long hydrostatic gravity waves when a non-uniform scorer parameter exists. This is done in terms of a transmission factor calculated from the two-layer analysis used for lee waves and applied to the surface gravity wave stress.

(v) *Saturation stress hypothesesis*
In regions of the atmosphere where high drag states are not operating the vertical profile of gravity wave stress is determined in a similar manner to the current scheme in that if the stress in any layer exceeds a saturation wave stress, then the stress is reset to the saturation value, and a drag applied to the winds.

The new gravity wave drag scheme includes a number of 'tuneable' coefficients, and results from two versions of the scheme are discussed each run with slightly different values for some of these coefficients. The coefficient values are listed below and the reader is referred to the original documentation for a full discussion of their significance.

Version 1 α= 0.3, 2/3 of total gravity wave stress applied below Ho in high drag regime, K_Lee = $10^6/16$, Phase of Lee waves = 0.7π

Version 2 α = 0.4, 4/5 of total gravity wave stress applied below Ho in high drag regime, K_Lee = 1.5E+5 ,Phase of Lee waves = 0.6π, surface wind (U) is integrated from the lift height above a blocked layer to the height of the average peak above the mean value, $\sqrt{2}\sigma^{1/2.}$

The effect of increasing α between version 1 and 2 is twofold. Firstly, the onset of the 'high drag' state is dependent upon α, the larger the value the more often a 'high drag' state is encountered. Secondly the ratio α/β appears in the saturation stress criterion (β is another tuneable constant currently set to 1). Hence the larger α the larger the saturation stress, which makes it less likely for the stress to be deposited in a layer for given values of wind (U) and stability (N).

3.2 Orographic Roughness.

The use of roughness lengths to parametrize the form drag due to subgridscale orography is prompted by modelling studies (Wood and Mason, 1993) and observations in hilly terrain (Grant and Mason, 1990) that show the areally averaged flow behaves logarithmically even over large roughness elements such as hills. The effective roughness length for momentum (z_{om}^{eff}) is determined by averaging the expressions for the stress due to the form drag and non-orographic roughness elements to give

$$\frac{k^2}{\left[\ln\left(\frac{h/2}{z_{0m}^{eff}}\right)\right]^2} = \frac{1}{2} C_D^{OROG} \frac{A}{S} f_D(Ri) + \frac{k^2}{\left[\ln\left(\frac{h/2}{z_{0m}}\right)\right]^2}$$

Where k is Von Karmans constant, C_D^{OROG} the drag coefficient for orography, z_{om} is the roughness length for momentum based on vegetative effects, and h is the mean peak to trough height of unresolved orography. The first term on the RHS of the equation is that due to form drag arising from subgridscale orography and the second is the 'non orographic' stress term. The key parameter is A/S, where A is the frontal area of orography and S the mean surface area. Thus A/S measures the total silhouette area of unresolved orography. This is currently parametrized in the global model from the standard deviation of the orography. The term $f_D(Ri)$ is a stability factor set to 1 when Ri<0 and reducing linearly to zero as Ri increases to 1.

3.3 New Ancillary Fields.

Four new ancillary fields associated with the subgridscale orography are introduced into the UM. For the gravity wave drag scheme we have the terms associated with anisotropy in the orography (h) which appear in the expression for the surface gravity wave stress

$$\sigma_{xx} = \left[\frac{\partial h}{\partial x}\right]^2, \sigma_{yy} = \left[\frac{\partial h}{\partial y}\right]^2, \sigma_{xy} = \left[\frac{\partial h}{\partial x}\right]\left[\frac{\partial h}{\partial y}\right]$$

and for the inclusion of orographic roughness the field of A/S is also needed. Ideally this should be calculated directly from high resolution orography datasets, but in lieu of such data it has been parametrized using the following relation

$$\frac{A}{S} = \frac{2k^2/C_D^{OROG}}{\left[\ln\left[\frac{\bar{h}/2}{z_0^{OROG}}\right]\right]^2}$$

Where Z_o^{OROG} is an effective roughness ignoring vegetative effects which is a function of the subgridscale orographic variance, formulated to agree with measurements of A/S made over Britain. The roughness lengths have increased from values of order 0.1-1.0 metres for purely vegetative roughness elements to values in excess of 50m for orographic roughness lengths over the Himalayas and Andes. The magnitude of such orographic roughness lengths over high orography is one of the main areas of uncertainty in the parametrization.

4. EXPERIMENTS

4.1 Case Studies

A set of 5 forecasts were run to T+120 with each of the following configurations

OP - Operational.
GW - New Gravity Wave Drag scheme (Version 1).
RO - Orographic roughness.
ROGW - New Gravity Wave Drag (Version 2) + Orographic roughness.

Initial analyses from 00Z on 1/12/93, 5/12/93, 10/12/93, 15/12/93, and 20/12/93 were used. No assimilation was performed in any of the above experiments, all of the initial analyses being from the operational version of the global UM. All validation of the forecasts was performed against the UKMO operational analyses. These expermiments are referred to in the text by their acronyms.

4.2 One Week Trials with Data Assimilation

Two one week trials were also run with both OP and ROGW configurations for the periods 7/1/94 to 13/1/94 and 11/8/93 to 17/08/93. Both model configurations were run through a full assimilation cycle. These forecasts allow us to verify the forecasts against observations (Radiosondes and Aireps) as opposed to model analyses.

4.3 Climate Integrations at Operational Resolution

A number of climate integrations have been conducted at operational resolution in order to determine the longer term climate of the model with the new parametrizations included. Two DJF seasons from a 10 year integration of the OP configuration were taken as a control, and two 90 day re-runs were

performed using the ROGW configuration . The first for DJF 1978/79 run from an operational analysis and the second for DJF 1979/80 initialised from a model dump of the OP integration.

5. RESULTS

5.1 Case Studies

In this section the impact of the new parametrizations on systematic errors and objective verification scores are discussed. The momentum budgets from each experiment are also examined in order to try and understand the changes in the general circulation which occur.

5.1.1 Zonally averaged fields U,V,T

Figure 4 shows the impact of the new parametrizations upon the zonal wind at T+120 compared to the operational forecasts. GW reduces the westerlies between 40°N-70°N by -0.5m/s to -1.0m/s (Fig 4b) which is in the correct sense to reduce the SE. The largest response to the new GWD scheme is over Antarctica where the easterly flow is increased at 70°S. This is a consequence of the reduction in gravity wave drag over the Antarctic Plateau in GW, caused by the introduction of anisotropy in the orography (see section 5.1.3). The impact in RO is much larger, and is consistent with increasing the surface drag (Fig. 4(c)). In most areas the difference, RO-OP, is the mirror image of the SE in zonal wind (Fig. 1). RO reduces the westerly SE in midlatitudes by up to 2m/s and the easterly SE over the poles and the tropical boundary layer. Over Antarctica RO makes the flow more westerly/less easterly, acting in the opposite sense to GW. It is also of note that by T+120 the impact in RO is not confined to the boundary layer. The response in the stratosphere in RO occurs indirectly through an interaction of the orographic roughness and operational gravity wave drag scheme which reduces the diagnosed gravity wave surface stress. This makes the model more westerly at 50°N and 100hPa where less gravity wave drag is applied in RO compared to OP (see section 5.1.3). This reduces the easterly SE in this region thought to be caused by applying excessive gravity wave drag in OP. Finally ROGW gives a similar response to RO, reflecting the larger impact of the orographic roughness change compared to that of the new GWD scheme.

Figure 5 shows the impact of the new parametrizations upon the mean error in the zonal wind at T+120. OP has a similar error distribution to that shown in Figure 1 for the December 1993 monthly mean. In GW there is a reduction of the westerly SE between 40°N and 50°N in the lower troposphere but an increase in the tropical easterly SE between 0°N-20°N and over Antarctica. In RO and ROGW the SE are reduced almost everywhere, both in the boundary layer and at jet level and most noteably over Antarctica. However ROGW does show an increase in the easterly SE between 0°N-20°N similar to that in GW. This may suggest that it is the new gravity wave drag scheme which makes the SE worse in this latitude band.

Given the large changes in zonal wind in RO and ROGW one might expect changes in the temperature distribution in order to maintain thermal wind balance. Both RO and ROGW cool relative to OP between 900hPa and 400hPa polewards of 70°N, and at 200hPa between 50°N and 70°N (Fig. 6). Both of these features are consistent with increasing the westerly component of the wind at 80°N in the troposphere and 50°N between 300hPa and 30hPa (Fig. 5). This cooling acts to increase the zonally averaged mean cold bias at 300hPa in the NH averaged over the 5 cases (Figure 7). There is also a tendency for RO and ROGW to warm by up to 1K below 900hPa in NH mid-latitudes.

Finally we consider the changes to the v component of wind (Fig. 8). A diagnostic equation relating the streamfunction associated with the mean meridional circulation ([v],[w]) to the sources/sinks of momentum and heat and the eddy transports is the Kuo-Eliassen equation (see Grotjahn (1993), p260). This states that boundary layer friction induces an indirect (clockwise in NH and anti-clockwise in SH) meridional circulation in the middle latitude westerlies and a direct circulation in the Tropics. This is

a consequence of the need to maintain geostrophic and hydrostatic balance in the face of friction which acts to destroy this balance. The coriolis term due to the mean meridional circulation (f[v]) opposes the original frictional dissipation in the zonal momentum budget. The act of increasing the boundary layer friction by including orographic roughness should therefore enhance the mean meridional circulation. In the NH both RO and ROGW show an increased indirect circulation between 40°N-60°N. There is also some evidence of an increase in the poleward flow in the upper tropospheric portion of the Hadley cell at 0°N, with a weaker return flow below. The Hadley circulation in OP is already too intense and ROGW tends to make this bias worse.

The largest changes in [v] occur over Antarctica. OP shows a large equatorward component at 70°S near the surface (Fig. 8(a)). Such intense meridional flows have been observed over Antarctica and are related to the katabatic winds which blow off the continent. However, compared to analyses this flow is too intense in OP. This equatorward flow is increased in GW (Fig 8(b)) and reduced in RO/ROGW, consistent with the fact that GW has a reduced drag at this location compared to OP, and RO and ROGW have increased drag. Over Antarctica the increase/decreases in drag act directly upon the meridional flow in the boundary layer over Antarctica, whereas in mid-latitudes the effect on the meridional circulation is a secondary one induced by changes in the zonal flow. In summary, RO/ROGW are more accurate than OP over Antarctica for both meridional and zonal winds suggesting that the increased drag is beneficial.

5.1.2 MSLP

The zonally averaged profile of MSLP at T+120 (Fig.9) shows that OP has too deep a trough at 60°N and 70°S and subtropical highs are too intense at 30°N and 30°S consistent with excessive westerlies in mid-latitudes. ROGW acts to correct these deficiencies and is consequently much closer to the analysed profile. However in the Tropics the pressures are now lower than analysed. This is a consequence of the increased divergent circulation suggested by the increased Hadley cell.

The geographical distributions of GW-OP (Figure 10(a)) and ROGW-OP (Figure 10(b)) in the NH show that both schemes act to increase the pressure poleward of 40°N, with the largest increases over land. The T+120 mean errors in MSLP in OP (Figure 11(b)) consist of erroneous low pressures poleward of 40°N. Both GW (Fig 11(c)) and ROGW (Fig 11(d)) reduce this mean error. ROGW has the largest impact removing a large proportion of the negative errors, although in some regions there is a slight tendency to make areas of positive mean error slightly worse, for example in the north Atlantic.

As expected the impact of the new parametrizations in the Southern Hemisphere (SH) is smaller (Fig. 12). Both parametrization schemes increase pressure in the circumpolar trough at T+120. Again ROGW has the larger impact, with the maximum response downstream of the Andes and Antarctic Peninsula. The mean error in OP is for generally lower pressures in the circumpolar trough (Fig 13(b)). Both GW and R OGW lead to improvements, in particular the negative error close to South America and positive errors equatorwards of this and downstream near South Africa are all reduced.

5.1.3 Zonal Momentum Budgets.

The zonally averaged zonal momentum budget is used in this section as a tool for understanding the impacts on the model's climate in terms of the changes to the parametrized sources/sinks of momentum which occur when the new gravity wave drag and orographic roughness schemes are introduced.

The tendencies (m/s/day) to the zonal wind from the gravity wave drag schemes in the four experiments OP, GW, RO and ROGW are shown in figure 14 averaged over the first day of the forecasts. OP shows most of the gravity wave drag to be applied in the stratosphere in NH

midlatitudes. In GW we see an increase in the low level easterly drag between 30°N and 60°N, but little change in the drag applied to the stratosphere. There is a considerable reduction in the gravity wave drag applied at 70°S over Antarctica due to the introduction of anisotropic effects in the orography which leads to the erroneously strong easterly winds in GW as discussed in section 5.1.1. The inclusion of orographic roughness has a major impact on the gravity wave drag applied in RO (Fig. 14(c)), reducing it dramatically compared to OP, even though the formulation of gravity wave drag in OP and RO is identical. This occurs because the current GWD scheme diagnoses the surface gravity wave stress from layer 2 winds which are significantly reduced by the introduction of the orographic roughness. This 'switching off' of the gravity wave drag scheme has been alleviated by estimating the 'surface' wind (U) used in the surface gravity stress formula as an integral of the wind between the 'lift' height above a blocked layer and a height given by $\sqrt{2}\sigma^{1/2}$. This reformulation is used in ROGW, and the gravity wave drag (Fig 14(d)) now shows a sizeable component below model level 6, associated with the high drag states and lee waves. The low level drag is larger in ROGW than in GW partly because of the larger fraction of stress removed below the hydraulic jump height and also due to the larger value of α. The stratospheric drag in ROGW is reduced compared to OP which is in the correct sense to reduce the stratospheric easterly SE (Fig. 1). However the value such drag should take in reality is unknown, and long climate integrations suggest some tuning of the scheme may still be neccessary (section 5.3). Over Antarctica the gravity wave drag is considerably smaller than that applied in OP or GW. However it is compensated by the form drag arising from the large orographic roughness in this region.

The inclusion of orographic roughness in the UM leads to large increases in the drag at all latitudes applied to the zonally averaged zonal wind by the UM boundary layer scheme (Figure 15(c)). Largest increases are in NH midlatitudes (4 m/s/day) and over Antarctica at 70°S (5 m/s/day). There is also evidence that in layer 1 there is actually a reduction in the drag in RO compared to OP. This may be explained by the fact that changes to the near surface velocity profile in ROGW actually leads to less momentum being mixed down in this layer.

The change in the total parametrized drag (Fig 16(c)) between ROGW and OP is for increased drag in the boundary layer. This comes largely from the orographic roughness with a smaller contribution from the new gravity wave drag scheme. In the free troposphere and stratosphere there is a source of westerly momentum in ROGW compared to OP due to the reduction in the gravity wave drag in ROGW. The changes in parametrized drag are largely compensated by changes in the dynamical increments (Fig 16(d)), which show increased westerly tendencies in the boundary layer at 30°N-60°N and increased easterly tendencies in the free troposphere at the same latitudes. These changes in the dynamics are consistent with the induced meridional circulation changes such as the noted earlier. The difference (ROGW-OP) in the total tendency (parametrizations + dynamics, Fig 16(e)) is smaller in magnitude (~ 0.5 to 1.0 m/s/day) than the change in the parametrized forcing, but still in the sense to reduce the systematic errors in the 'initial tendencies' shown in figure 2, and hence improve the initial momentum balance of the UM.

Finally, we look at the zonally averaged surface stresses (Fig. 17). For the boundary layer scheme the inclusion of orographic roughness in RO and ROGW leads to a 25% increase in surface stress between 30°N and 60°N. Smaller increases also occur in the easterly trade regions (20°N and 25°S), in SH mid-latitudes and at 70°S over the Antarctic. Unfortunately the gravity wave stress was not output from the OP runs, although the distribution of gravity wave drag in the zonally averaged cross sections (Figure 14(a) and 14(b)) suggests that OP and GW may apply a similar surface gravity wave stress at most latitudes (with the exception of the Antarctic). Compared to GW we see that RO diagnoses much less gravity wave stress for reasons already discussed, but the use of the new definition of surface wind (U) in the new GWD scheme increases this value in ROGW. However ROGW still applies less surface gravity wave stress than GW (and OP?).

In summary we have

(i) An increase in parametrized surface stress (BL + GWD) in ROGW compared to OP.
(ii) An increased drag in the lower troposphere in ROGW compared to OP.
(iii) A reduced drag in the stratosphere in ROGW compared to OP.

These features lead to a better initial momentum balance in the UM, and consequently a reduction in systematic error growth.

5.1.4 Objective Verification.

In this section we consider the objective verification of the 5 case studies against operational analyses. All scores are averages across the 5 individual cases and are given for T+24, T+72 and T+120. RMS error and bias are the two verification scores used, and only the Northern Hemisphere extratropics (90N-30N) is considered in this section.

(a) MSLP

GW, RO and ROGW all have smaller RMS errors than OP in all forecast ranges (Fig 18(a)). The largest improvement is in RO with a 15% reduction in RMSE at T+72. OP develops a large negative bias in MSLP with pressures too low by ~ -2hPa at T+120 (Fig 18(b)). GW reduces this bias to -1.3hPa and RO to -0.5 hPa. In ROGW the bias becomes slightly positive, although it is a marked improvement over OP in terms of magnitude. All of these scores are in agreement with the earlier discussions concerning MSLP.

(b) 500hPa Geopotential Height

For 500hPa geopotential height we see very much the same signal, with reductions in RMSE (Fig 19(a)) and reductions in a large negative bias (Fig 19(b)). Most of these improvements probably arise from a more accurate surface pressure field. Again there is an indication of a change of sign in the bias of ROGW compared to OP.

(c) Winds at 850hPa and 250hPa

For 850hPa winds there are reductions in RMS vector wind error at T+72 and T+120 in GW, RO and ROGW (Figure 20(b)), with RO again the most skilful. At 250hPa the RMS vector wind error is made marginally worse by T+120, although the impact is neutral in the earlier forecast ranges. The 850hPa wind speed shows a reduction in RMS error beyond T+24 in GW, RO and ROGW (Fig. 21(a)). The wind speed bias (Fig 21(b)) shows operational winds are too strong at low levels and GW reduces this bias. However RO and ROGW reverse its sign so that winds are now too weak. At 250hPa none of the schemes impact significantly upon the RMS error in the wind speed (Fig. 22(a)). The 250hPa wind speed bias at T+24 shows OP has too weak winds in line with operational experience, and this bias is made worse by RO and ROGW. However by T+120 the wind speeds in OP are too strong and RO and ROGW act to reduce this bias.

(d) 500hPa Temperatures

Finally we consider the temperature biases at 500hPa (Figure 23). OP shows the characteristic cold bias in all forecast ranges. GW has zero impact upon this bias, but RO and ROGW make it worse, which agrees with the discussion of the zonally averaged temperature bias in section 5.1.1. ROGW is a small improvement upon RO alone.

These verification results are summarised in Table 1 and Table 2 which shows where ROGW is an improvement over OP in terms of RMS errors and bias respectively.

TABLE 1 - Improvements in RMS errors - Y => ROGW has smaller RMS errors than OP

	T+24	T+72	T+120
MSLP	Y	Y	Y
500HPa HEIGHT	Y	Y	Y
850HPa RMS VWE	N	Y	Y
250HPa RMS VWE	Neutral	Neutral	N
850HPa W.SPEED	N	Y	Y
250HPa W.SPEED	Neutral	Neutral	Neutral

TABLE 2 - Improvements in Bias - Y => ROGW has smaller Bias magnitude than OP.

	T+24	T+72	T+120
MSLP	N	Y	Y
500HPa HEIGHT	Y	Y	Y
850HPa W.SPEED	N	Y	N
250HPa W.SPEED	N	N	Y
500HPa TEMP.	N	N	N

5.2 One Week Trials -Verification against Observations.

All of the verification against observations is performed on model levels using the layer mean values of each quantity from both model and observations. Statistics are calculated as observations-model and for

- 3 latitude bands ; NH extratropics (90N-30N), tropics (30N-30S), and SH extratropics (30S-90S).
- 3 forecast ranges, T+24, T+72, T+144.
- Verification against Radiosondes and Aireps.
- All 19 model levels.
- Two separate months (January and August).

In interpreting the verification results it is useful to bear in mind that the radiosondes are concentrated over the land masses and there are consequently far greater numbers of observations in the Northern Hemisphere compared to the Tropics or Southern Hemisphere. For example in the January week the average number of temperature observations over all model levels used in one day was NH~6000, Tropics~2000, and SH~500. On sampling grounds the verification scores are most reliable in the NH extratropics.

5.2.1 January Results

(a) Winds

Against radiosondes ROGW is an improvement over OP in RMS vector wind error at all forecast ranges in the NH extratropics between levels 1 (~997hPa) and 6(~700hPa) and levels 15 (~100hPa) and 19 (~5hPa) (Fig. 24). This improvement in the stratosphere strengthens one of the initial hypotheses that OP extracted too much drag in the stratosphere, whereas in ROGW this drag has been reduced with beneficial results. At jet level where the RMS vector wind error is largest the verification against sondes suggests an improvement in ROGW at T+24 only. In the Tropics there is a similar signal of improvements in boundary layer levels 1-3 and in the stratosphere around level 15 (Fig. 25). However there is an increase in RMS vector wind error at jet level which becomes large by T+144 for both sondes and aireps. Improvements in the SH extratropics are largely confined to the boundary layer levels 1-4 with neutral impacts at other levels (Fig. 26).

In the NH extratropics (Fig. 27) there is a reduction in the westerly bias of the zonal wind at low levels in ROGW compared to OP against both sondes and aireps and a reduction in the easterly bias in the stratosphere. In the Tropics (Fig. 28) the signal is more complex with ROGW reducing the easterly bias in model levels 1-3, but increasing the bias above these levels. This pattern is most clear at T+144. The signal in the SH extratropics (Fig 29) is similar to that in the NH with a reduction of the westerly bias as measured against sondes, with the largest impacts for levels 1-6.

(b) Temperatures

The dominant signal in the verification of NH extratropical temperatures against sondes (Figure 30) is that the large low level cold bias in OP has been replaced by a *smaller* warm bias in ROGW. Additional cooling in the upper troposphere occurs in ROGW in agreement with the earlier discussion on the zonally averaged cold bias. The tropics shows a similar switch from a cold to warm bias at low levels, but no large increase in upper level cooling. In the SH extratropics the low level warm bias in OP is made slightly worse (Fig. 32).

(c) Relative Humidity

For the NH extratropics the results for January imply that the operational model is too dry compared to observations at T+144 (Fig. 33(a)). This would appear to contradict other results which show the UM has a large moist bias. However, careful examination of the RH bias at 850mb (A. Van der Waal, personal communication), shows a large seasonal variation with the moist bias is largest in JJA and smallest in DJF, and in January 1994 large areas of land over Canada and Asia show a dry bias. ROGW has a large impact on this dry bias reducing it considerably. The RMS error is also reduced. In the Tropics (Fig. 33(b)) and most noteably the Southern Hemisphere extratropics (Fig. 33(c)) the operational model shows the more familiar moist bias. In the lowest layer ROGW produces a drying which is consistent with the warmer boundary layer.

5.2.2 August Results

In this section results are only presented where conclusions differ significantly from those of the January integrations.

(a) Winds

The RMS vector wind errors in the NH extratropics show an improvement in ROGW against sondes up to level 13 at all forecast ranges with the largest impact in the lowest levels. Similar improvements can be seen in the verification against aireps. One striking difference with the January trial is that no improvement in stratospheric winds can be seen. In the Tropics (Fig. 35) improvements at T+24 are confined to levels 1-4, but by T+144 ROGW shows a reduction in RMS vector wind errors at most levels. This is the reverse of the results for January where the tropical scores are worse. In the SH

extratropics ROGW reduces the RMS vector wind error most noteably in the lowest model layers.

(b) Temperatures and Relative Humidity
For all latitude bands ROGW has a warmer and drier boundary layer than OP and in NH extratropics the cold bias is increased in ROGW in the mid and upper troposphere.

Summarising, the objective verification against observations shows that,

-ROGW is a consistent improvement over OP in both RMS vector wind error and zonal wind bias for low level and stratospheric winds.
-The impact at jet level is generally neutral or positive with the exception of the tropical winds in January.
-ROGW has a consistently warmer boundary layer which generally acts to improve the OP forecasts.
-The upper tropospheric cold bias is made worse.

5.2.3 Synoptic Assessment.
Comparing the ROGW and OP forecasts subjectively it is apparent that the new gravity wave drag and orographic roughness have a significant impact on synoptic development in the Northern Hemisphere.

At T+24,the main impact is a reduction in low level westerly wind speeds over land and a slight filling of depressions, which is sometimes overdone. In a comparison of 22 depressions at T+24, 21 ROGW depressions are less deep by 2 to 7hPa. Eleven of these are filled correctly but the remaining ten fill too much or too soon. The favoured area for over-filled depressions is over Canada. 500hPa heights over Canada and north of the Himalayas are slightly higher but the impact on 250hPa jets is generally small. No changes in evolution are seen at T+24.

At T+72, the ROGW and OP forecasts are still similar. Differences have increased and some changes in evolution are evident. Most ROGW depressions are less deep by 4-8hPa, but differences as large as 10-20hPa can be seen. Again, half were filled correctly, and half filled too much or too soon. The majority of 250hPa jets are slightly weaker in ROGW due to a reduction in the westerly component. Comparison against the analysis is marginally in favour of the ROGW forecast jets.

At T+120/144 evolution changes dominate the comparison between ROGW and OP forecasts. Where comparison is still possible the majority of ROGW depressions and 500hPa lows are less deep, although on a few noteable occasions ROGW deepened a depression more than OP. For the jets as many in ROGW are stronger as are weaker compared to OP. Subjective assessment is generally in favour of the ROGW.

Out of the seven forecasts compared, the subjective assessment preferred the ROGW forecasts on 4 occasions, the OP on two occasions with 1 draw.

The following examples illustrate the kind of differences seen between ROGW and OP forecasts over North America and the North Atlantic.

An example of the filling of depressions by the ROGW forecasts over Canada is shown in Figure 37. Comparing the T+72 MSLP forecasts verifying at 00Z 11/01/94, the forecast evolution is similar in both cases but the ROGW depression near Hudson Bay (Figure 37(a)) is 12hPa less deep than the OP depression (Figure 37(b)). Also the anticyclone just west of this depression is stronger in the ROGW forecast. The ROGW forecasts of 1009hPa and 1032hPa for these features are closer to the values of 1006hPa and 1034hPa in the verifying analysis for 00Z 11/01/94 (Figure 38).

The tendency for the ROGW to predict less deep depressions and cold pools over Canada is again illustrated in the next example. Figure 39 compares the ROGW and OP MSLP forecasts at T+72 over Canada, verifying at 00Z 12/01/94. Both versions predict a low centre west of Winnipeg but the OP depression, 1000hPa, is deeper by 13hPa. Similarly, the OP depression of 996hPa over Hudson Bay is deeper by 15hPa than the ROGW depression. The verifying analysis for 00Z 12/01/94 (Figure 40(a)) has only a weak low of 1016hPa east of Winnipeg which supports the ROGW forecast. The analysed centre over the Hudson Bay of 1003hPa is midway between the ROGW (1011hPa) and OP (996hPa) forecasts. The main feature over Canada in the 500hPa analysis (Figure 40(b)) is the cold pool of 495dm over Hudson Bay. The ROGW and OP T+72 500hPa forecasts verifying at this time (Figure 41) show the OP forecast was very accurate, but the ROGW forecast filled the 500hPa low too quickly on this occasion.

From T+72 onwards occasional large differences occur in the development over Newfoundland. The next case illustrates this with the most important feature to compare in the two T+120 forecasts (Figure 42) being the complex depression off the Labrador coast. The OP forecast has the deeper depression, 953hPa, centred over the coast of Labrador, with a strong westerly gradient to the south over Newfoundland. The ROGW forecast predicts two centres, one at 979hPa near the Hudson Strait and the other at 975hPa further south close to Newfoundland. The verifying analysis for 00Z 17/01/94 (Figure 43(a)), agrees better with the ROGW forecast, with one centre, 981hPa, between Greenland and the Hudson Strait and a smaller centre, 1002hPa just east of Newfoundland.

The final example, taken from the same forecast run, is a comparison between the T+144 forecasts for the North Atlantic and U.K.. The MSLP analysis for 00Z 18/01/94 (Figure 43(b)) has a deep depression of 949hPa over southern Greenland and a ridge of high pressure extending across Southern England. The depression over southern Greenland is better represented in the ROGW T+144 forecast (Figure 44(a)), and the high pressure over Europe is also predicted although pressures are too high over the U.K. In contrast, the OP T+144 forecast (Figure 43(b)) fails to capture the deep depression and is too cyclonic over Europe with a depression 988hPa giving a northeasterly flow through the Dover Straits. At 500hPa the analysis (Figure 43(c)) has a deep low of 478dm over Greenland, a strong ridge over the U.K. and a trough over the continent The cold pool over Greenland and cut-off low over North Africa are better represented by the ROGW forecast (Figure 45(a)). Neither forecast predicts a strong ridge over the U.K. but the higher contours in the ROGW forecast verifies better. The OP forecast was much too cold, with the 522dm contour over the U.K. (Figure 45(b)).

In summary the synoptic assessment of the January cases shows

1. Subjective assessment preferred the ROGW forecasts for 4 cases out of 7, with one equal.
2. ROGW forecasts were less cyclonic, with higher mean sea level pressure and 500hPa contours usually verifying better.
3. Significant reduction in low level wind speeds.
4. ROGW forecasts were slightly warmer near the surface.
5. Reduction in westerly bias.
6. Above effects sometimes overdone downwind of Rockies early in forecast.

5.3 Climate Integrations

A stringent test of any new parametrization is that it be able to perform on both short range (1-5 days) and climate timescales (Seasonal to Decadal). The Unified Model system provides us with the ability to carry out such tests, and the 'new parametrizations' have been run in long climate integrations at full OP resolution (see section 4.3). Figure 46(a) shows the time-mean zonally averaged zonal wind from a 90 day integration of OP (plotted on log pressure) for the 1978/79 season, and figure 46(b) shows the difference of OP from the UK climatology of analyses (1985-1990), which can be

interpreted as the model SE. This shows similar SE structures to the 5 day forecasts, with westerly errors in mid-latitudes and large easterly errors in the tropics. Most of the amplitude in the error at these longer time ranges is concentrated in the stratosphere. Fig 46(c) shows ROGW-OP and comparison with the SE in OP shows that ROGW acts everywhere to reduce the SE. This reduction can clearly be seen in the comparison of SE in ROGW (fig 46(d)) and OP (fig 46(b)) . The NH SE has been greatly reduced, particularly above 100hPa, and similar reductiuons are evident in the SH. A further ROGW integration is initialised on 1/12/79 from a model dump generated by the OP integration during its second winter. The difference ROGW-OP (Fig. 46(e)) has a similar structure to that from the previous winter. However the magnitude of the westerlies at 60N and 25hPa has almost doubled. This acts to make the SE in OP worse. The SE from ROGW is shown in the final panel (Fig. 46(f)). This error may suggest that the gravity wave drag has been decreased by too much in the stratosphere in the ROGW formulation.

These changes in the zonal wind are accompanied by large changes in the zonally averaged temperature in the UM. There is a cooling of -5K above 200hPa at 60N, which is associated with the increased westerlies in ROGW at 50°N in the stratosphere. This is an identical response to that in the 5 day forecasts and is such as to make the cold bias in temperatures worse.

6. CONCLUSIONS

The following conclusions can be drawn about the impact of including the new gravity wave drag scheme and the orographic roughness together as a package in the global Unified Model.

BENEFITS

- Reduction in westerly bias in zonal wind at most latitudes.
- Reduction in MSLP and 500hPa geopotential height bias/RMS errors in mid latitudes.
- Improved low level winds in NH,SH and Tropics (vs analyses and observations).
- Improved stratospheric winds in January integrations.
- Neutral impact on 250hPa winds in mid-latitudes in December/January.
- Improved winds at all levels in August.
- Improved 'initial momentum balance'.

DISADVANTAGES

- Increase in cold bias in the upper troposphere.
- Degradation in tropical winds above the boundary layer in December/January.
- Tendency to overfill lows over land ?
- MSLP too low in the Tropics (Increased meridional circulation)
- Long timescale spin-up in westerlies in the stratosphere in climate integrations.

OTHER IMPACTS (BENEFITS or DISADVANTAGES?)

- Near surface cold bias replaced by warm bias.

Many uncertainties remain in the implementation of the orographic roughness and new gravity wave drag scheme, not least of which is the fact that there are few observations of pressure drag or vertical fluxes of horizontal momentum against which to test the parametrizations. Other uncertainties include the values that the silhouette area of orography(A/S) should take over steep orography. Accurate specification of this field requires high resolution orography datasets. The A/S parameter should also probably have a directional dependence to allow for the anisotropy in the orography in a similar fashion to that done in the new gravity wave drag scheme. Further refinements to the parametrizations will undoubtedly be required in the future. A further issue not addressed in this study is the impact the new parametrizations have upon the variability in the Unified Model. This is best addressed in climate simulations.

On the whole these results suggest that inclusion of orographic roughness and the revised formulation for the gravity wave drag scheme are beneficial on both the 5 day and climate timescales. Of primary importance is the fact that these new parametrizations attempt to improve the physical realism of the model by including processes which are known to occur in the real atmosphere. They directly address deficiencies in the model's momentum budget suggested by other studies, namely that the model has insufficient parametrized drag, and lead to a marked reduction in the systematic errors of the Unified Model.

ACKNOWLEDGEMENTS

The new gravity wave drag scheme has been coded into the UM by James Mitchell and Dave Gregory of the parametrizations group in the Climate Research Division. The orographic roughnesses have been coded into the UM by Simon Jackson and Roderick Smith of the Mesoscale group in FR Division. Thanks to Ernst Klinker for providing ECMWF results (Fig. 3(b))

REFERENCES.

Bretherton, F.P., 1969: Momentum Transport by Gravity Waves. *Quart. J.R.Meteor.Soc*,95,21-234

Grant, A.L.M. and P.J. Mason, 1990: Observations of boundary-layer structure over complex terrain. *Quart. J.R.Meteor.Soc*,116,159-186.

Grotjahn, R. ,1993: Global Atmospheric Circulations : Observations and Theories. Oxford University Press.

Kim, Y-J and A. Arakawa, 1994 : Improvement of Orographic Gravity Wave Parameterization Using a Mesoscale Gravity Wave Model. Part I - Simulations with a mesoscale model and evaluation of a test parametrization scheme. (Submitted to *Journal of the Atmospheric Sciences*).

Klinker, E. and P.D. Sardesmukh, 1987: The Diagnosis of Mechanical Dissipation in the Atmosphere from Large-Scale Balance Requirements. *Journal of the Atmospheric Sciences*, 49, pp608-627.

Klinker, E. and P.D. Sardesmukh, 1992: The Diagnosis of Systematic erros in Numerical Weather Prediction Models. *ECMWF Workshop proceedings on 'Diabatic forcing', 30 Nov-2 Dec, pp 209-244.*

Mason , P.J., 1985: On the Parametrization of Orographic Drag. *Pp 139-165 in ECMWF seminar on physical parametrization for numerical models of the atmosphere.*

Miller, M.J., 1989: The Parametrization of Momentum Fluxes in the free Atmosphere. From ECMWF Semeinar on 'Ten Years of Medium Range Weather prediction', pp 67-92.

Milton, S.F., 1994: Diagnosing Systematic Errors in the Unified Model. - II Momentum Budget. *Fr Division Technical Report No. 74.*

Palmer, T.N., G.J. Shutts,and R.Swinbank, 1986:Alleviation of systematic westerly bias in general circulation and numerical weather prediction models through an orographic gravity wave drag parametrization. *Quart. J.R.Meteor.Soc*,112, 1001-1040.

Peltier, W.L and T.L. Clark, 1979: The evolution and stability of finite amplitude mountain waves. Part II: Surface wave drag and severe downslope windstorms. *Journal of the Atmospheric Sciences*, 36, pp1489-1529.

Shutts, G.J., 1990: A New Gravity Wave drag Parametrization Scheme for the Unified Model. *Available from the Forecasting research Division of UKMO.*

Smith, R.B., 1985: On Severe Downslope Windstorms. *Journal of the Atmospheric Sciences*, 42, pp2597-2603.

Wood, N. and P.J. Mason, 1993: The Pressure Force Induced by Neutral Turbulent Flow over Hills. *Quart. J.R.Meteor.Soc*,119,1233-1268.

FIGURE CAPTIONS

Figure 1 Zonally averaged pressure-latitude cross sections from the Unified Model of December 1993 monthly averaged (a) zonal wind calculated from 00Z analyses, and (b) Mean error (Forecast - analysis) at T+72.

Figure 2 Zonally averaged pressure-latitude cross sections from the Unified Model of December 1993 monthly averaged (a) zonal wind calculated from 00Z analyses, and (b) Residual tendency (Dynamics + Parametrized tendencies) in zonal wind calculated from two timetsep integrations of the Unified Model (see Milton (1994) for details of the calculations).

Figure 3 Zonally averaged pressure-latitude cross sections of December 1993 monthly averaged (a) tendencies from the Unified Model gravity wave drag scheme as calculated from two timestep integrations, and (b) as (a) but for the ECMWF model and calculated from a set of two hour integrations.

Figure 4 Zonally averaged pressure-latitude cross sections of December 1993 monthly averaged (a) zonal wind from the operational model forecasts at T+120 (b) zonal wind differences , New GWD - Operational , at T+120 (c) as (b) but for Orographic roughness - Operational , and (d) as (b) but for the Orographic Roughness + New GWD - Operational.

Figure 5 Zonally averaged pressure-latitude cross sections of December 1993 monthly averaged (a) zonal wind mean error (model - analyses) for the operational model forecasts at T+120 (b) as (a) but for the New GWD forecasts , (c) as (a) but for Orographic Roughness forecasts , and (d) as (a) but for the Operational Roughness + New GWD forecasts.

Figure 6 As Figure 4 but for zonally averaged temperatures.

Figure 7 Zonally averaged pressure-latitude cross sections of December 1993 monthly averaged (a) temperature mean error from the operational model forecasts at T+120 (b) as (a) but for Orographic Roughness + New GWD - Operational.

Figure 8 As for Figure 4 but for the meridional wind.

Figure 9 Zonally averaged profile of MSLP for Analysis, Operational forecasts, and Orographic Roughness + New GWD forecasts at T+120. Results averaged over the 5 cases from December 1993.

Figure 10 Northern Hemisphere MSLP difference fields at T+120 for (a) New GWD - Operational forecasts, and (b) Orographic Roughness + New GWD - Operational forecasts.Results averaged over the 5 cases from December 1993.

Figure 11 Northern Hemisphere MSLP fields showing (a) Analyses corresponding to forecasts at T+120, (b) mean error in MSLP (forecast - analysis) for the operational forecasts at T+120, (c) as (b) but for New GWD forecasts, and (c) as (b) but for Orographic Roughness + New GWD Forecasts. Results averaged over the 5 cases from December 1993.

Figure 12 As figure 10 but for the Southern Hemisphere.

Figure 13 As figure 11 but for the Southern Hemisphere.

Figure 14 Zonally averaged, daily averaged (T+00 to T+24) zonal wind tendencies due to the Unified Model gravity wave drag scheme for (a) Operational forecasts, (b) New GWD forecasts, (c) Orographic Roughness forecasts, and (d) Orographic Roughness + New GWD forecasts. Units are m/s/day.

Figure 15 Zonally averaged, daily averaged (T+00 to T+24) zonal wind tendencies due to the Unified Model boundary layer turbulent mixing scheme for (a) Operational forecasts, (b) Orographic Roughness forecasts, and (c) the difference in forecasts, Orographic Roughness - Operational. Units are m/s/day.

Figure 16 Zonally averaged, daily averaged (T+00 to T+24) zonal wind tendencies due to the Unified Model parametrization schemes (GWD + Boundary Layer Turbulent Mixing + Vertical Diffusion) for (a) Operational forecasts, (b) Orographic Roughness + New GWD forecasts, (c) the difference in forecasts, Orographic Roughness +New GWD - Operational, (d) . Also shown are (d) as (c) but for the Unified model dynamical tendencies, and (e) as (c) but for the total (residual) tendencies.

Figure 17 Zonally averaged surface stresses at T+24 for (a) Boundary layer turbulent mixing scheme , and (b) the gravity wave drag schemes. Units are N/m^2 .

Figure 18 Northern Hemisphere (90N-30N) verification scores for MSLP (a) RMS error, and (b) Bias.

Figure 19 As Figure 18 but for 500hPa geopotential height.

Figure 20 Northern Hemisphere (90N-30N) RMS vector wind error for (a) 250hPa winds (b) 850 hPa winds.

Figure 21 As Figure 18 but for 850 hPa wind speeds.

Figure 22 As Figure 18 but for 250 hPa wind speeds.

Figure 23 Northern Hemisphere (90N-30N) 500hPa temperature bias scores.

Figure 24 RMS vector wind error for Observations - Model for Northern Hemisphere extratropics (90N-30N) and for forecasts from 07/01/94 to 13/01/94. Observations are Radiosondes and Aireps and verification scores are shown for each model level at (a) T+24, (b) T+72, and (c) T+144.

Figure 25 As Figure 24 but for the tropical region (30N-30S)

Figure 26 As Figure 24 but for the Southern Hemisphere extratropics (30S-90S)

Figure 27 Bias in zonal winds for Observations - Model for Northern Hemisphere extratropics (90N-30N) and for forecasts from 07/01/94 to 13/01/94. Observations are Radiosondes and Aireps and verification scores are shown for each model level at (a) T+24, (b) T+72, and (c) T+144.

Figure 28 As Figure 27 but for the tropical region (30N-30S)

Figure 29 As Figure 27 but for the Southern Hemisphere extratropics (30S-90S).

Figure 30 Bias in temperatures for Observations - Model for Northern Hemisphere extratropics (90N-30N) and for forecasts from 07/01/94 to 13/01/94. Observations are Radiosondes and verification scores are shown for each model level at (a) T+24, (b) T+72, and (c) T+144.

Figure 31 As Figure 30 but for the tropical region (30N-30S)

Figure 32 As Figure 30 but for the Southern Hemisphere extratropics (30S-90S).

Figure 33 Bias and RMS error in Relative Humidity for Observations - Model at T+144 for forecasts from 07/01/94 to 13/01/94. Observations are Radiosondes and verification scores are shown for each model level for (a) Northern Hemisphere extratropics (90N-30N), (b) Tropics (30N-30S), and (c) Southern Hemisphere extratropics (30S-90S)

Figure 34 RMS vector wind error for Observations - Model for Northern Hemisphere extratropics (90N-30N) and for forecasts from 11/08/93 to 17/08/93. Observations are Radiosondes and Aireps and verification scores are shown for each model level at (a) T+24, (b) T+72, and (c) T+144.

Figure 35 As Figure 34 but for the tropical region (30N-30S)

Figure 36 As Figure 24 but for the Southern Hemisphere extratropics (30S-90S)

Figure 37 T+72 forecasts of mean-sea level pressure verifying at 00Z on 11/01/94 for (a) ROGW and (b) OP.

Figure 38 Verifying analysis (Operational) of mean-sea level pressure valid at 00Z on 11/01/94.

Figure 39 T+72 forecasts of mean-sea level pressure verifying at 00Z on 12/01/94 for (a) ROGW and (b) OP.

Figure 40 Verifying analysis (Operational) valid at 00Z on 11/01/94 of (a) mean-sea level pressure and (b) 500hPa geopotential height,

Figure 41 T+72 forecasts of 500hPa geopotential height verifying at 00Z on 12/01/94 for (a) ROGW and (b) OP.

Figure 42 T+120 forecasts of mean-sea level pressure verifying at 00Z on 17/01/94 for (a) ROGW and (b) OP.

Figure 43 Verifying analysis (Operational) of (a) mean-sea level pressure valid at 00Z on 17/01/94, (b) mean-sea level pressure valid at 00Z on 18/01/94 and (c) 500hPa geopotential height valid at 00Z on 18/01/94.

Figure 44 T+144 forecasts of mean-sea level pressure verifying at 00Z on 18/01/94 for (a) ROGW and (b) OP.

Figure 45 T+144 forecasts of 500hPa geopotential height verifying at 00Z on 18/01/94 for (a) ROGW and (b) OP.

Figure 46 90-day means of zonally averaged (a) Zonal wind from OP run December-January-February (DJF) 1978-79, (b) Zonal wind difference (OP - Climatology of UKMO analyses 1985- 90) for DJF 1978-79 (c) Zonal wind difference ROGW - OP for DJF 1978-79, (d) Zonal wind difference (ROGW - Climatology of UKMO analyses 1985-90) for DJF 1978-79, (e) as (c) but for DJF 1979-80, (f) as (d) but for DJF 1979-80.

Figure 47 90-day means of zonally averaged (a) Temperature for ROGW run December-January-February (DJF) 1978-79, (b) Temperature difference ROGW - OP for DJF 1978-79.

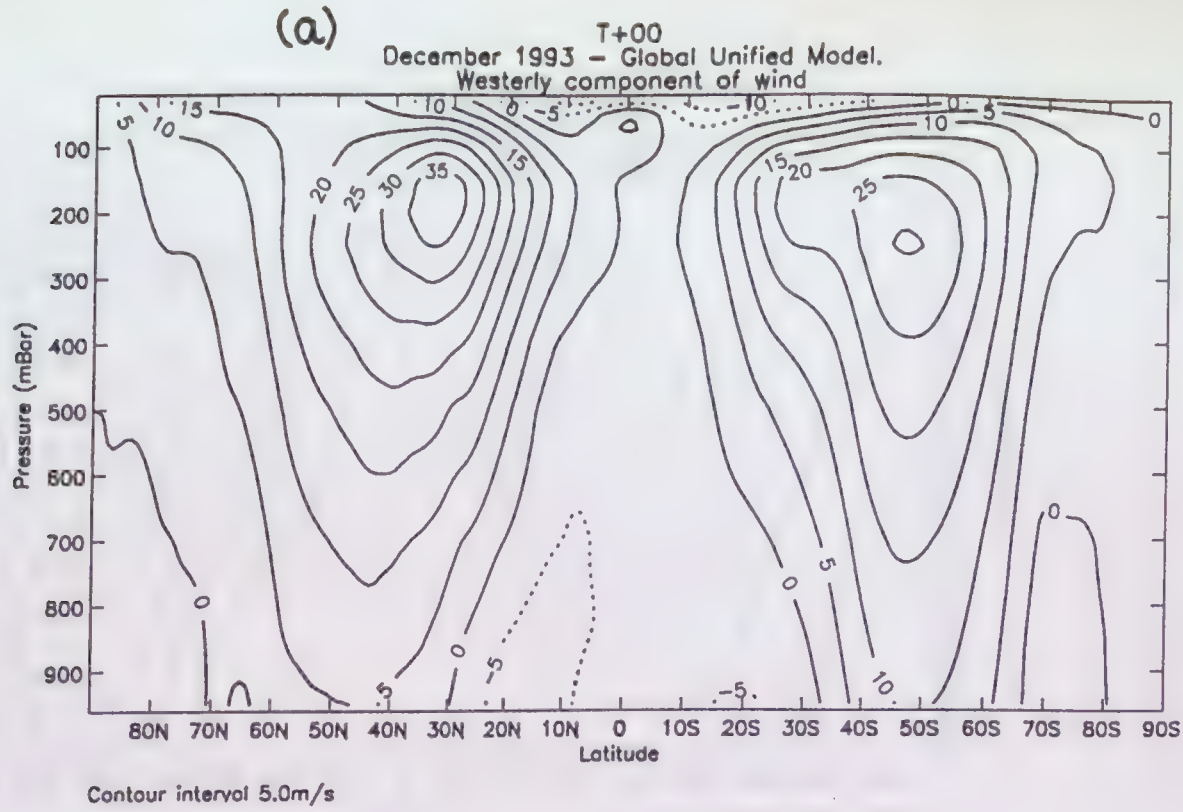
(a)
T+00
December 1993 – Global Unified Model.
Westerly component of wind
Pressure (mBar)
100
200
300
400
500
600
700
800
900
80N 70N 60N 50N 40N 30N 20N 10N 0 10S 20S 30S 40S 50S 60S 70S 80S 90S
Latitude
Contour interval 5.0m/s

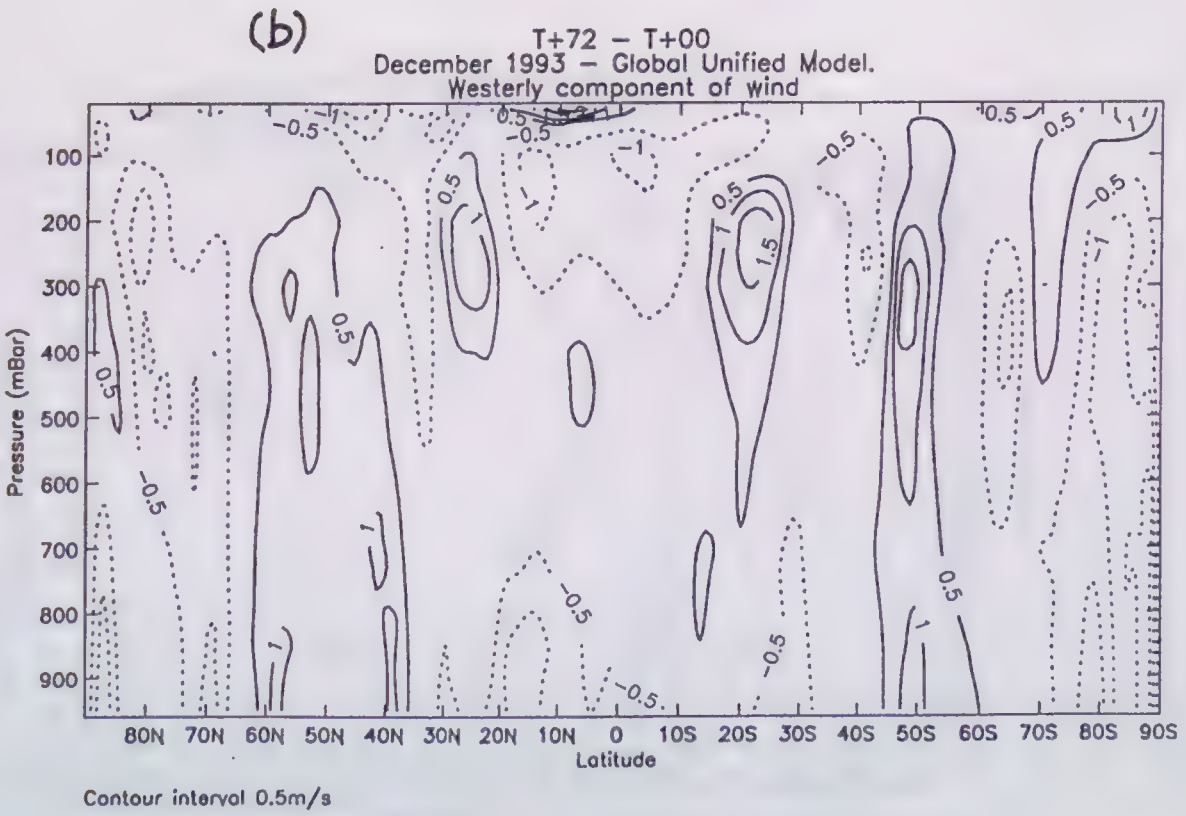
(b)
T+72 – T+00
December 1993 – Global Unified Model.
Westerly component of wind
Pressure (mBar)
100
200
300
400
500
600
700
800
900
80N 70N 60N 50N 40N 30N 20N 10N 0 10S 20S 30S 40S 50S 60S 70S 80S 90S
Latitude
Contour interval 0.5m/s

Figure 1

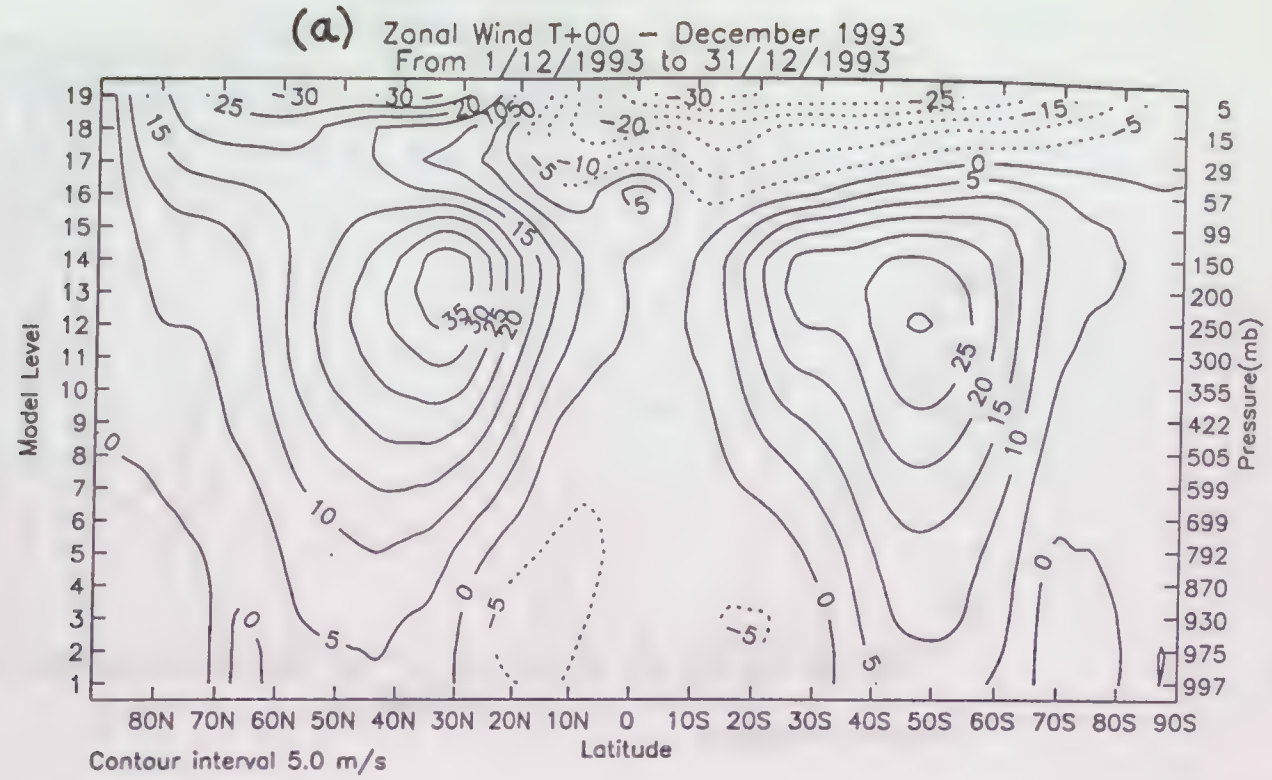
(a) Zonal Wind T+00 – December 1993
From 1/12/1993 to 31/12/1993
Model Level
Pressure(mb)
80N 70N 60N 50N 40N 30N 20N 10N 0 10S 20S 30S 40S 50S 60S 70S 80S 90S
Latitude
Contour interval 5.0 m/s

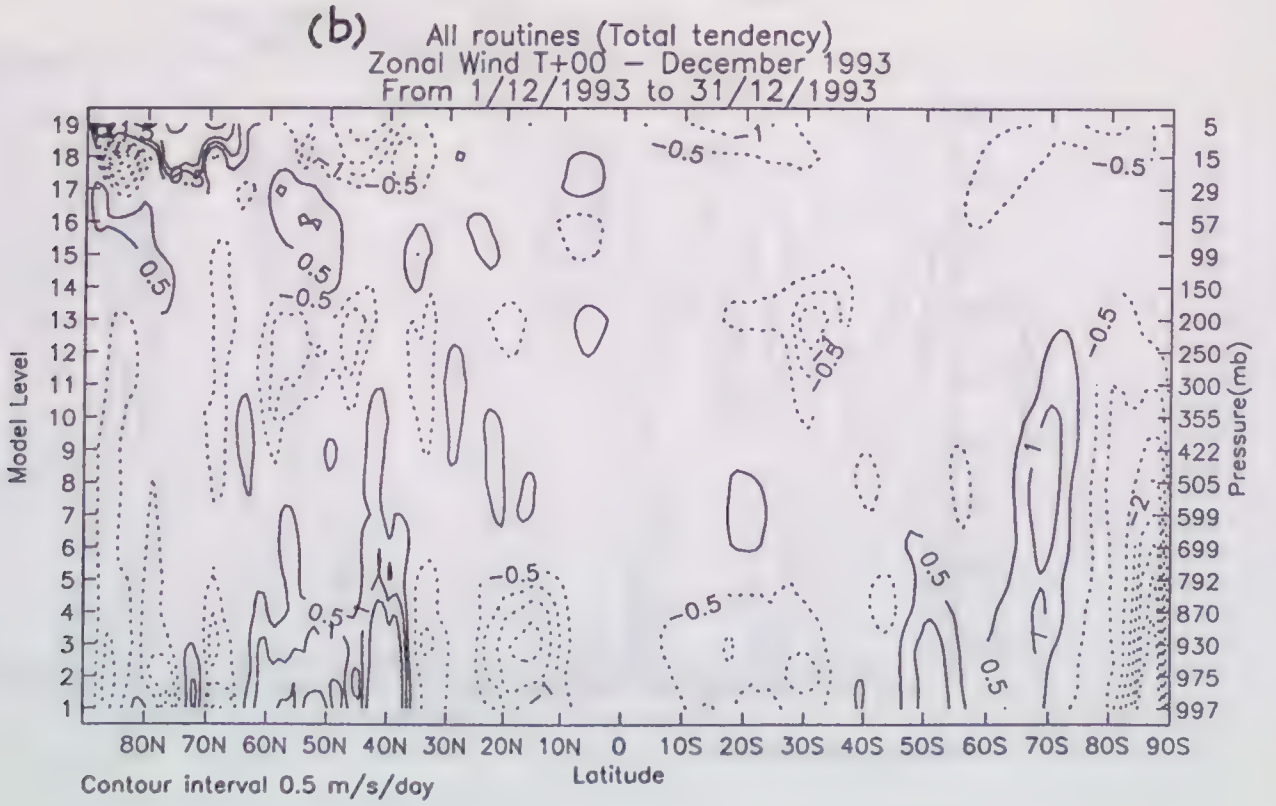
(b) All routines (Total tendency)
Zonal Wind T+00 – December 1993
From 1/12/1993 to 31/12/1993
Model Level
Pressure(mb)
80N 70N 60N 50N 40N 30N 20N 10N 0 10S 20S 30S 40S 50S 60S 70S 80S 90S
Latitude
Contour interval 0.5 m/s/day

Figure 2

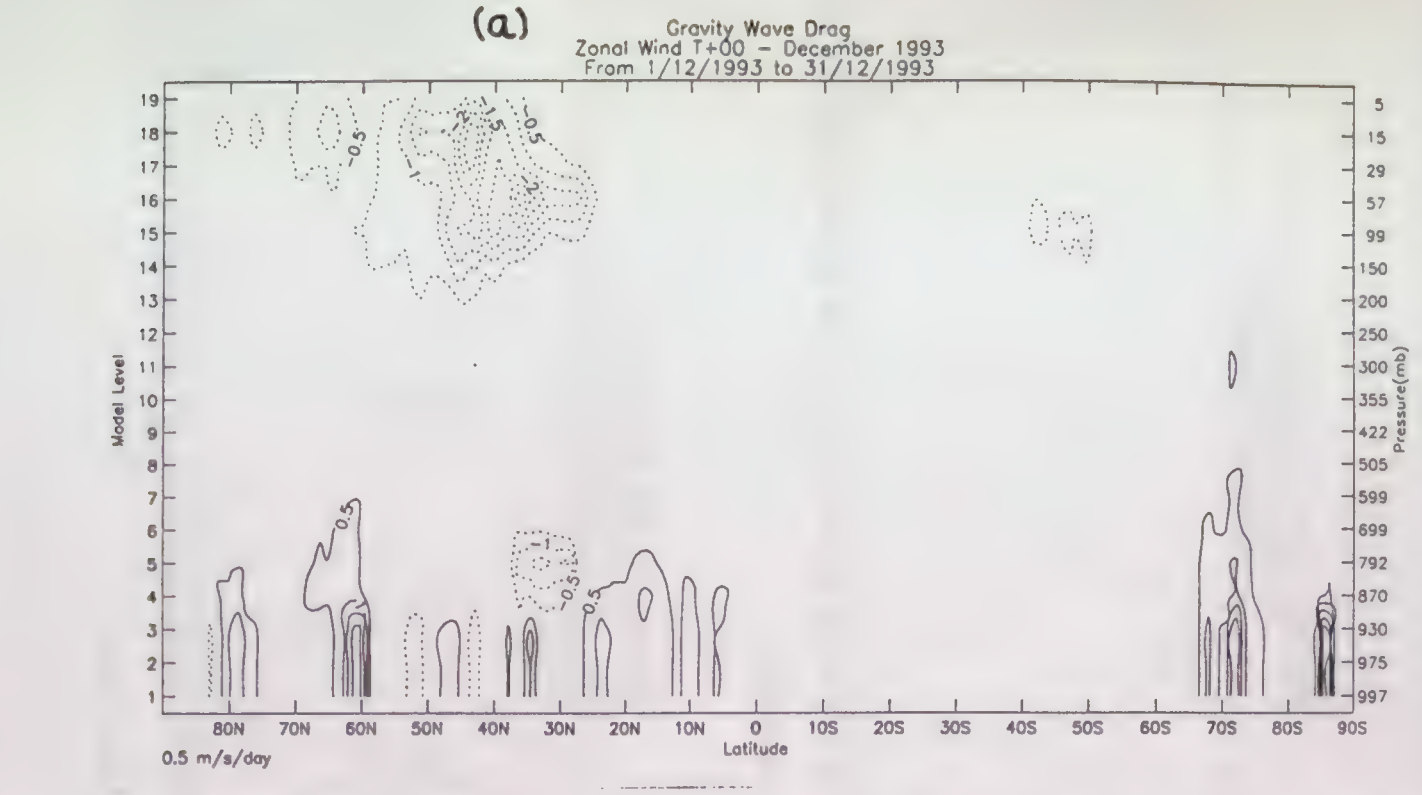
(a)
Gravity Wave Drag
Zonal Wind T+00 – December 1993
From 1/12/1993 to 31/12/1993
Model Level
Pressure(mb)
Latitude
0.5 m/s/day

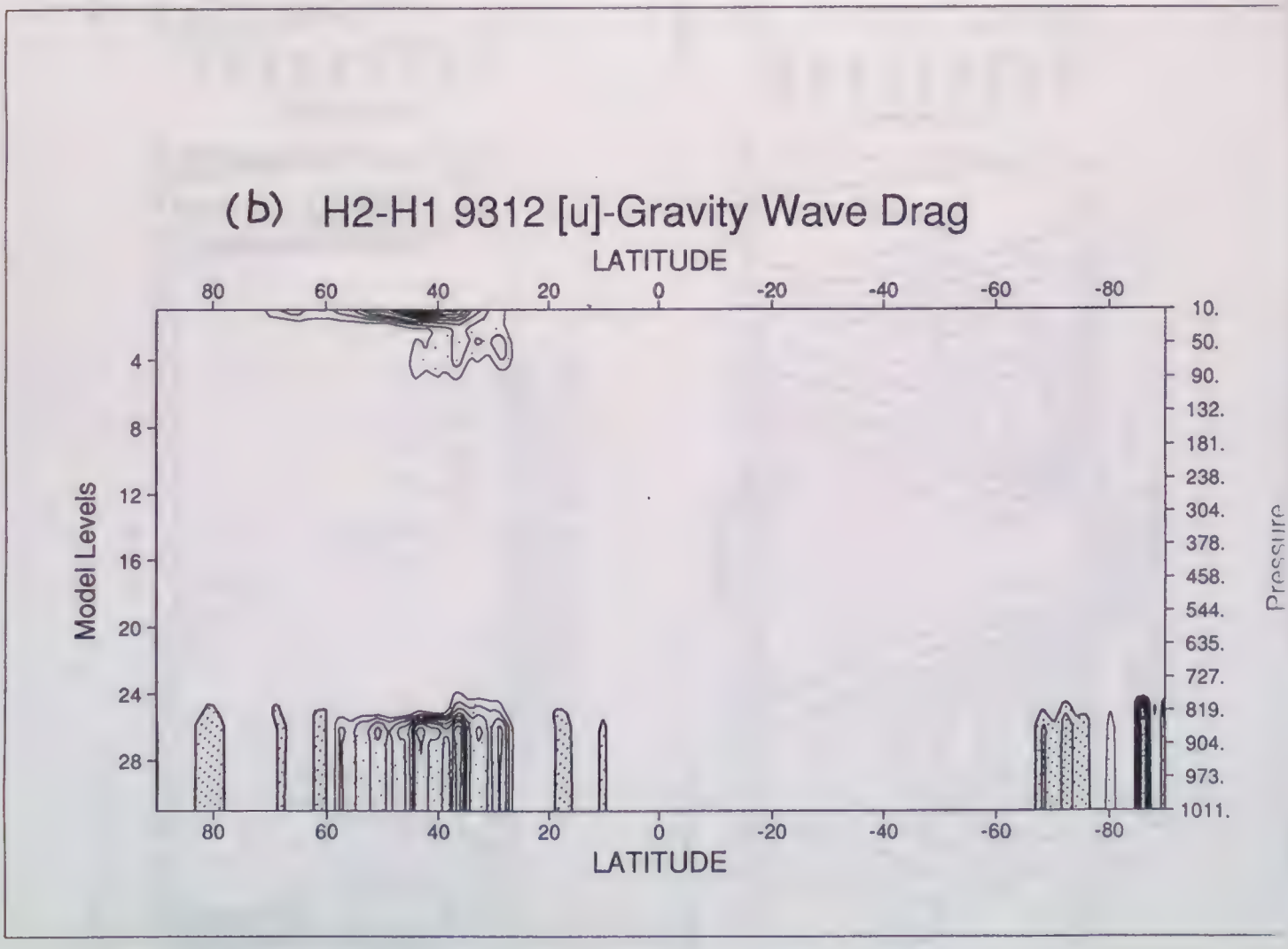
(b) H2-H1 9312 [u]-Gravity Wave Drag
LATITUDE
Model Levels
Pressure
LATITUDE

Figure 3

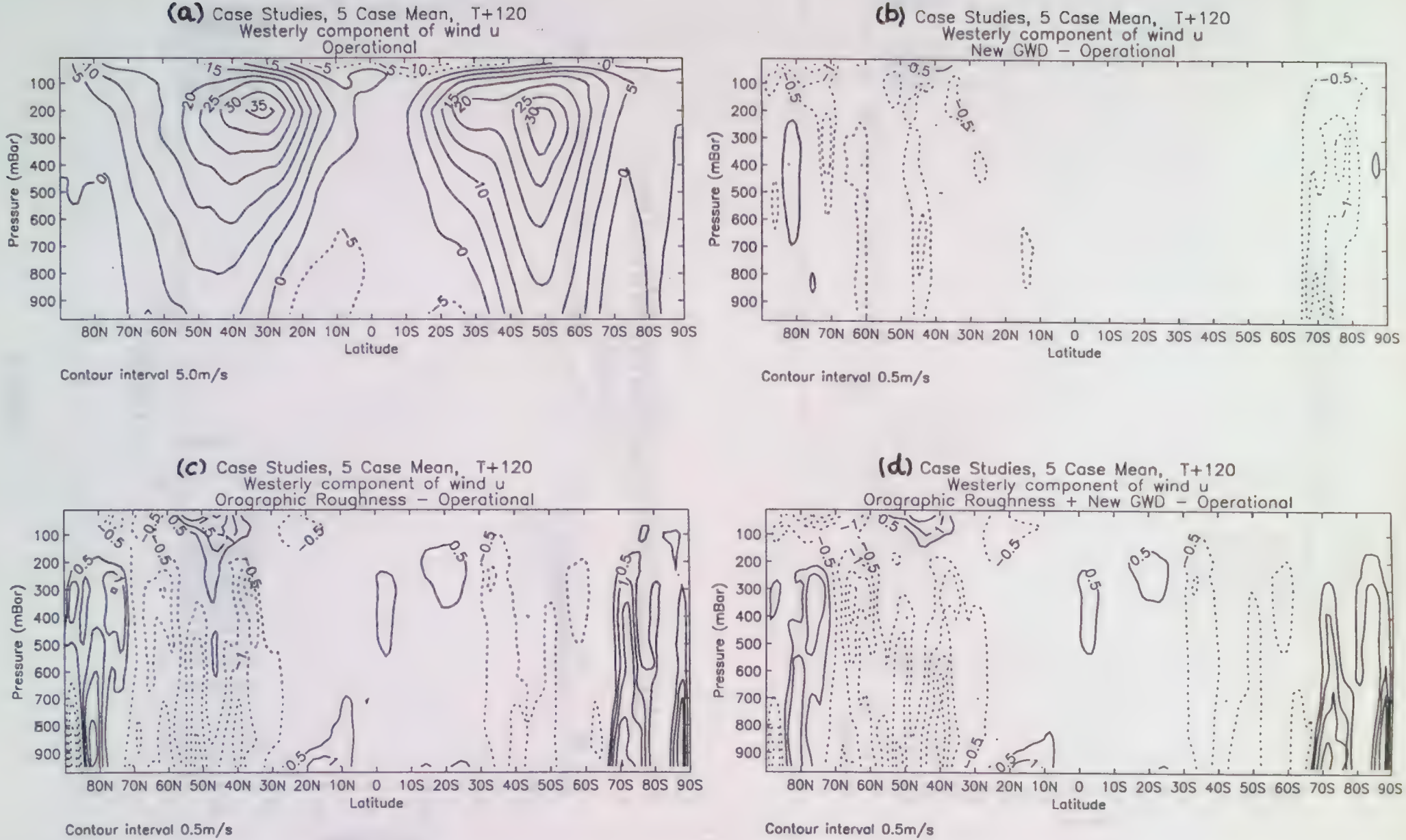
(a) Case Studies, 5 Case Mean, T+120
Westerly component of wind u
Operational
Pressure (mBar)
Latitude
80N 70N 60N 50N 40N 30N 20N 10N 0 10S 20S 30S 40S 50S 60S 70S 80S 90S
Contour interval 5.0m/s
(b) Case Studies, 5 Case Mean, T+120
Westerly component of wind u
New GWD − Operational
Pressure (mBar)
Latitude
Contour interval 0.5m/s
(c) Case Studies, 5 Case Mean, T+120
Westerly component of wind u
Orographic Roughness − Operational
Pressure (mBar)
Latitude
Contour interval 0.5m/s
(d) Case Studies, 5 Case Mean, T+120
Westerly component of wind u
Orographic Roughness + New GWD − Operational
Pressure (mBar)
Latitude
Contour interval 0.5m/s

Figure 4

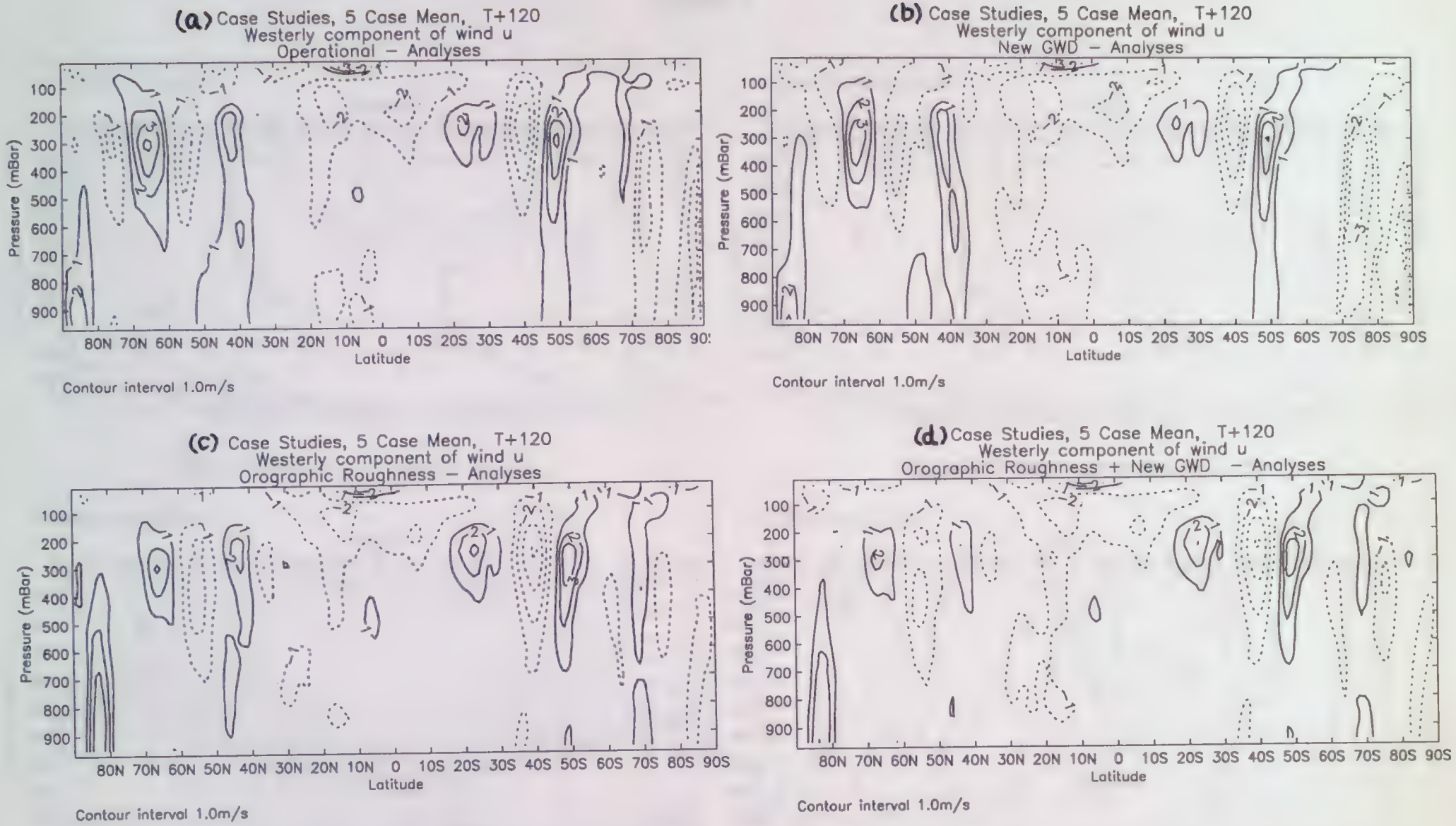
(a) Case Studies, 5 Case Mean, T+120
Westerly component of wind u
Operational – Analyses
Pressure (mBar)
100
200
300
400
500
600
700
800
900
80N 70N 60N 50N 40N 30N 20N 10N 0 10S 20S 30S 40S 50S 60S 70S 80S 90S
Latitude
Contour interval 1.0m/s
(b) Case Studies, 5 Case Mean, T+120
Westerly component of wind u
New GWD – Analyses
Pressure (mBar)
100
200
300
400
500
600
700
800
900
80N 70N 60N 50N 40N 30N 20N 10N 0 10S 20S 30S 40S 50S 60S 70S 80S 90S
Latitude
Contour interval 1.0m/s
(c) Case Studies, 5 Case Mean, T+120
Westerly component of wind u
Orographic Roughness – Analyses
Pressure (mBar)
100
200
300
400
500
600
700
800
900
80N 70N 60N 50N 40N 30N 20N 10N 0 10S 20S 30S 40S 50S 60S 70S 80S 90S
Latitude
Contour interval 1.0m/s
(d) Case Studies, 5 Case Mean, T+120
Westerly component of wind u
Orographic Roughness + New GWD – Analyses
Pressure (mBar)
100
200
300
400
500
600
700
800
900
80N 70N 60N 50N 40N 30N 20N 10N 0 10S 20S 30S 40S 50S 60S 70S 80S 90S
Latitude
Contour interval 1.0m/s

Figure 5

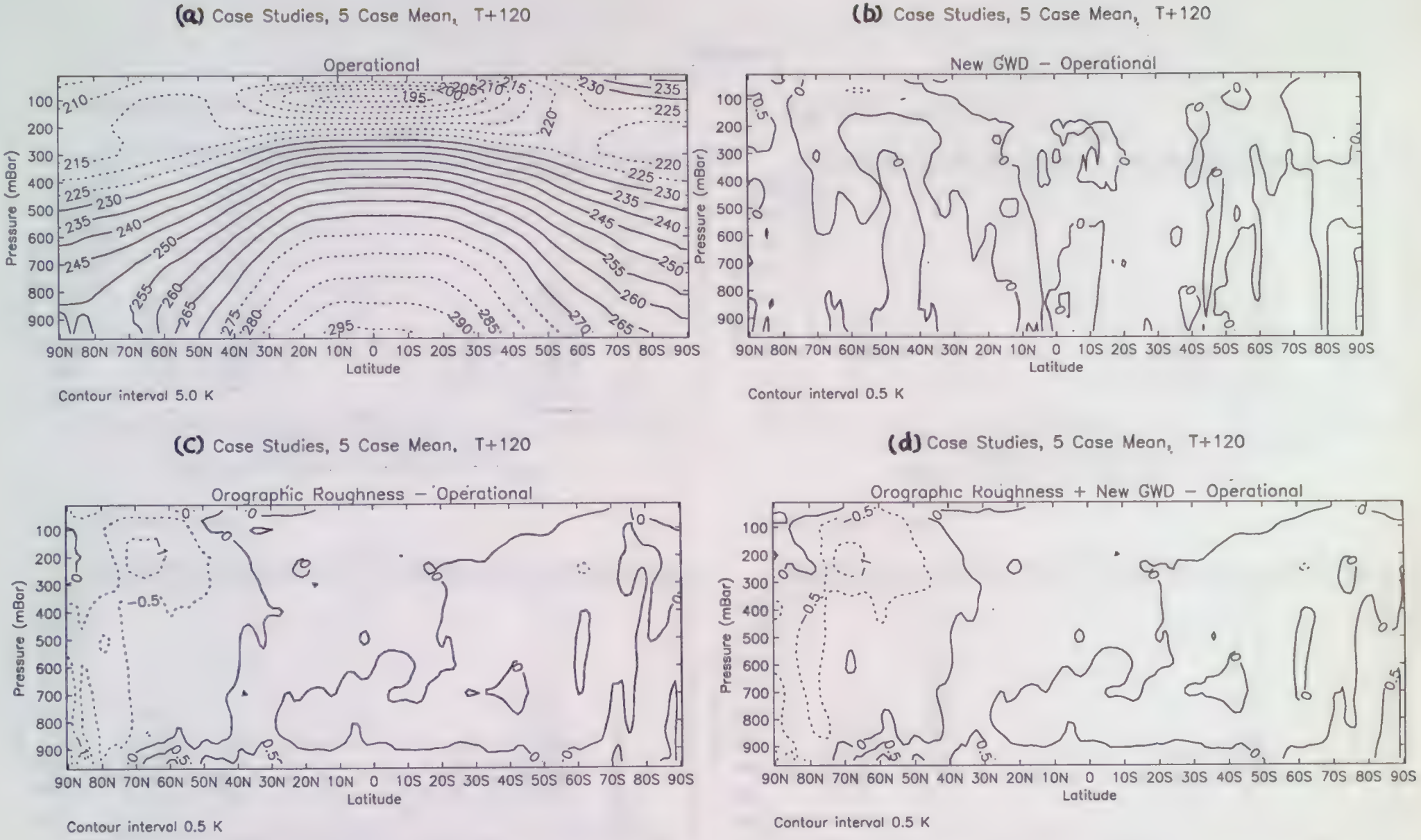
(a) Case Studies, 5 Case Mean, T+120
Operational
Pressure (mBar)
Latitude
90N 80N 70N 60N 50N 40N 30N 20N 10N 0 10S 20S 30S 40S 50S 60S 70S 80S 90S
Contour interval 5.0 K
(b) Case Studies, 5 Case Mean, T+120
New GWD – Operational
Pressure (mBar)
Latitude
Contour interval 0.5 K
(c) Case Studies, 5 Case Mean, T+120
Orographic Roughness – Operational
Pressure (mBar)
Latitude
Contour interval 0.5 K
(d) Case Studies, 5 Case Mean, T+120
Orographic Roughness + New GWD – Operational
Pressure (mBar)
Latitude
Contour interval 0.5 K

Figure 6

(a) Case Studies, 5 Case Mean, T+120

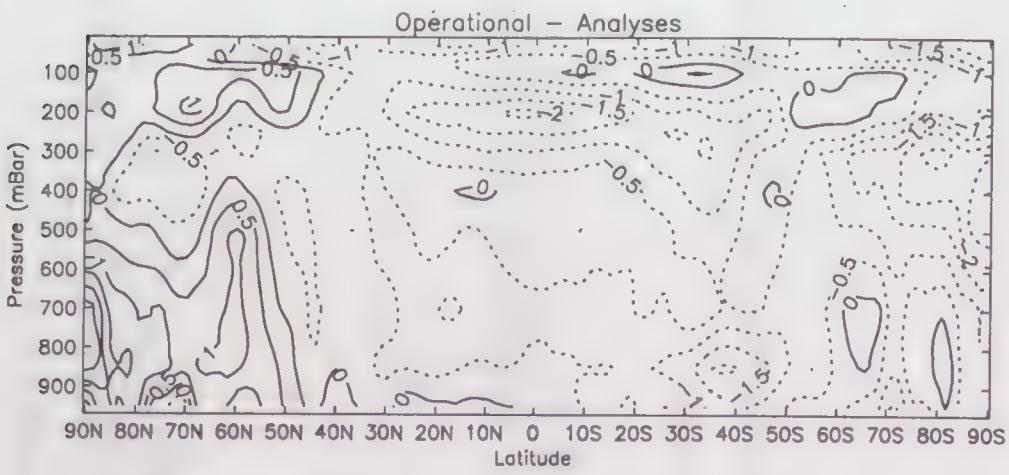

(b) Case Studies, 5 Case Mean, T+120

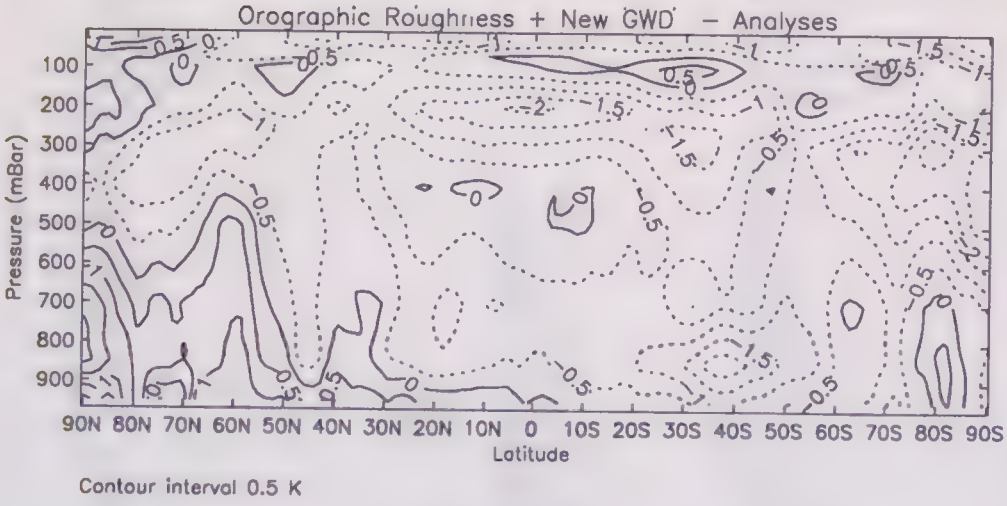

Figure 7

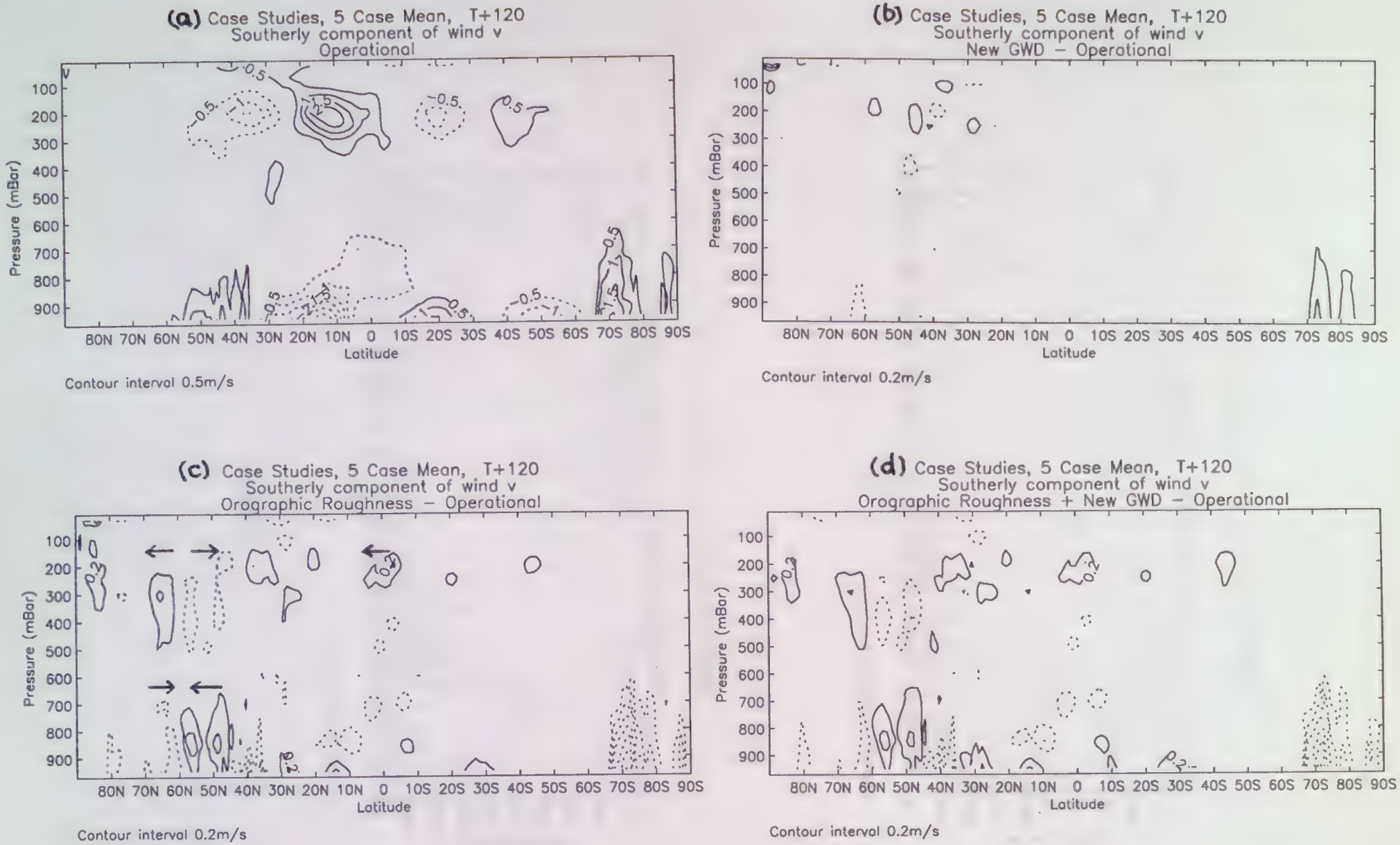
(a) Case Studies, 5 Case Mean, T+120
Southerly component of wind v
Operational
Pressure (mBar)
Latitude
80N 70N 60N 50N 40N 30N 20N 10N 0 10S 20S 30S 40S 50S 60S 70S 80S 90S
Contour interval 0.5m/s
(b) Case Studies, 5 Case Mean, T+120
Southerly component of wind v
New GWD − Operational
Pressure (mBar)
Latitude
Contour interval 0.2m/s
(c) Case Studies, 5 Case Mean, T+120
Southerly component of wind v
Orographic Roughness − Operational
Pressure (mBar)
Latitude
Contour interval 0.2m/s
(d) Case Studies, 5 Case Mean, T+120
Southerly component of wind v
Orographic Roughness + New GWD − Operational
Pressure (mBar)
Latitude
Contour interval 0.2m/s

Figure 8

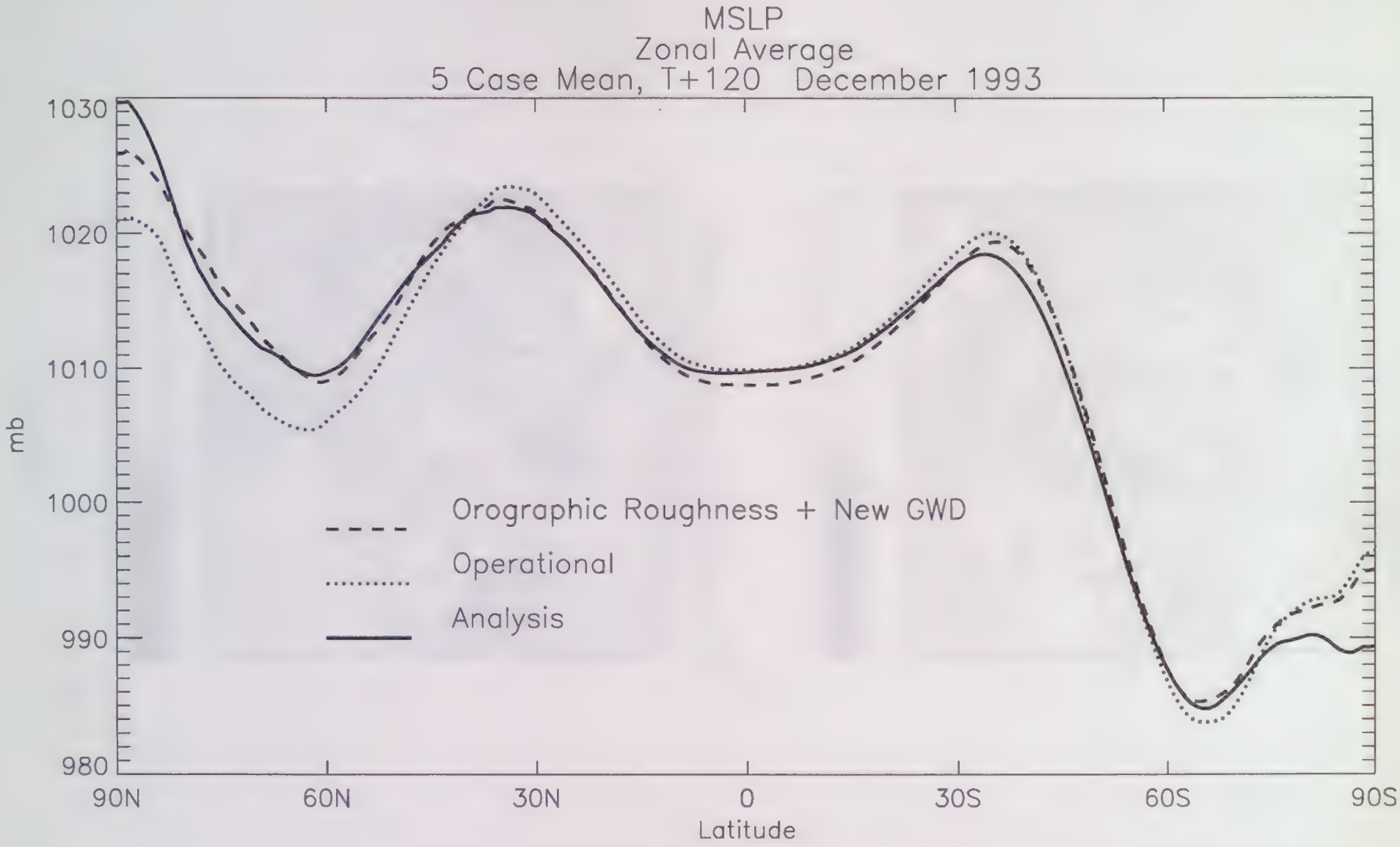
MSLP
Zonal Average
5 Case Mean, T+120 December 1993
1030
1020
1010
1000
990
980
mb
Orographic Roughness + New GWD
Operational
Analysis
90N
60N
30N
0
30S
60S
90S
Latitude

Figure 9

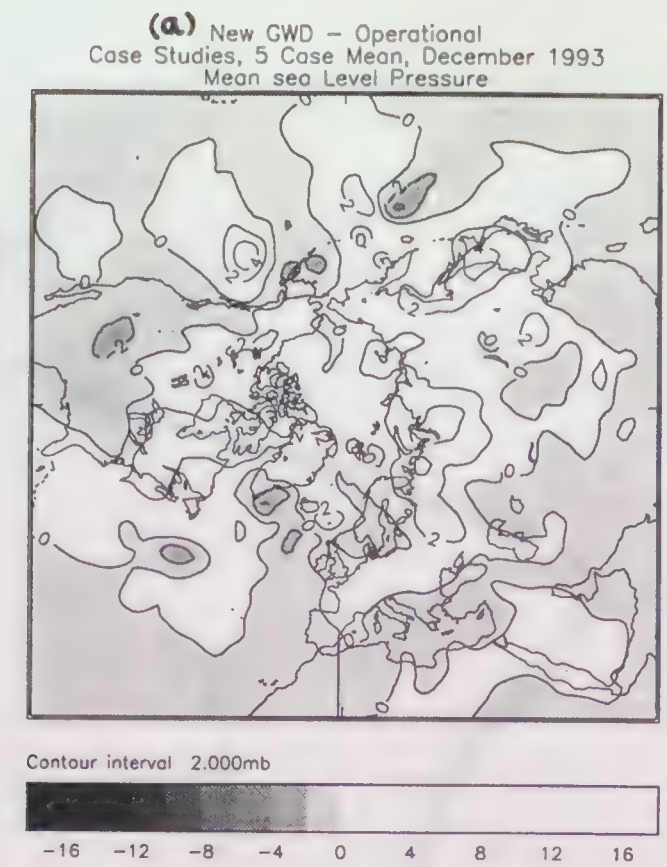
(a) New GWD – Operational
Case Studies, 5 Case Mean, December 1993
Mean sea Level Pressure
Contour interval 2.000mb
−16 −12 −8 −4 0 4 8 12 16
(b) Orographic Roughness + New GWD – Operational
Case Studies, 5 Case Mean, December 1993
Mean sea Level Pressure
Contour interval 2.000mb
−16 −12 −8 −4 0 4 8 12 16

Figure 10

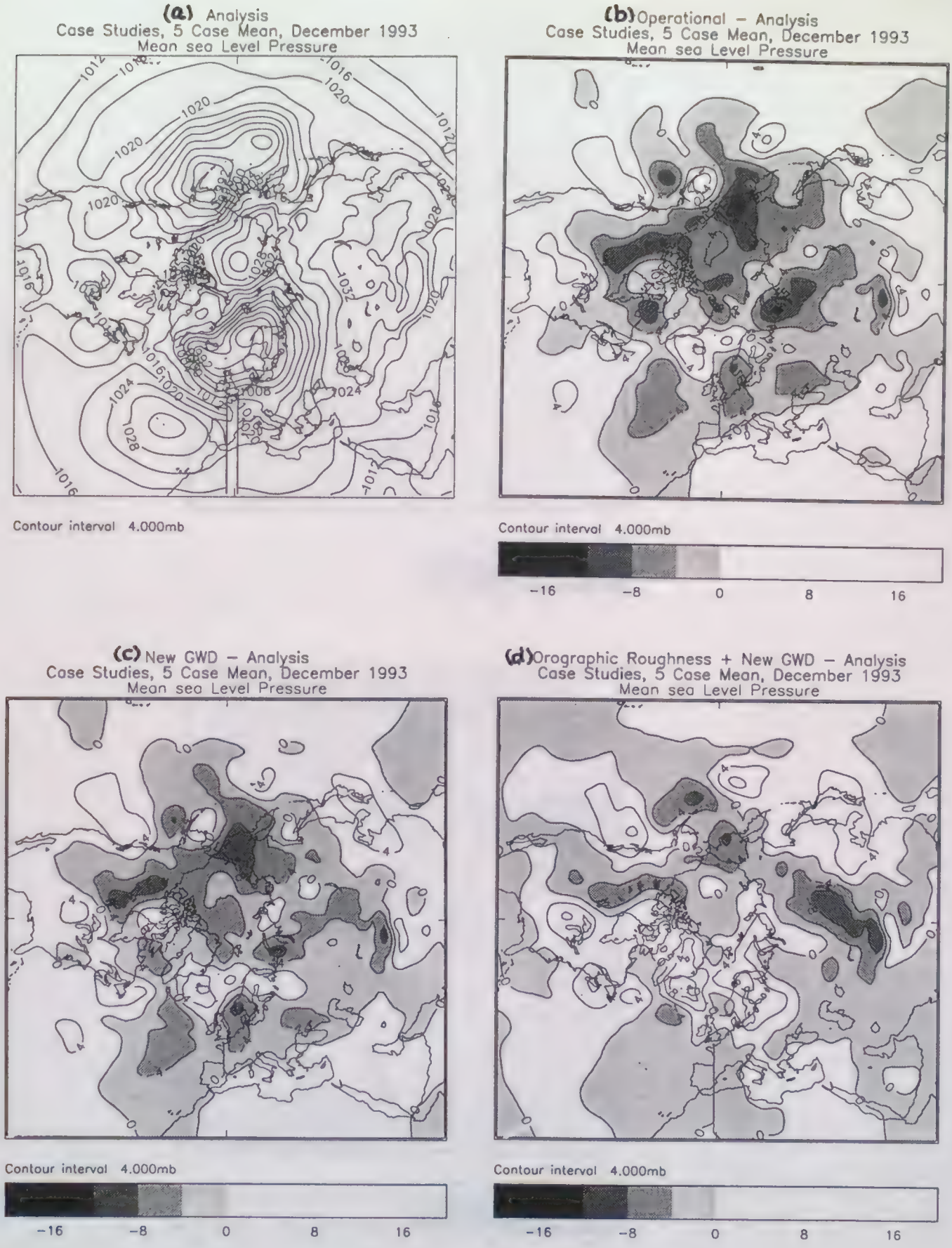
(a) Analysis
Case Studies, 5 Case Mean, December 1993
Mean sea Level Pressure
Contour interval 4.000mb
(b) Operational – Analysis
Case Studies, 5 Case Mean, December 1993
Mean sea Level Pressure
Contour interval 4.000mb
−16 −8 0 8 16
(c) New GWD – Analysis
Case Studies, 5 Case Mean, December 1993
Mean sea Level Pressure
Contour interval 4.000mb
−16 −8 0 8 16
(d) Orographic Roughness + New GWD – Analysis
Case Studies, 5 Case Mean, December 1993
Mean sea Level Pressure
Contour interval 4.000mb
−16 −8 0 8 16

Figure 11

(a) New GWD – Operational
Case Studies, 5 Case Mean, December 1993
Mean sea Level Pressure
Contour interval 2.000mb
−16 −12 −8 −4 0 4 8 12 16

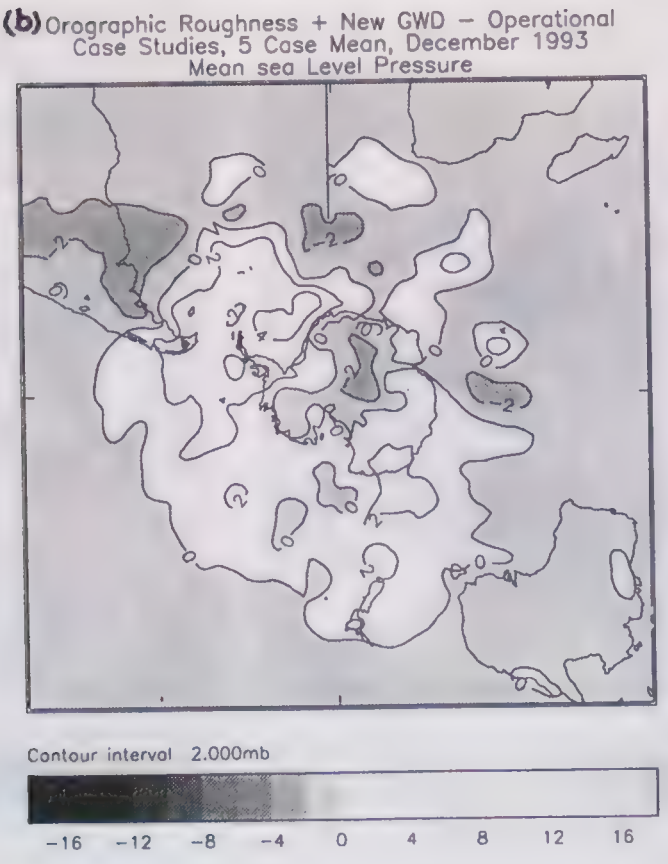
(b) Orographic Roughness + New GWD – Operational
Case Studies, 5 Case Mean, December 1993
Mean sea Level Pressure
Contour interval 2.000mb
−16 −12 −8 −4 0 4 8 12 16

Figure 12

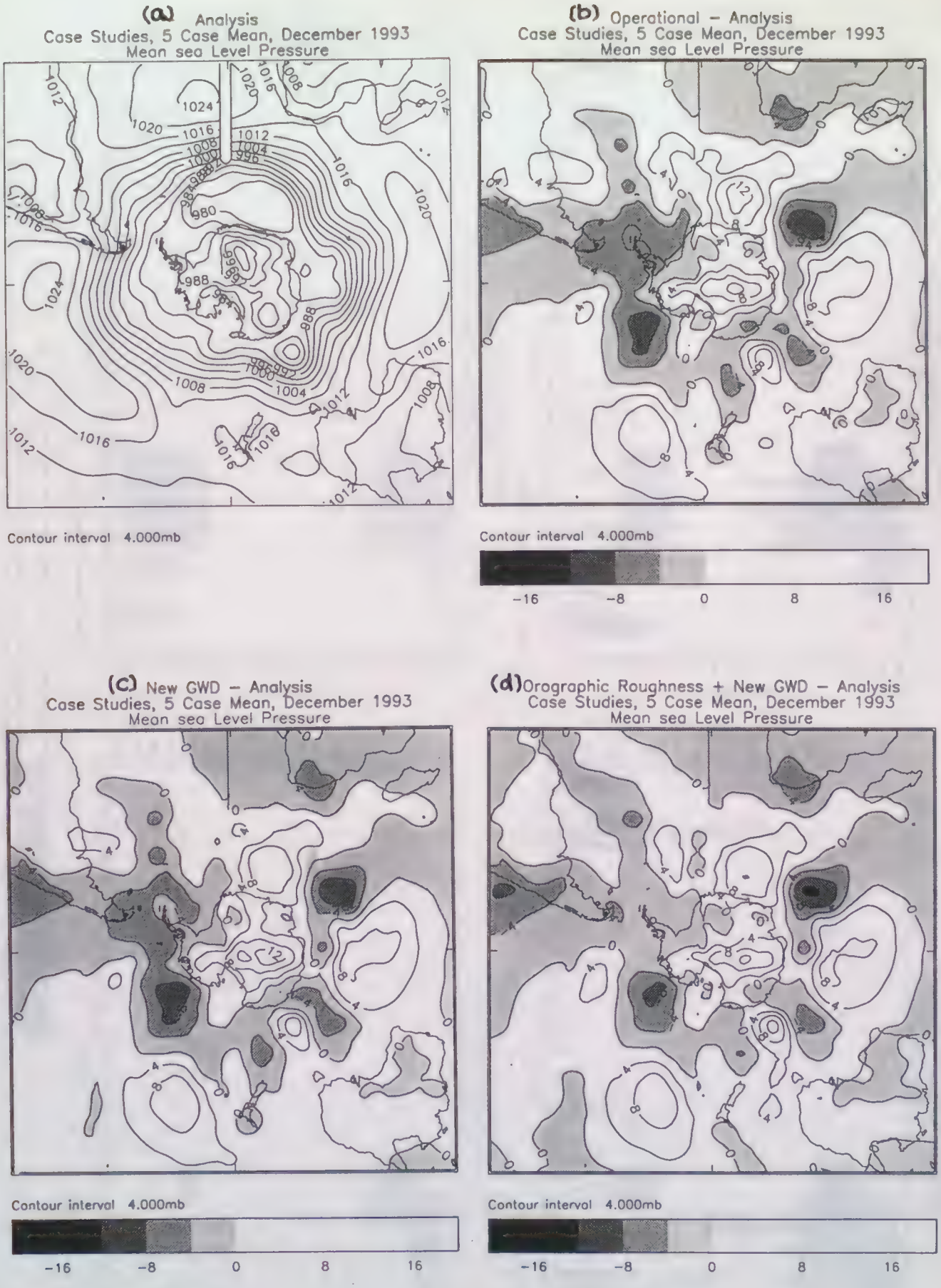
(a) Analysis
Case Studies, 5 Case Mean, December 1993
Mean sea Level Pressure
Contour interval 4.000mb
(b) Operational – Analysis
Case Studies, 5 Case Mean, December 1993
Mean sea Level Pressure
Contour interval 4.000mb
−16 −8 0 8 16
(c) New GWD – Analysis
Case Studies, 5 Case Mean, December 1993
Mean sea Level Pressure
Contour interval 4.000mb
−16 −8 0 8 16
(d) Orographic Roughness + New GWD – Analysis
Case Studies, 5 Case Mean, December 1993
Mean sea Level Pressure
Contour interval 4.000mb
−16 −8 0 8 16

Figure 13

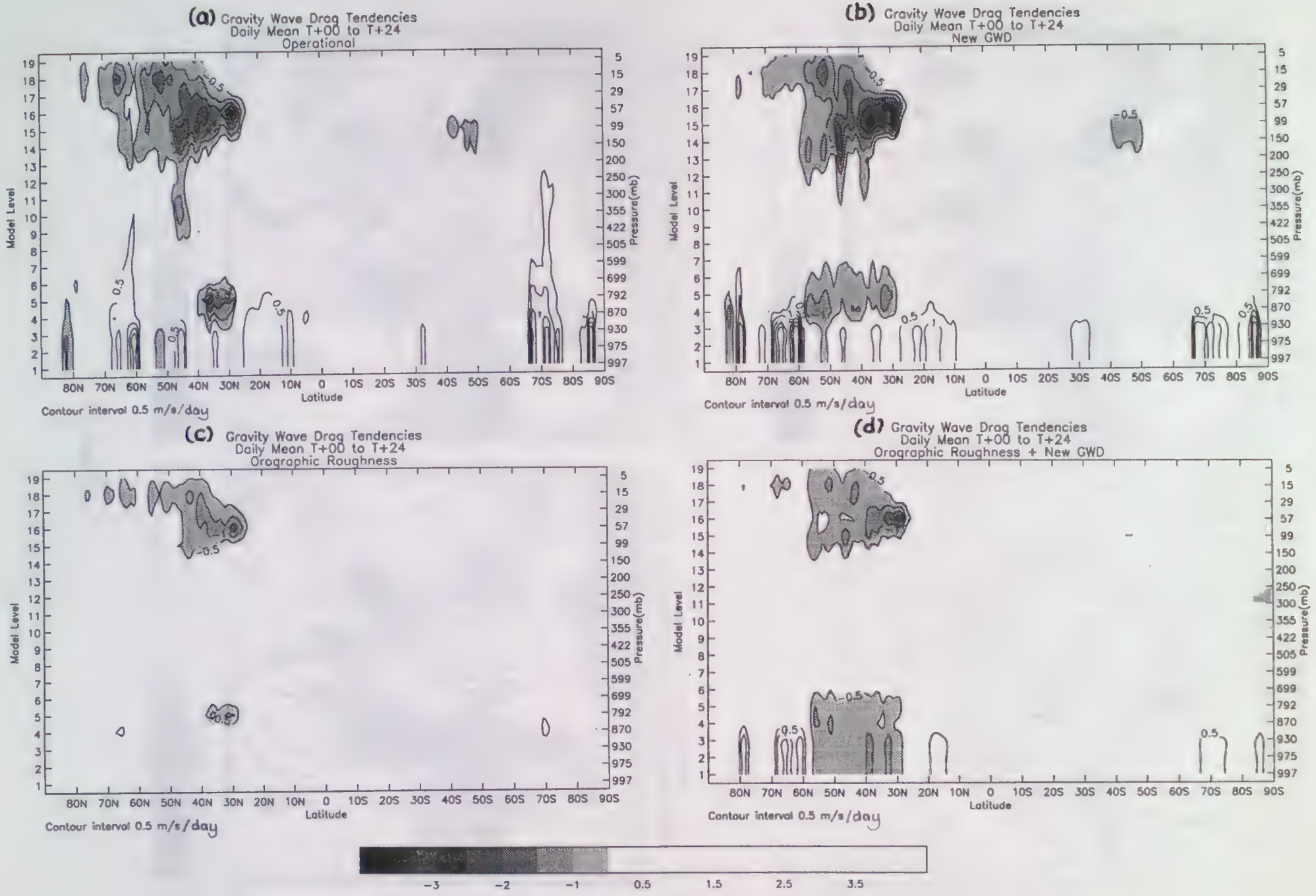
(a) Gravity Wave Drag Tendencies
Daily Mean T+00 to T+24
Operational
(b) Gravity Wave Drag Tendencies
Daily Mean T+00 to T+24
New GWD
(c) Gravity Wave Drag Tendencies
Daily Mean T+00 to T+24
Orographic Roughness
(d) Gravity Wave Drag Tendencies
Daily Mean T+00 to T+24
Orographic Roughness + New GWD
Model Level
Pressure(mb)
Latitude
80N 70N 60N 50N 40N 30N 20N 10N 0 10S 20S 30S 40S 50S 60S 70S 80S 90S
Contour interval 0.5 m/s/day
-3 -2 -1 0.5 1.5 2.5 3.5

Figure 14

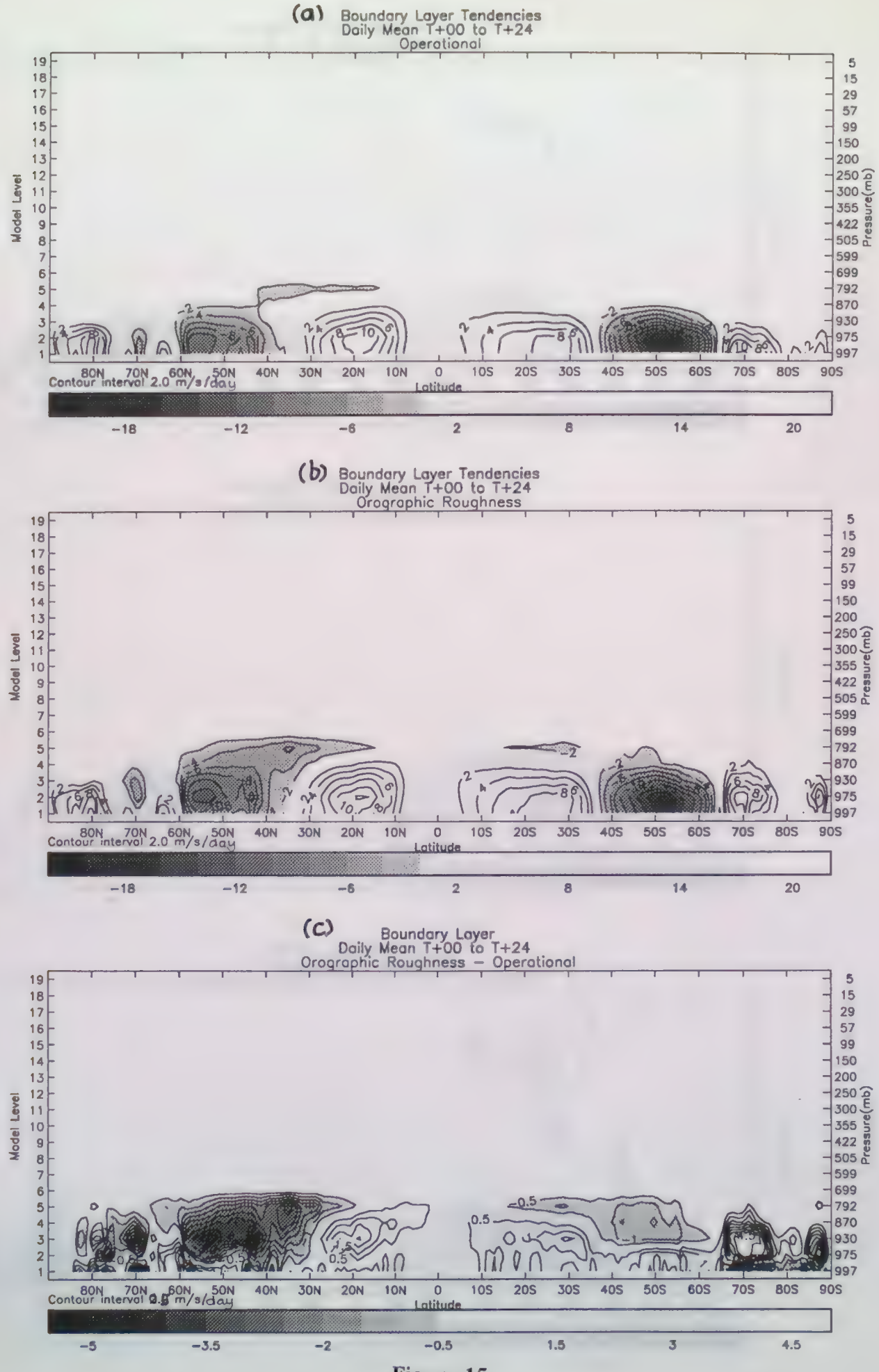
(a) Boundary Layer Tendencies
Daily Mean T+00 to T+24
Operational
Model Level
Pressure(mb)
Latitude
80N 70N 60N 50N 40N 30N 20N 10N 0 10S 20S 30S 40S 50S 60S 70S 80S 90S
Contour interval 2.0 m/s/day
-18 -12 -6 2 8 14 20
(b) Boundary Layer Tendencies
Daily Mean T+00 to T+24
Orographic Roughness
Model Level
Pressure(mb)
Latitude
80N 70N 60N 50N 40N 30N 20N 10N 0 10S 20S 30S 40S 50S 60S 70S 80S 90S
Contour interval 2.0 m/s/day
-18 -12 -6 2 8 14 20
(c) Boundary Layer
Daily Mean T+00 to T+24
Orographic Roughness - Operational
Model Level
Pressure(mb)
Latitude
80N 70N 60N 50N 40N 30N 20N 10N 0 10S 20S 30S 40S 50S 60S 70S 80S 90S
Contour interval 0.5 m/s/day
-5 -3.5 -2 -0.5 1.5 3 4.5

Figure 15

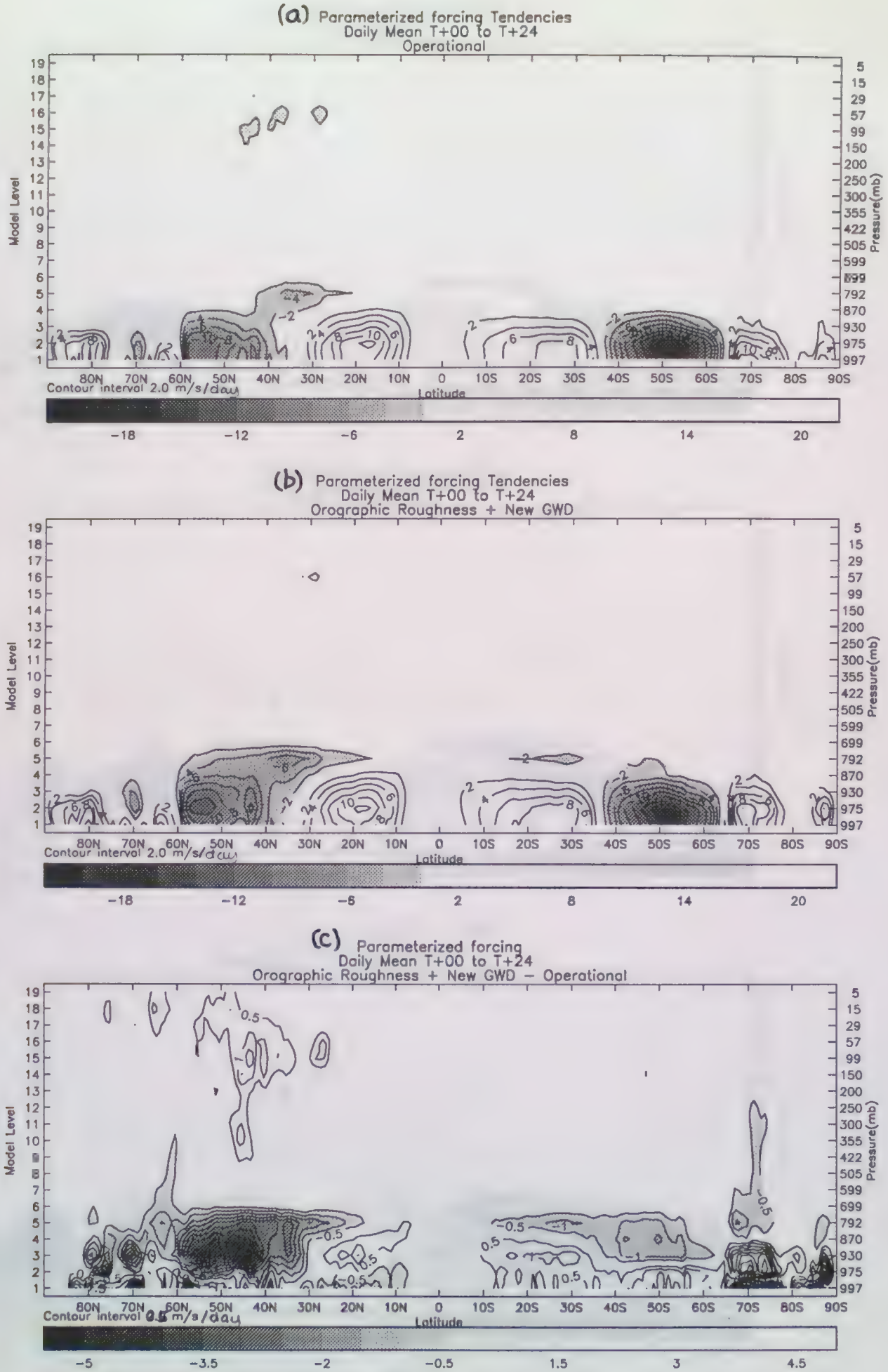
(a) Parameterized forcing Tendencies
Daily Mean T+00 to T+24
Operational
Model Level
Pressure(mb)
Latitude
Contour interval 2.0 m/s/day
(b) Parameterized forcing Tendencies
Daily Mean T+00 to T+24
Orographic Roughness + New GWD
Model Level
Pressure(mb)
Latitude
Contour interval 2.0 m/s/day
(c) Parameterized forcing
Daily Mean T+00 to T+24
Orographic Roughness + New GWD − Operational
Model Level
Pressure(mb)
Latitude
Contour interval 0.5 m/s/day

Figure 16

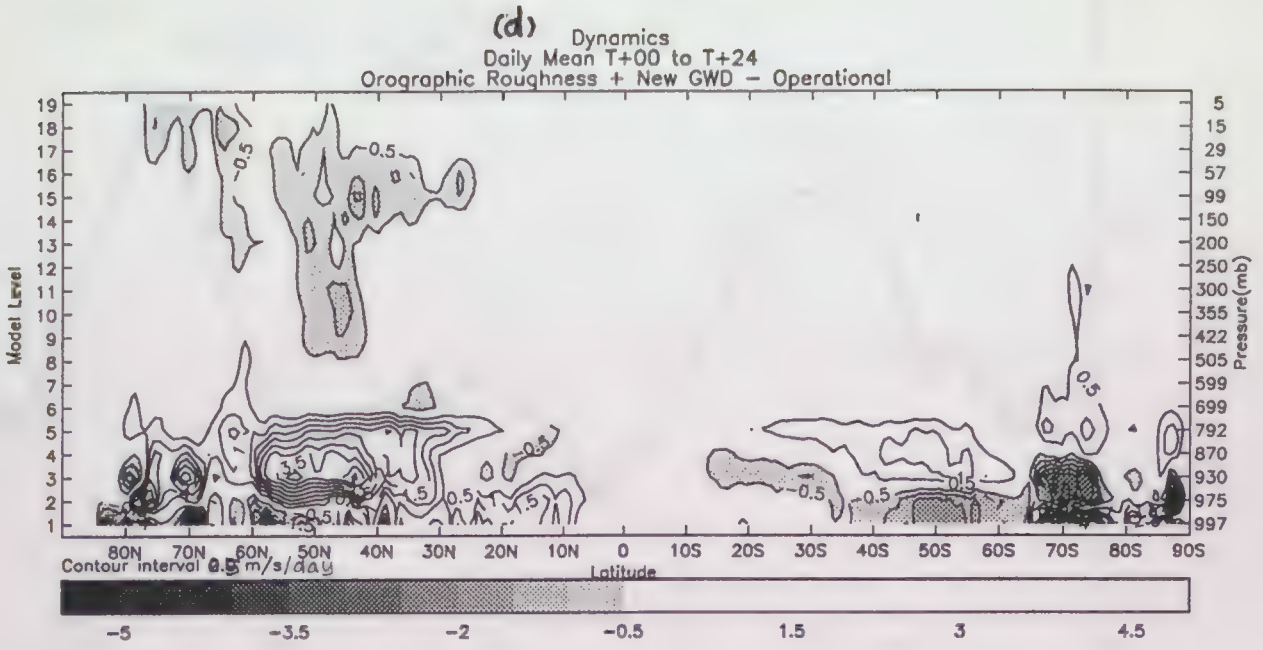

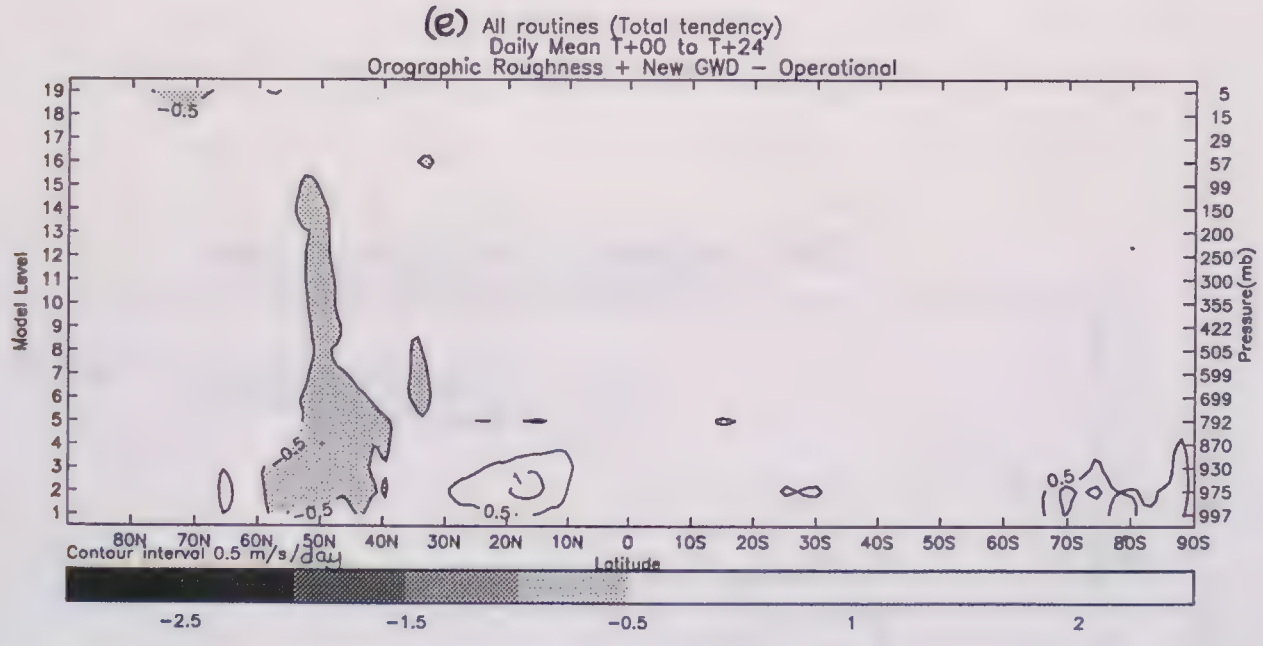

Figure 16 (Continued)

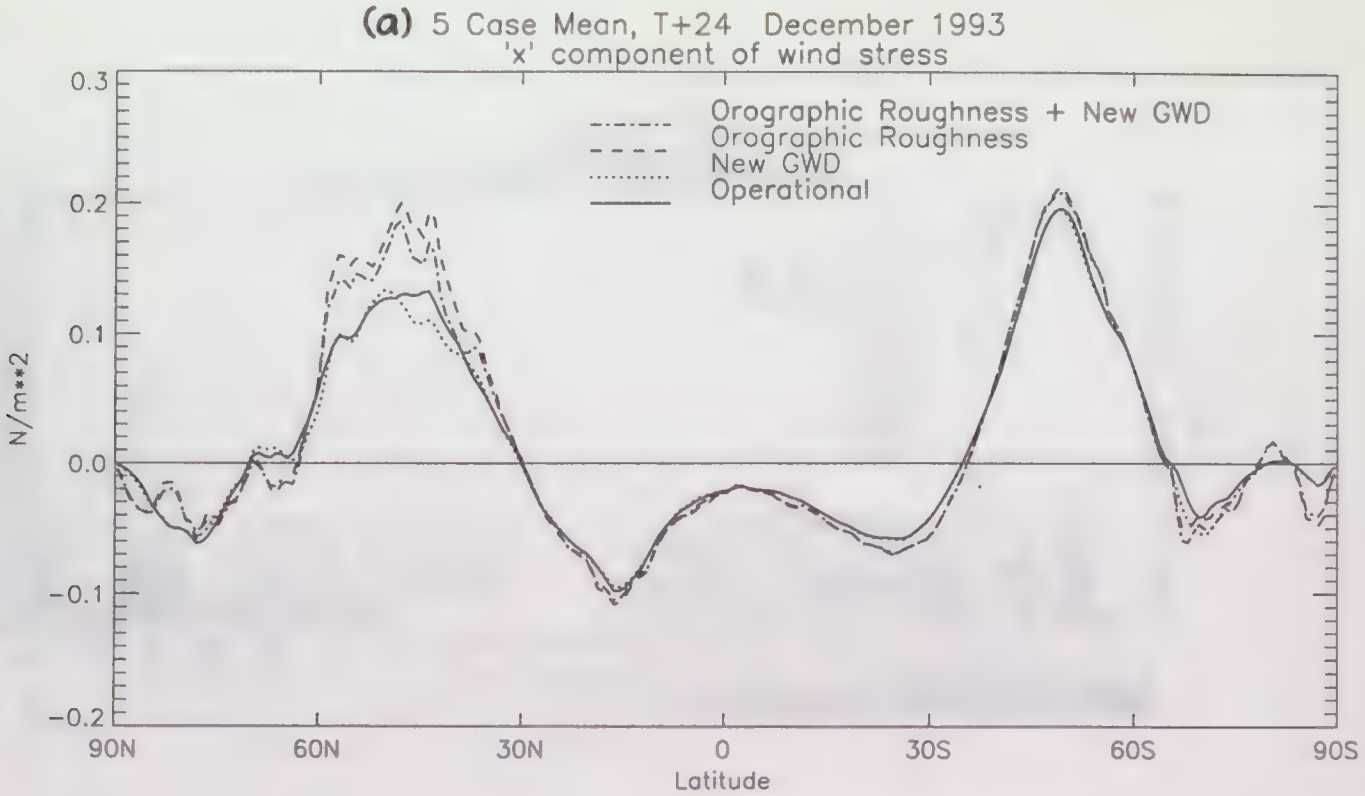
(a) 5 Case Mean, T+24 December 1993
'x' component of wind stress
Orographic Roughness + New GWD
Orographic Roughness
New GWD
Operational
N/m**2
0.3
0.2
0.1
0.0
−0.1
−0.2
90N
60N
30N
0
30S
60S
90S
Latitude

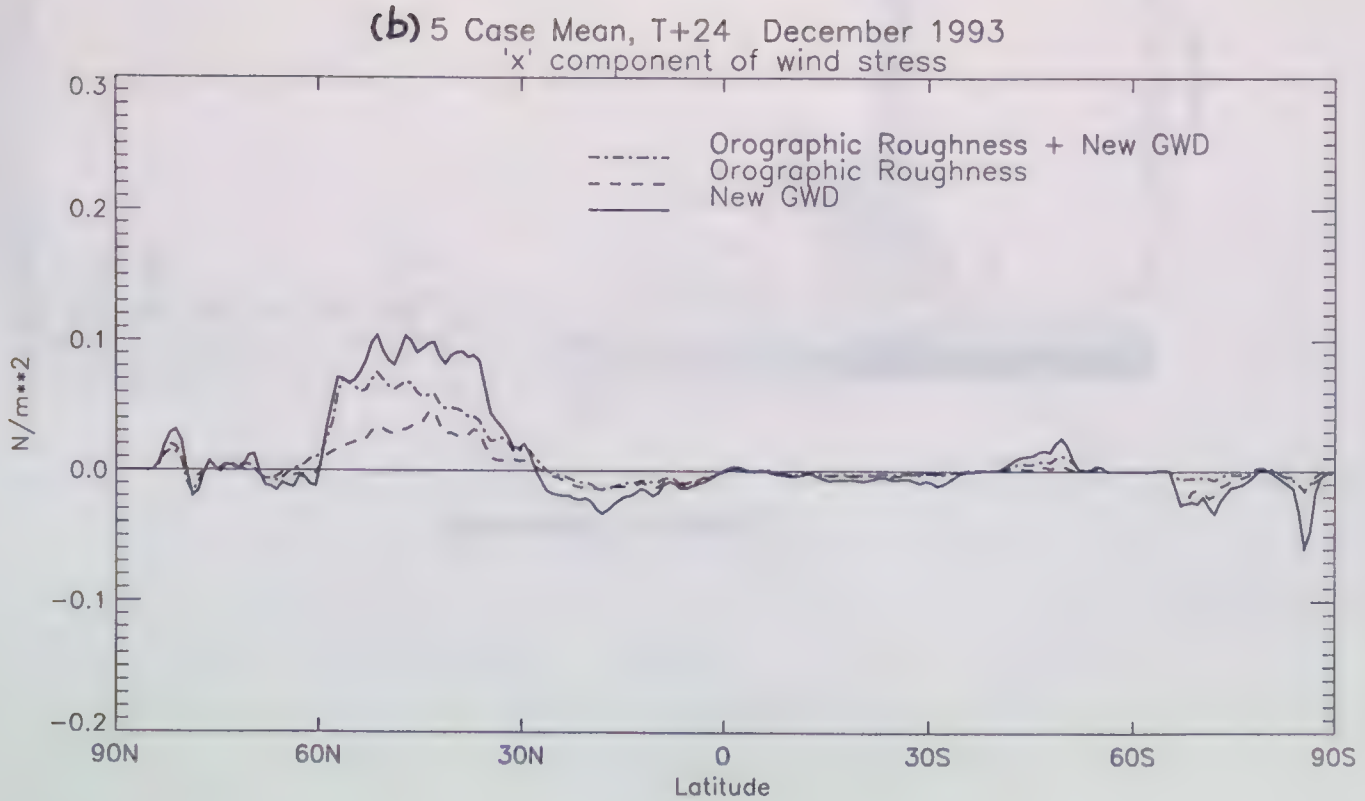
(b) 5 Case Mean, T+24 December 1993
'x' component of wind stress
Orographic Roughness + New GWD
Orographic Roughness
New GWD
N/m**2
0.3
0.2
0.1
0.0
−0.1
−0.2
90N
60N
30N
0
30S
60S
90S
Latitude

Figure 17

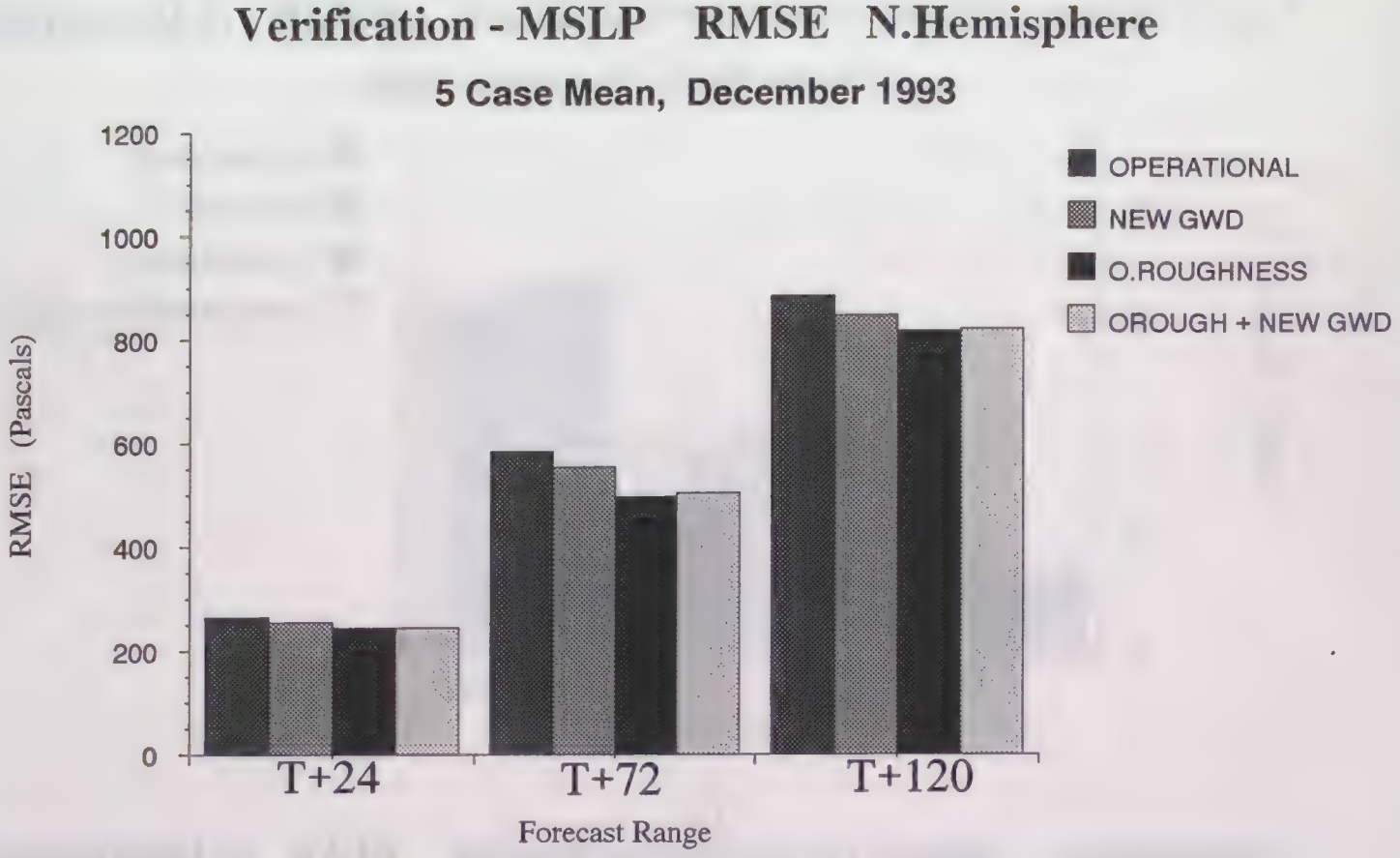
Verification - MSLP RMSE N.Hemisphere
5 Case Mean, December 1993
RMSE (Pascals)
1200
1000
800
600
400
200
0
T+24
T+72
T+120
Forecast Range
OPERATIONAL
NEW GWD
O.ROUGHNESS
OROUGH + NEW GWD

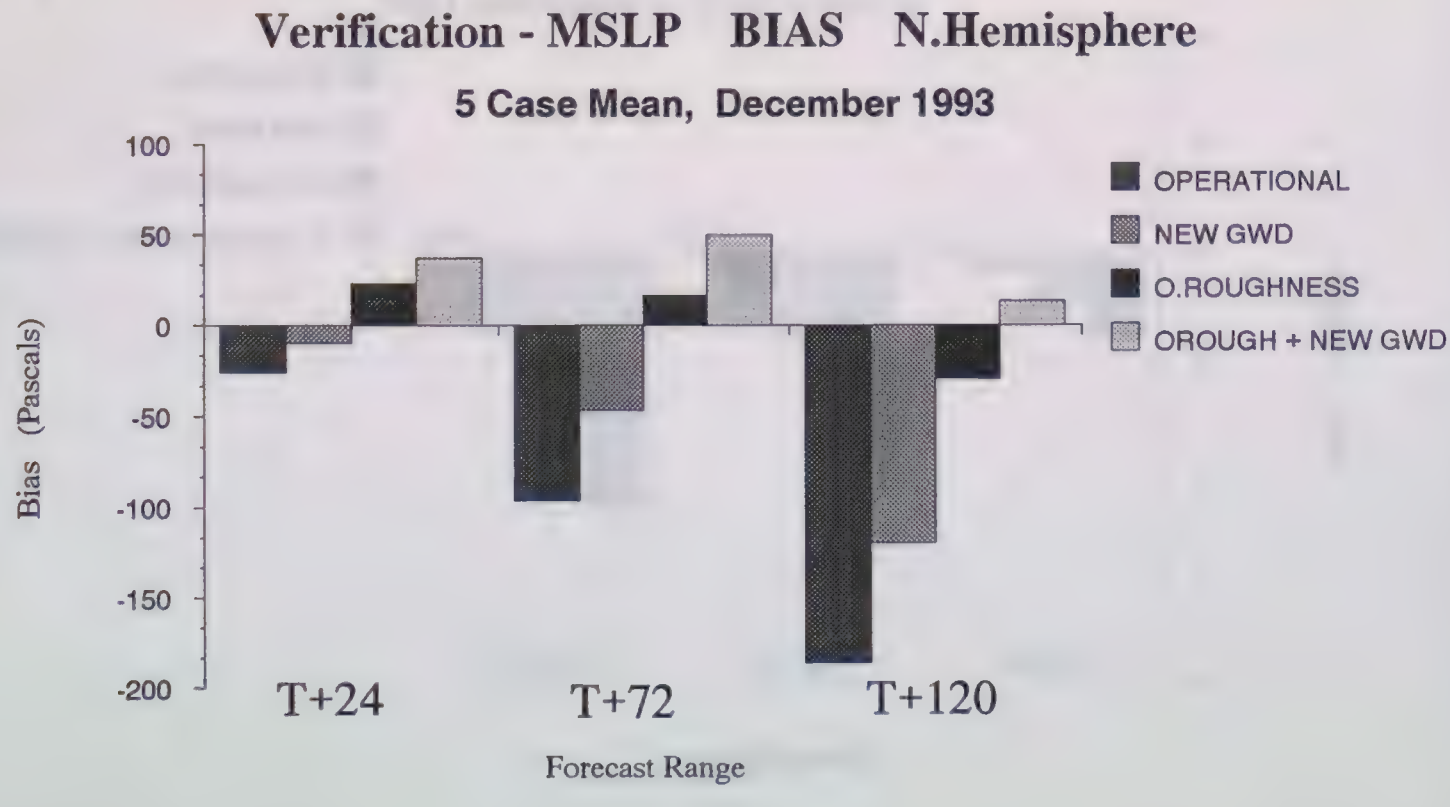
Verification - MSLP BIAS N.Hemisphere
5 Case Mean, December 1993
Bias (Pascals)
100
50
0
-50
-100
-150
-200
T+24
T+72
T+120
Forecast Range
OPERATIONAL
NEW GWD
O.ROUGHNESS
OROUGH + NEW GWD

Figure 18

(a)

Verification - 500mb Geopotential Height RMSE N.Hemisphere

5 Case Mean, December 1993

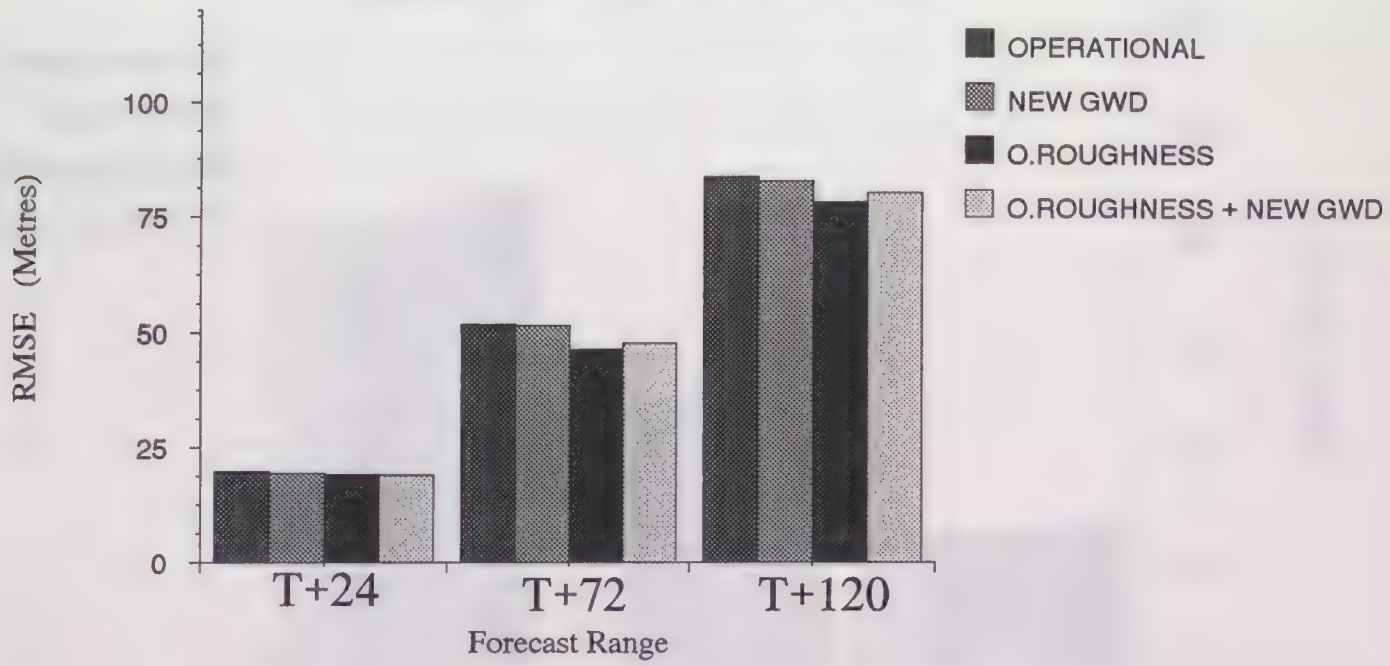

(b)

Verification - 500mb Geopotential Height BIAS N.Hemisphere

5 Case Mean, December 1993

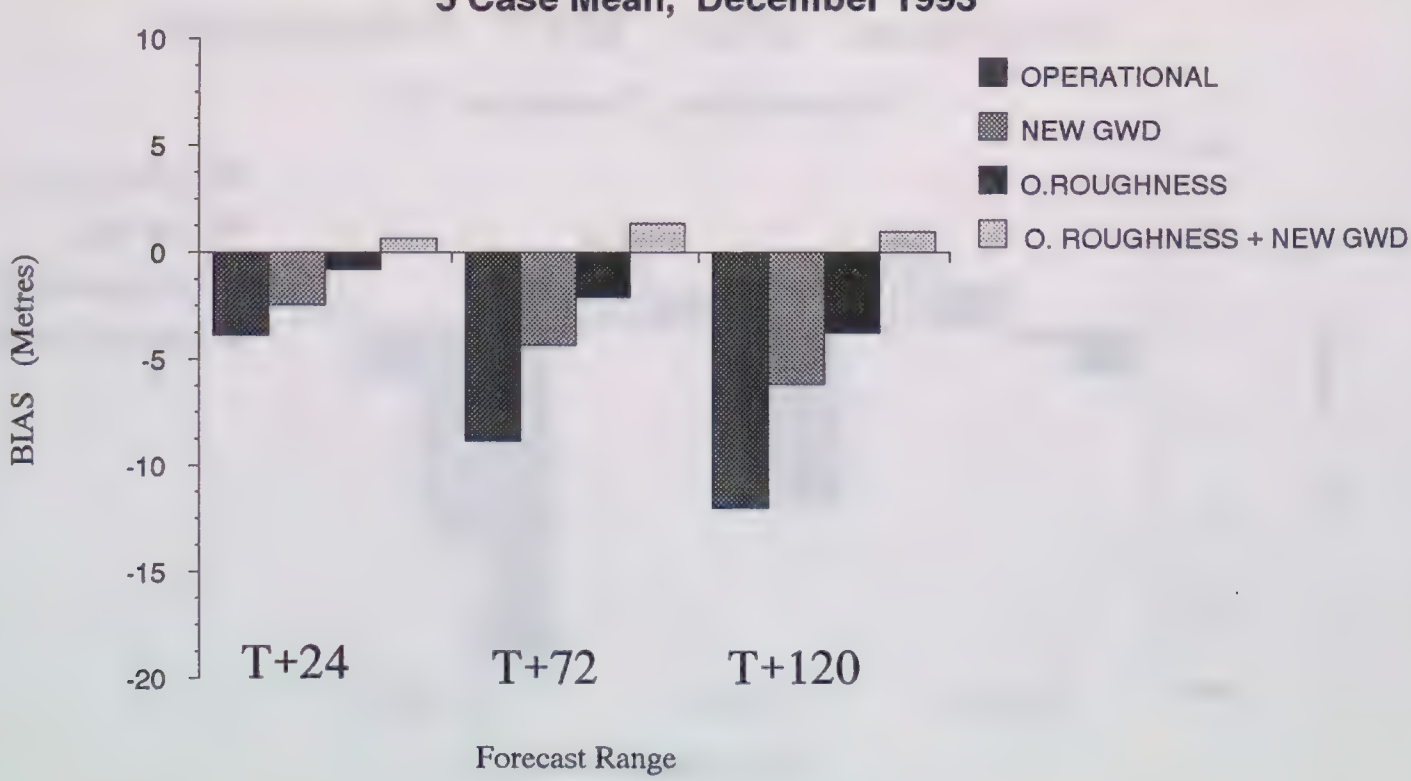

Figure 19

(a)

Verification - 250mb RMS VWE - N. Hemisphere

5 Case Mean, December 1993

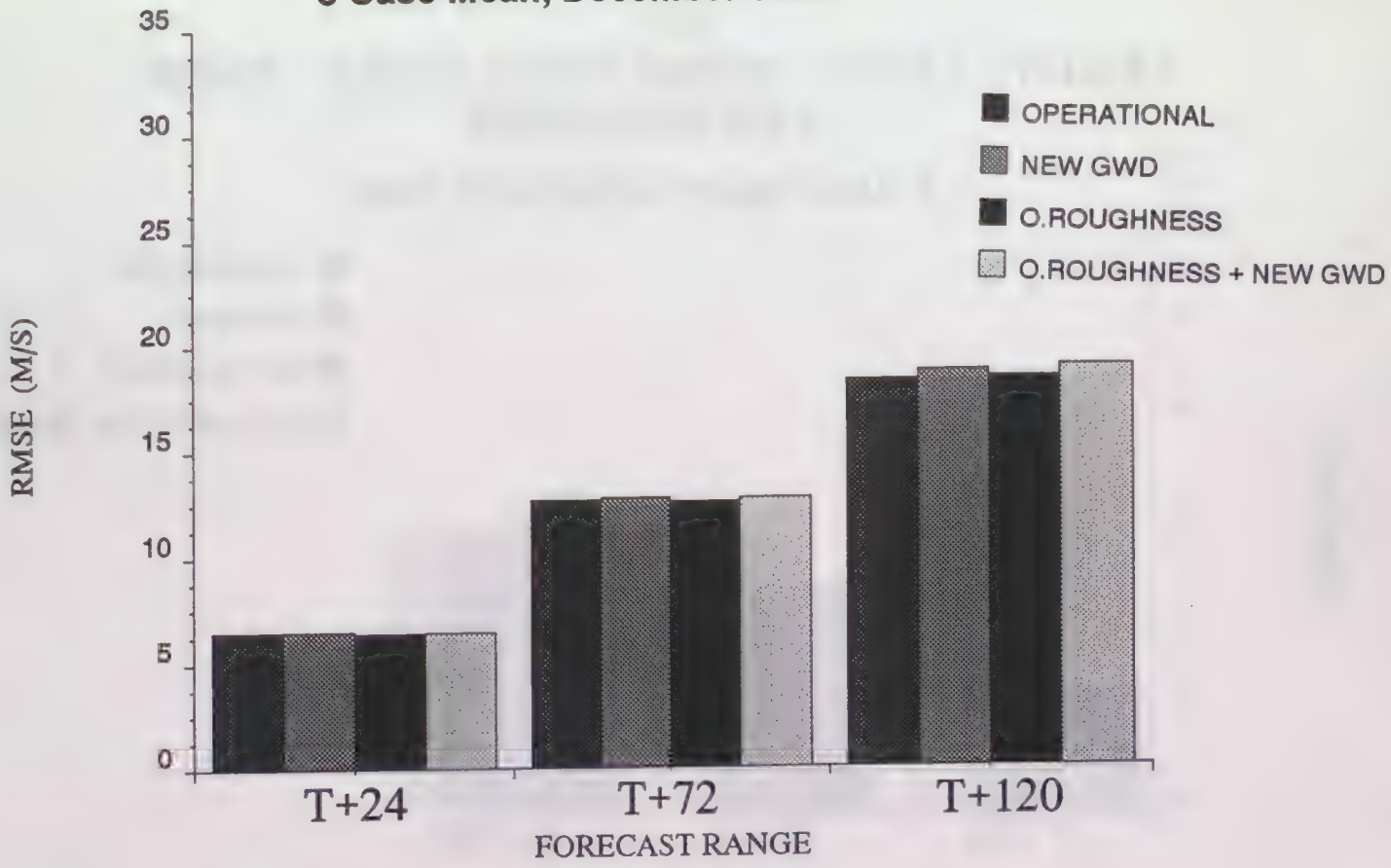

(b)

Verification - 850mb RMS VWE N.Hemisphere

5 Case Mean, December 1993

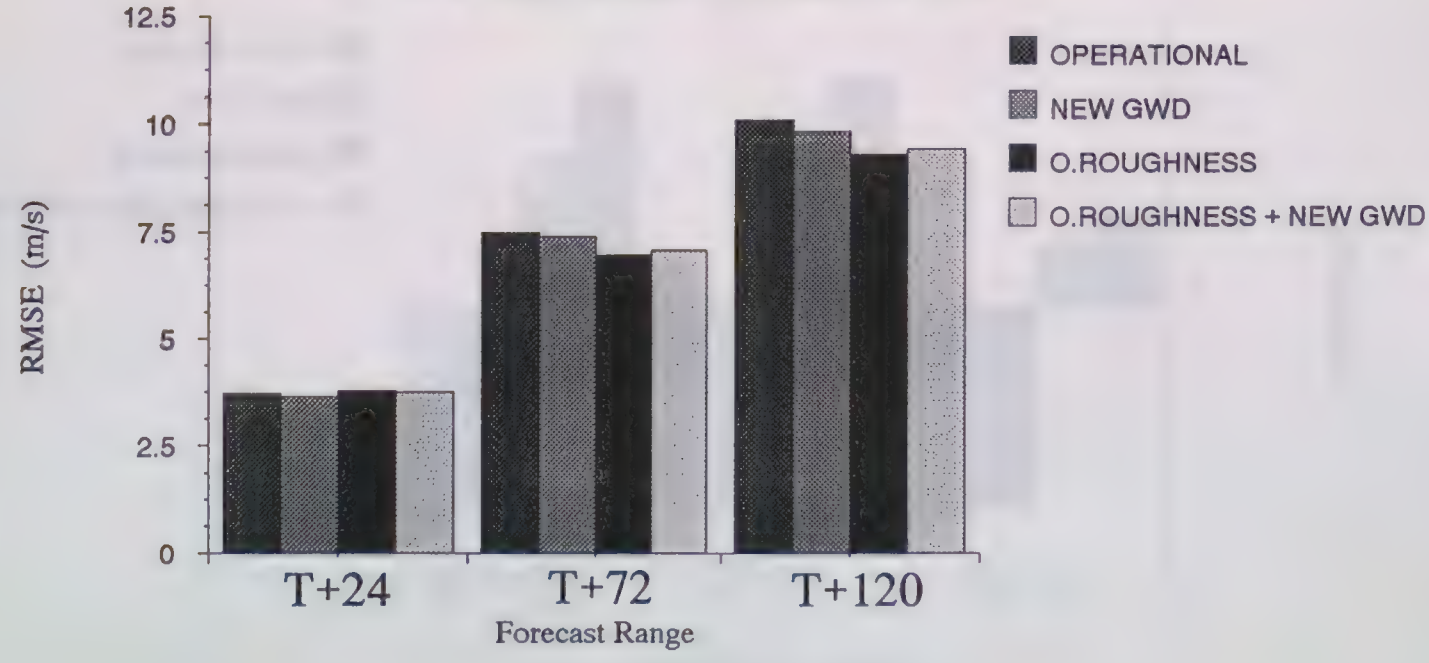

Figure 20

(a)

VERIFICATION - 850MB WIND SPEED - RMSE - N.HEMISPHERE

5 CASE MEAN, DECEMBER 1993

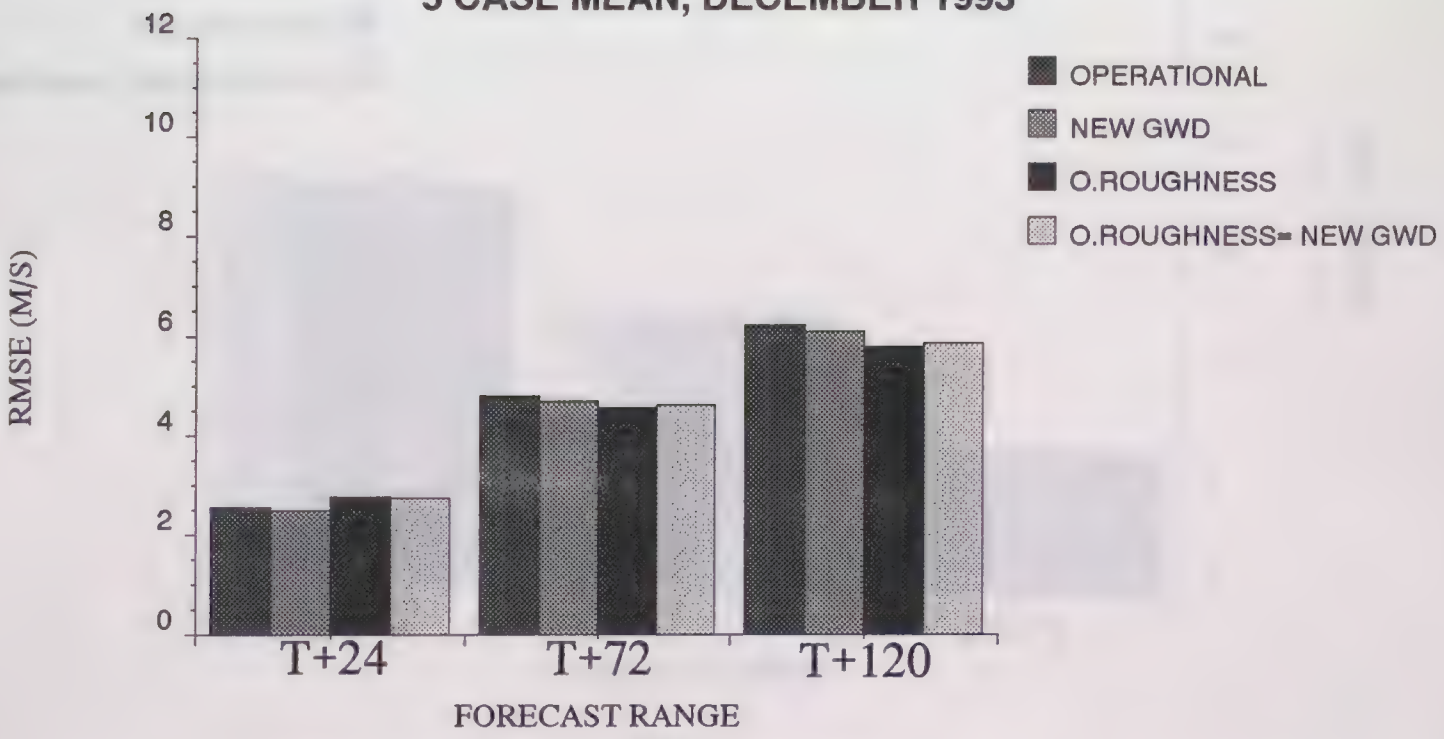

(b)

VERIFICATION - 850MB WIND SPEED - BIAS N.HEMISPHERE

5 CASE MEAN, DECEMBER 1993

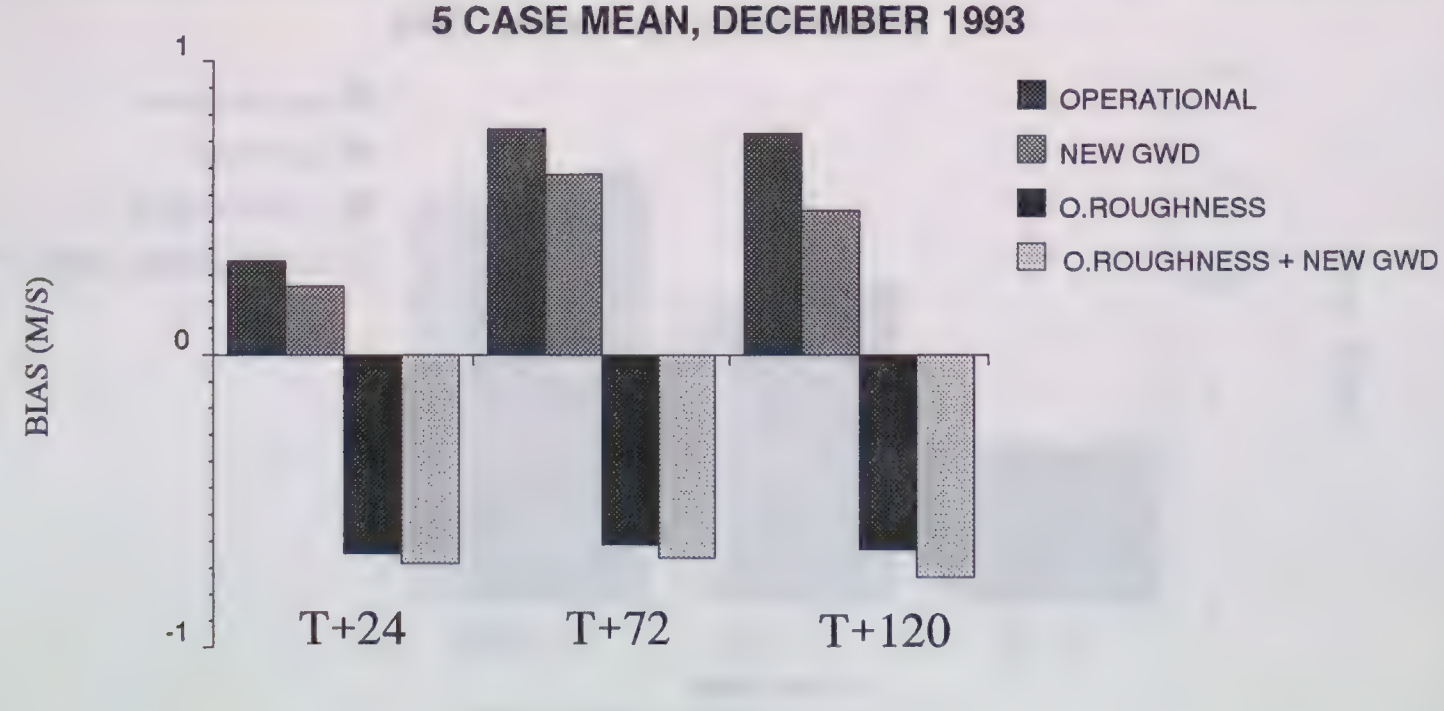

Figure 21

(a)

Verification - 250mb Wind speed - RMSE - N.hemisphere

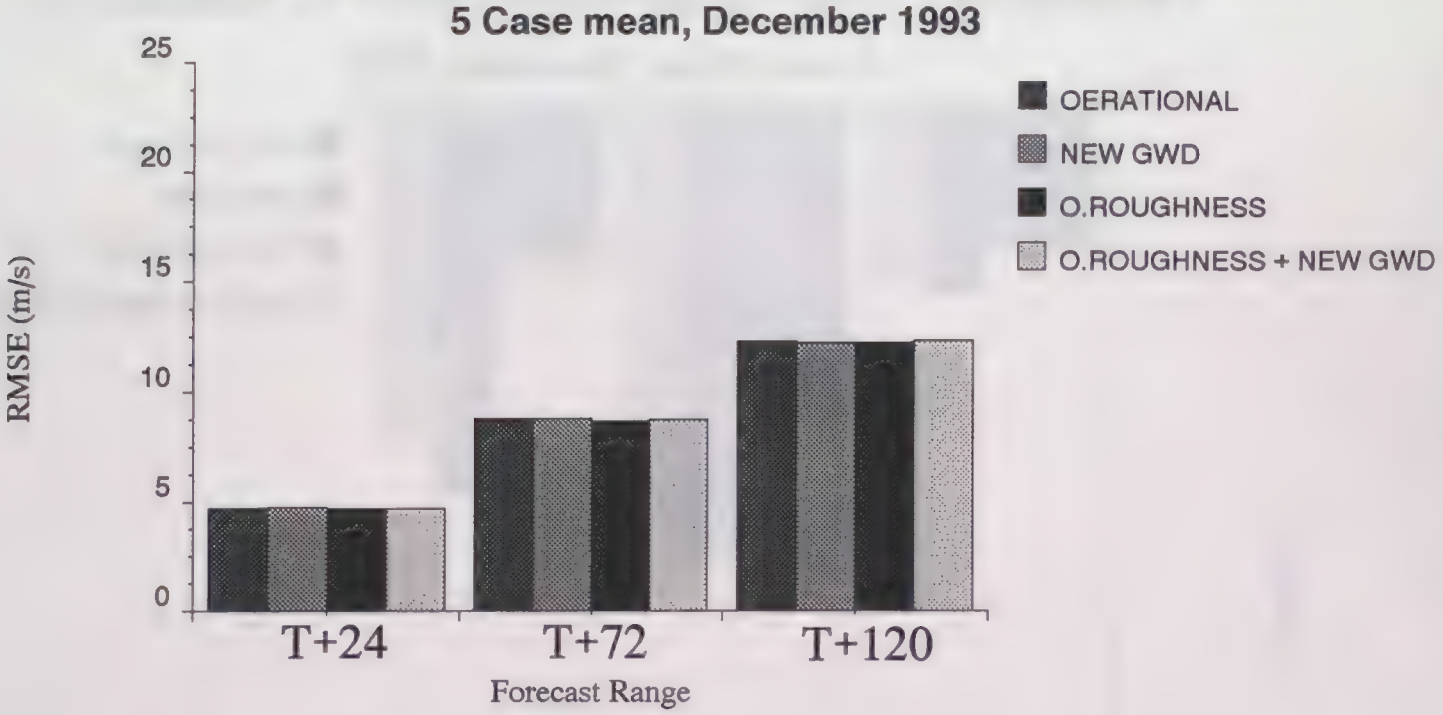

(b)

VERIFICATION - 250 MB WIND SPEED - BIAS - N.HEMISPHERE

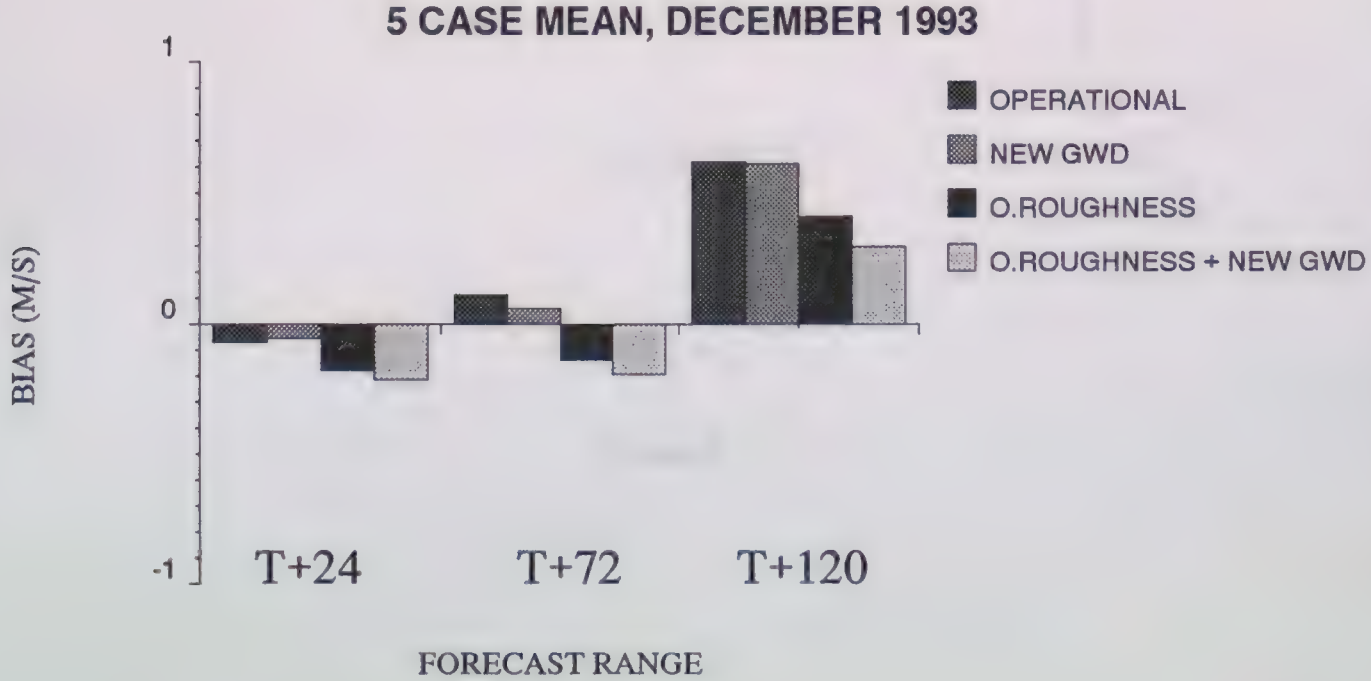

Figure 22

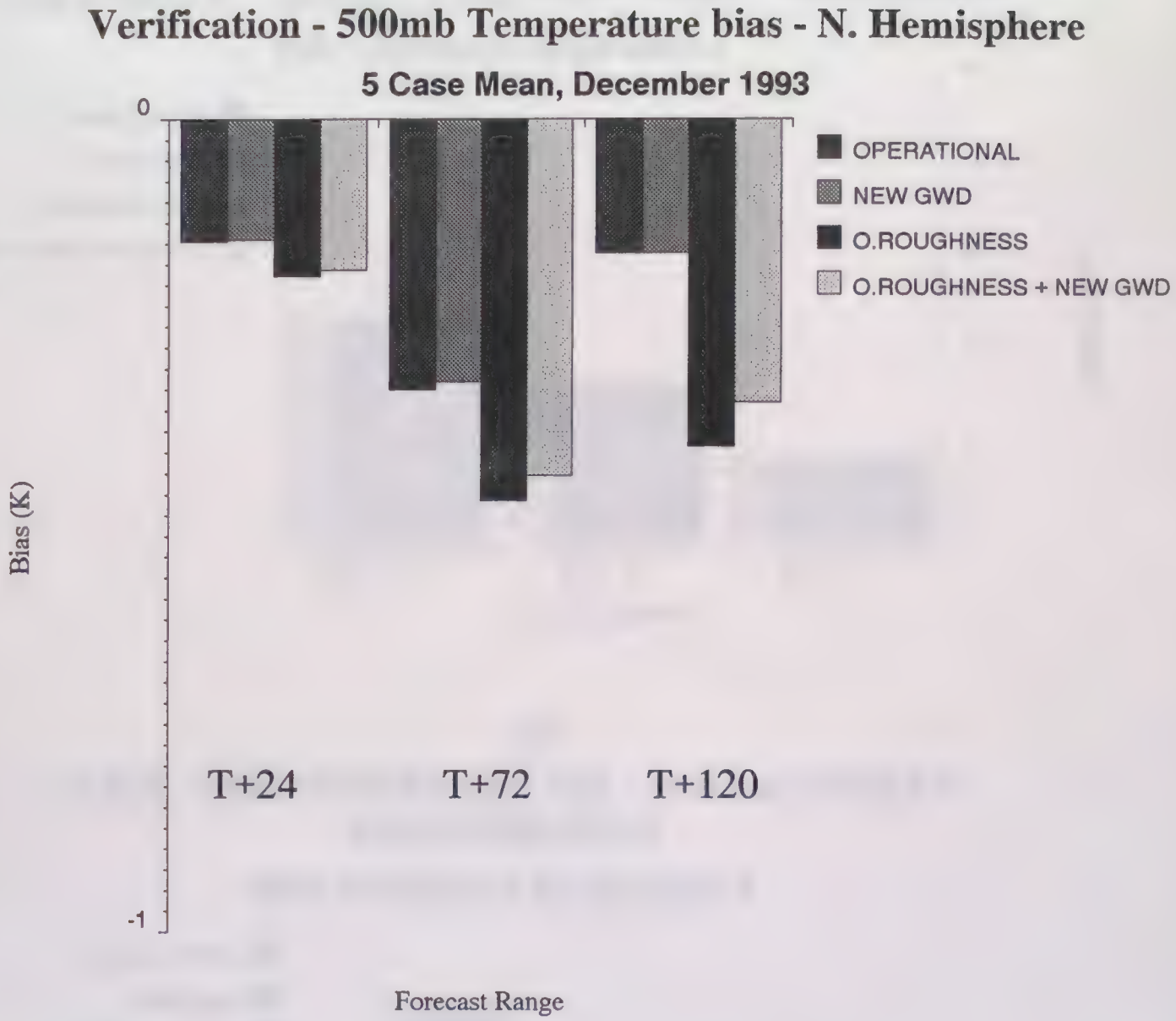
Verification - 500mb Temperature bias - N. Hemisphere
5 Case Mean, December 1993
0
-1
Bias (K)
OPERATIONAL
NEW GWD
O.ROUGHNESS
O.ROUGHNESS + NEW GWD
T+24
T+72
T+120
Forecast Range

Figure 23

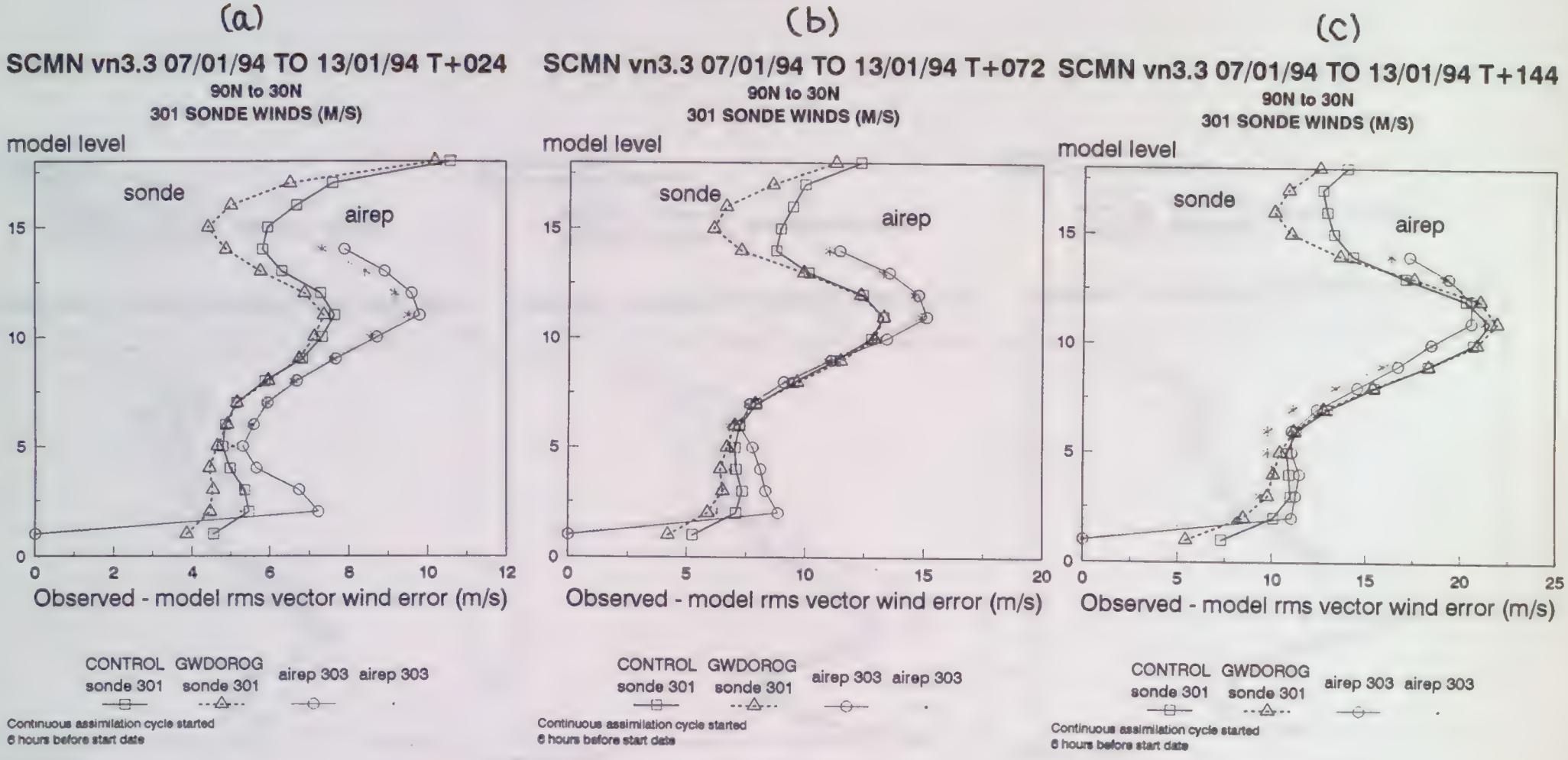
(a)
SCMN vn3.3 07/01/94 TO 13/01/94 T+024
90N to 30N
301 SONDE WINDS (M/S)
model level
sonde
airep
Observed - model rms vector wind error (m/s)
CONTROL sonde 301
GWDOROG sonde 301
airep 303
airep 303
Continuous assimilation cycle started
6 hours before start date
(b)
SCMN vn3.3 07/01/94 TO 13/01/94 T+072
90N to 30N
301 SONDE WINDS (M/S)
model level
sonde
airep
Observed - model rms vector wind error (m/s)
CONTROL sonde 301
GWDOROG sonde 301
airep 303
airep 303
Continuous assimilation cycle started
6 hours before start date
(c)
SCMN vn3.3 07/01/94 TO 13/01/94 T+144
90N to 30N
301 SONDE WINDS (M/S)
model level
sonde
airep
Observed - model rms vector wind error (m/s)
CONTROL sonde 301
GWDOROG sonde 301
airep 303
airep 303
Continuous assimilation cycle started
6 hours before start date

Figure 24

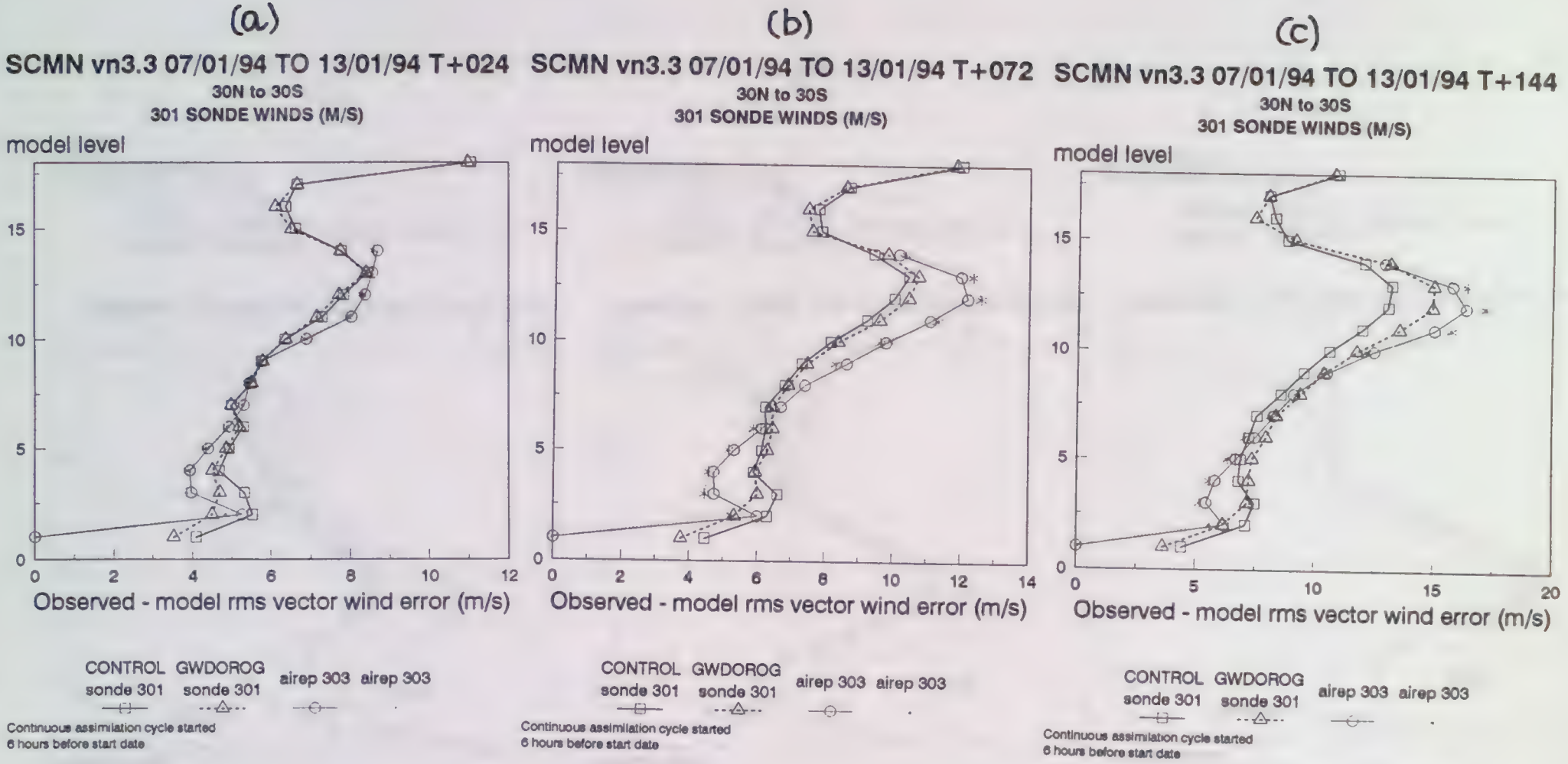
(a)
SCMN vn3.3 07/01/94 TO 13/01/94 T+024
30N to 30S
301 SONDE WINDS (M/S)
model level
Observed - model rms vector wind error (m/s)
CONTROL sonde 301
GWDOROG sonde 301
airep 303
airep 303
Continuous assimilation cycle started
6 hours before start date
(b)
SCMN vn3.3 07/01/94 TO 13/01/94 T+072
30N to 30S
301 SONDE WINDS (M/S)
model level
Observed - model rms vector wind error (m/s)
CONTROL sonde 301
GWDOROG sonde 301
airep 303
airep 303
Continuous assimilation cycle started
6 hours before start date
(c)
SCMN vn3.3 07/01/94 TO 13/01/94 T+144
30N to 30S
301 SONDE WINDS (M/S)
model level
Observed - model rms vector wind error (m/s)
CONTROL sonde 301
GWDOROG sonde 301
airep 303
airep 303
Continuous assimilation cycle started
6 hours before start date

Figure 25

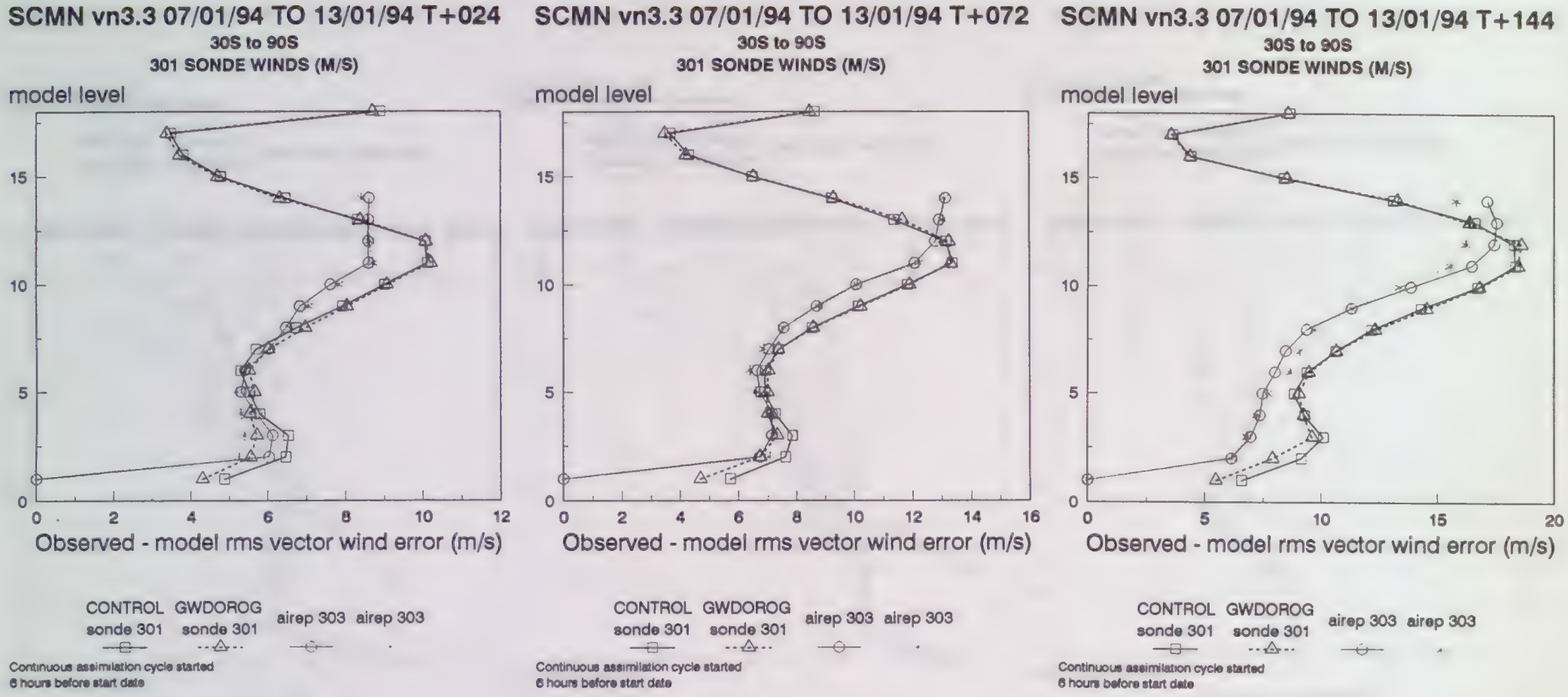
SCMN vn3.3 07/01/94 TO 13/01/94 T+024
30S to 90S
301 SONDE WINDS (M/S)
model level
Observed - model rms vector wind error (m/s)
SCMN vn3.3 07/01/94 TO 13/01/94 T+072
30S to 90S
301 SONDE WINDS (M/S)
model level
Observed - model rms vector wind error (m/s)
SCMN vn3.3 07/01/94 TO 13/01/94 T+144
30S to 90S
301 SONDE WINDS (M/S)
model level
Observed - model rms vector wind error (m/s)
CONTROL sonde 301
GWDOROG sonde 301
airep 303
airep 303
Continuous assimilation cycle started
6 hours before start date

Figure 26

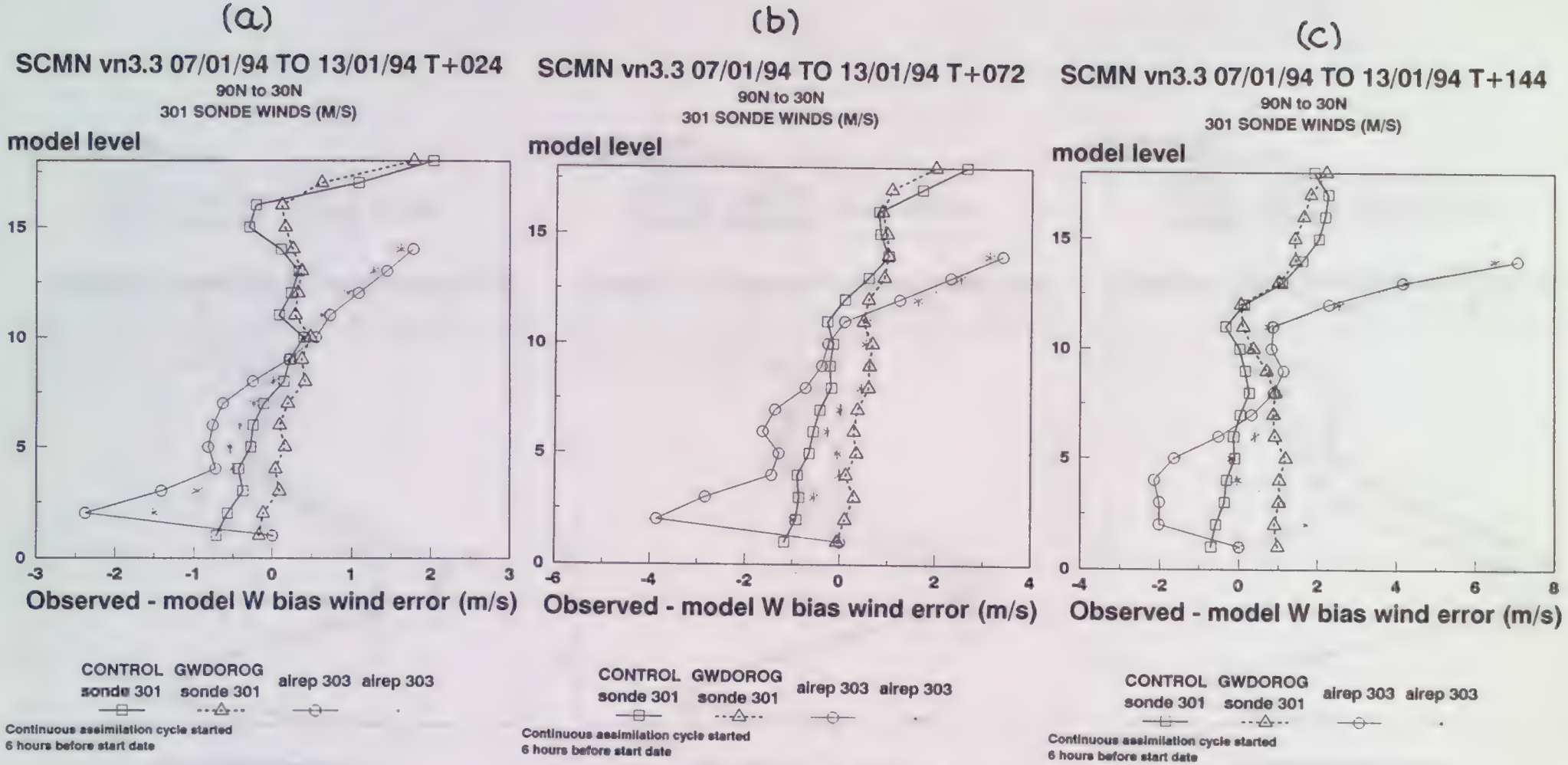
(a)
SCMN vn3.3 07/01/94 TO 13/01/94 T+024
90N to 30N
301 SONDE WINDS (M/S)
model level
Observed - model W bias wind error (m/s)
CONTROL sonde 301
GWDOROG sonde 301
airep 303
airep 303
Continuous assimilation cycle started 6 hours before start date
(b)
SCMN vn3.3 07/01/94 TO 13/01/94 T+072
90N to 30N
301 SONDE WINDS (M/S)
model level
Observed - model W bias wind error (m/s)
CONTROL sonde 301
GWDOROG sonde 301
airep 303
airep 303
Continuous assimilation cycle started 6 hours before start date
(c)
SCMN vn3.3 07/01/94 TO 13/01/94 T+144
90N to 30N
301 SONDE WINDS (M/S)
model level
Observed - model W bias wind error (m/s)
CONTROL sonde 301
GWDOROG sonde 301
airep 303
airep 303
Continuous assimilation cycle started 6 hours before start date

Figure 27

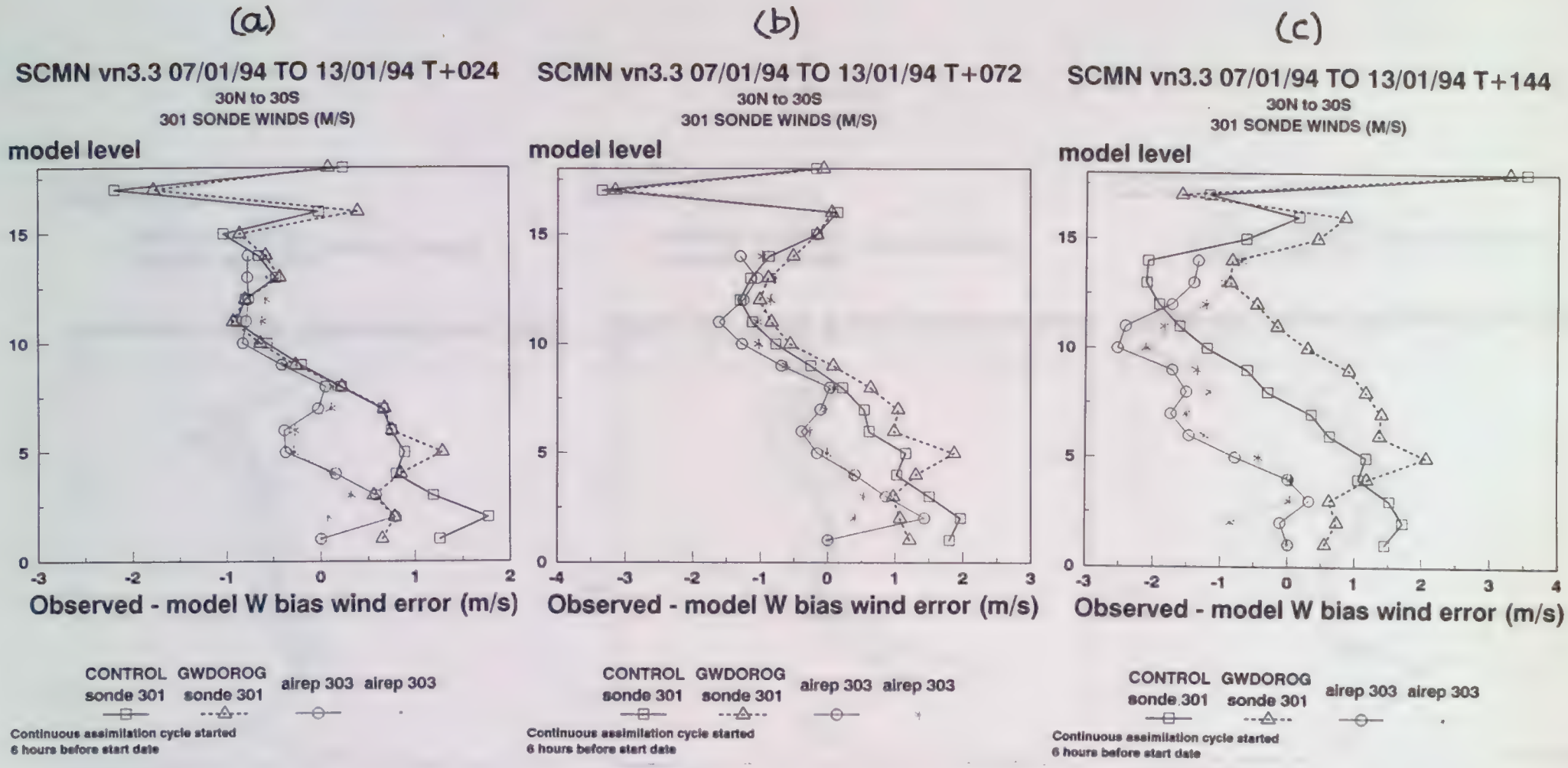
(a)
SCMN vn3.3 07/01/94 TO 13/01/94 T+024
30N to 30S
301 SONDE WINDS (M/S)
model level
Observed - model W bias wind error (m/s)
(b)
SCMN vn3.3 07/01/94 TO 13/01/94 T+072
30N to 30S
301 SONDE WINDS (M/S)
model level
Observed - model W bias wind error (m/s)
(c)
SCMN vn3.3 07/01/94 TO 13/01/94 T+144
30N to 30S
301 SONDE WINDS (M/S)
model level
Observed - model W bias wind error (m/s)
CONTROL sonde 301
GWDOROG sonde 301
airep 303
airep 303
Continuous assimilation cycle started
6 hours before start date

Figure 28

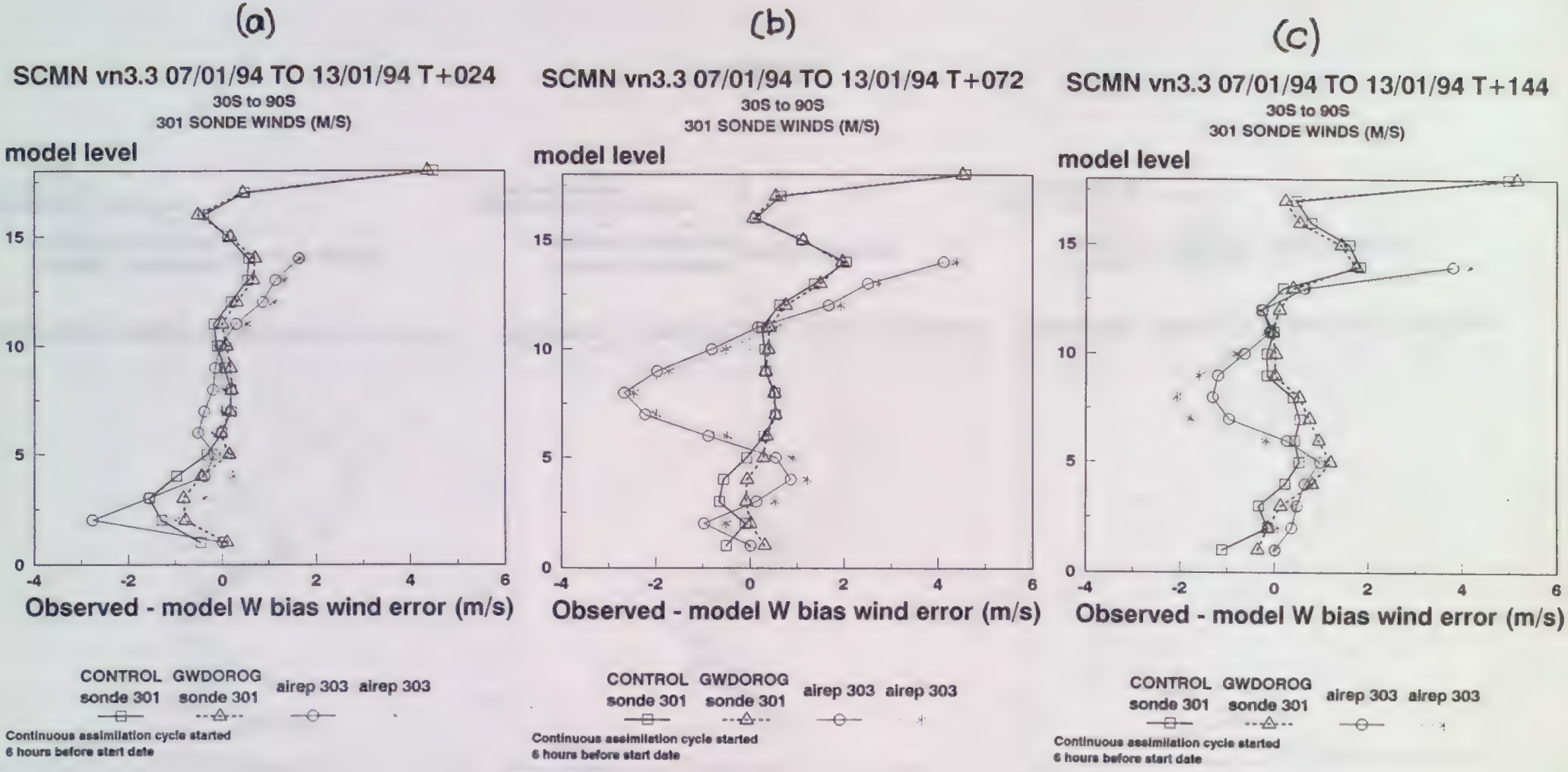
(a)
SCMN vn3.3 07/01/94 TO 13/01/94 T+024
30S to 90S
301 SONDE WINDS (M/S)
model level
0
5
10
15
-4
-2
0
2
4
6
Observed - model W bias wind error (m/s)
CONTROL sonde 301
GWDOROG sonde 301
airep 303
airep 303
Continuous assimilation cycle started
6 hours before start date
(b)
SCMN vn3.3 07/01/94 TO 13/01/94 T+072
30S to 90S
301 SONDE WINDS (M/S)
model level
0
5
10
15
-4
-2
0
2
4
6
Observed - model W bias wind error (m/s)
CONTROL sonde 301
GWDOROG sonde 301
airep 303
airep 303
Continuous assimilation cycle started
6 hours before start date
(c)
SCMN vn3.3 07/01/94 TO 13/01/94 T+144
30S to 90S
301 SONDE WINDS (M/S)
model level
0
5
10
15
-4
-2
0
2
4
6
Observed - model W bias wind error (m/s)
CONTROL sonde 301
GWDOROG sonde 301
airep 303
airep 303
Continuous assimilation cycle started
6 hours before start date

Figure 29

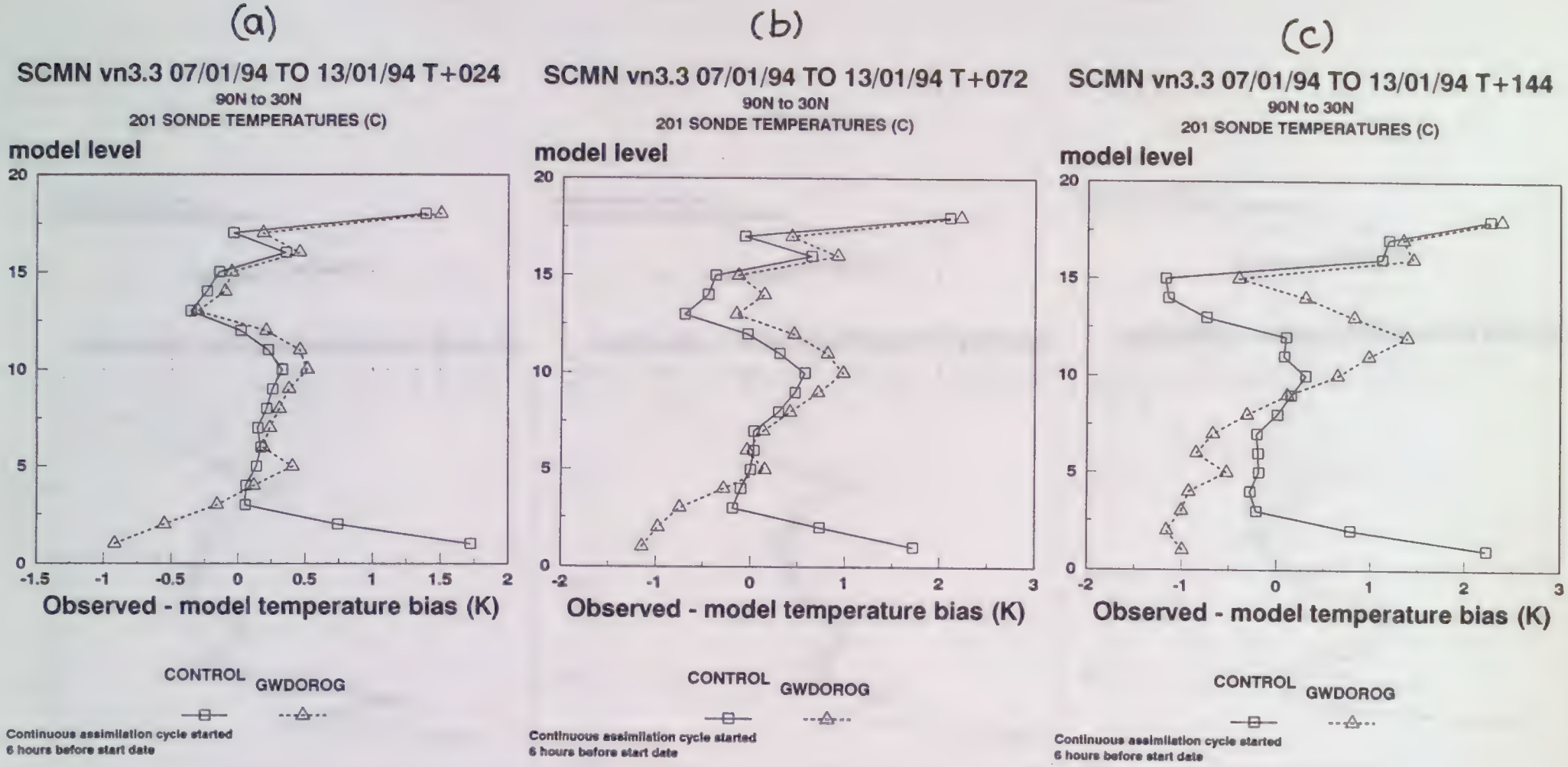
(a)
SCMN vn3.3 07/01/94 TO 13/01/94 T+024
90N to 30N
201 SONDE TEMPERATURES (C)
model level
20
15
10
5
0
-1.5
-1
-0.5
0
0.5
1
1.5
2
Observed - model temperature bias (K)
CONTROL
GWDOROG
Continuous assimilation cycle started
6 hours before start date
(b)
SCMN vn3.3 07/01/94 TO 13/01/94 T+072
90N to 30N
201 SONDE TEMPERATURES (C)
model level
20
15
10
5
0
-2
-1
0
1
2
3
Observed - model temperature bias (K)
CONTROL
GWDOROG
Continuous assimilation cycle started
6 hours before start date
(c)
SCMN vn3.3 07/01/94 TO 13/01/94 T+144
90N to 30N
201 SONDE TEMPERATURES (C)
model level
20
15
10
5
0
-2
-1
0
1
2
3
Observed - model temperature bias (K)
CONTROL
GWDOROG
Continuous assimilation cycle started
6 hours before start date

Figure 30

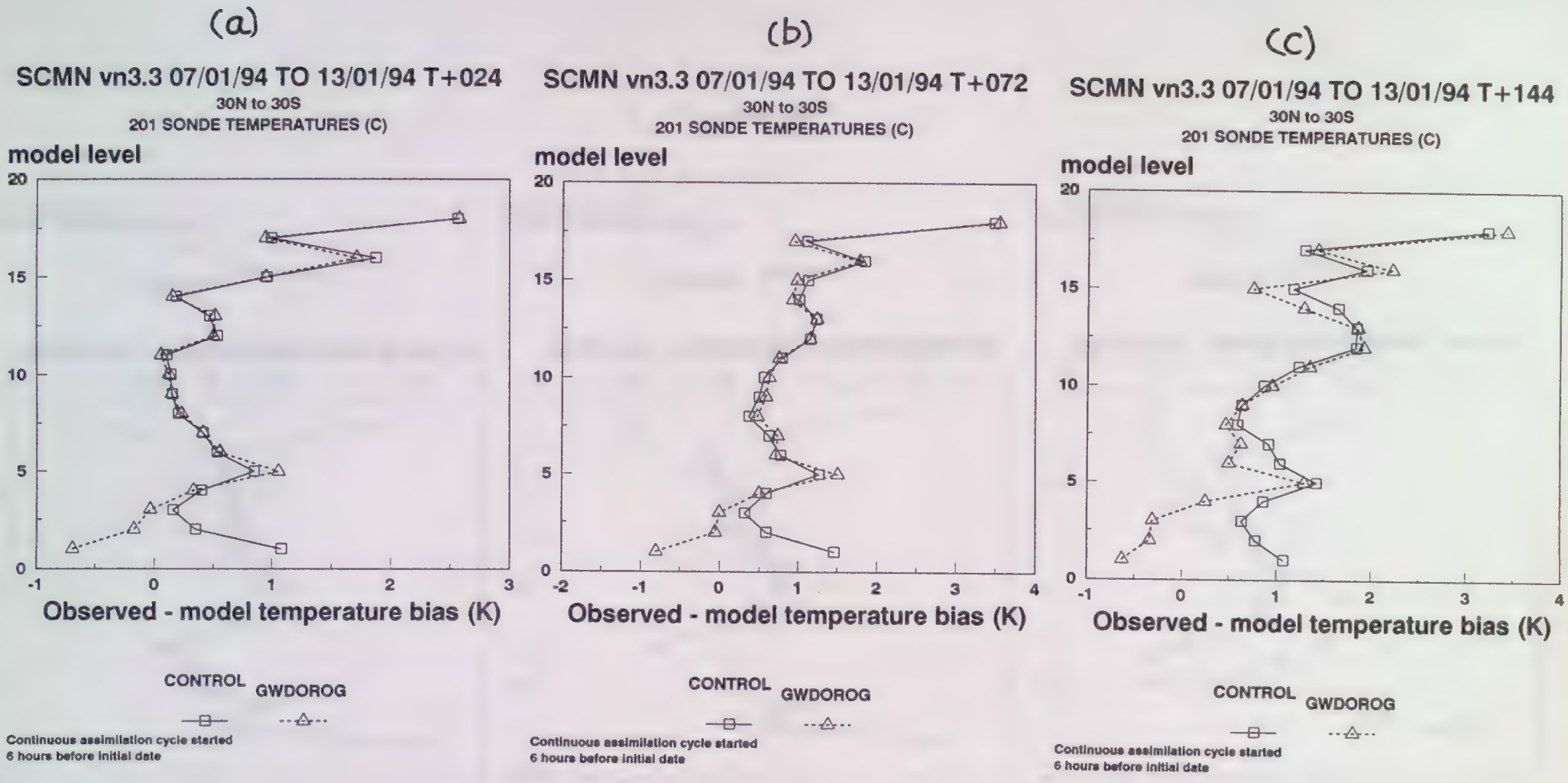
(a)
SCMN vn3.3 07/01/94 TO 13/01/94 T+024
30N to 30S
201 SONDE TEMPERATURES (C)
model level
Observed - model temperature bias (K)
CONTROL
GWDOROG
Continuous assimilation cycle started
6 hours before initial date
(b)
SCMN vn3.3 07/01/94 TO 13/01/94 T+072
30N to 30S
201 SONDE TEMPERATURES (C)
model level
Observed - model temperature bias (K)
CONTROL
GWDOROG
Continuous assimilation cycle started
6 hours before initial date
(c)
SCMN vn3.3 07/01/94 TO 13/01/94 T+144
30N to 30S
201 SONDE TEMPERATURES (C)
model level
Observed - model temperature bias (K)
CONTROL
GWDOROG
Continuous assimilation cycle started
6 hours before initial date

Figure 31

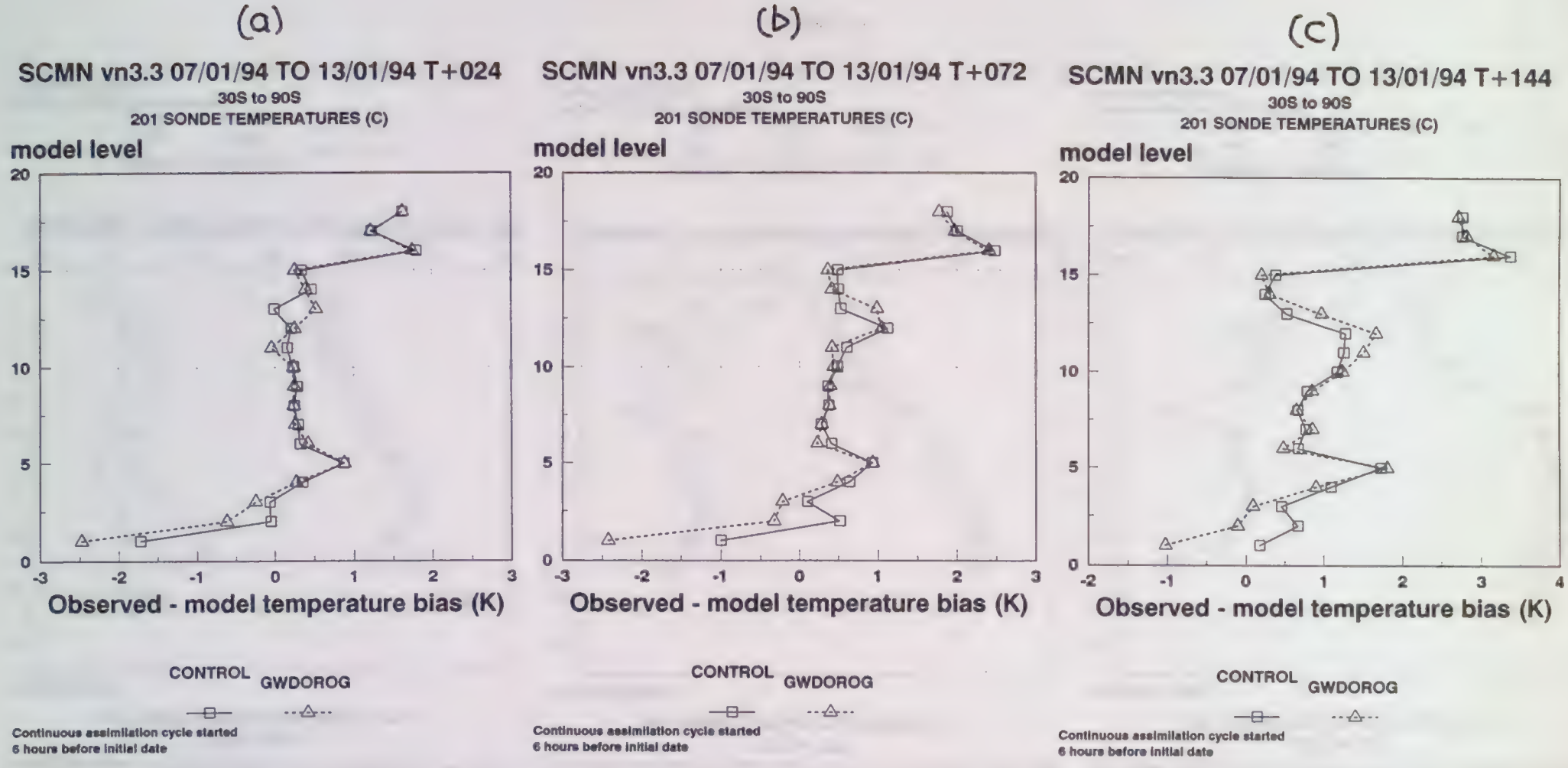
(a)
SCMN vn3.3 07/01/94 TO 13/01/94 T+024
30S to 90S
201 SONDE TEMPERATURES (C)
model level
Observed - model temperature bias (K)
CONTROL
GWDOROG
Continuous assimilation cycle started
6 hours before initial date
(b)
SCMN vn3.3 07/01/94 TO 13/01/94 T+072
30S to 90S
201 SONDE TEMPERATURES (C)
model level
Observed - model temperature bias (K)
CONTROL
GWDOROG
Continuous assimilation cycle started
6 hours before initial date
(c)
SCMN vn3.3 07/01/94 TO 13/01/94 T+144
30S to 90S
201 SONDE TEMPERATURES (C)
model level
Observed - model temperature bias (K)
CONTROL
GWDOROG
Continuous assimilation cycle started
6 hours before initial date

Figure 32

(a)

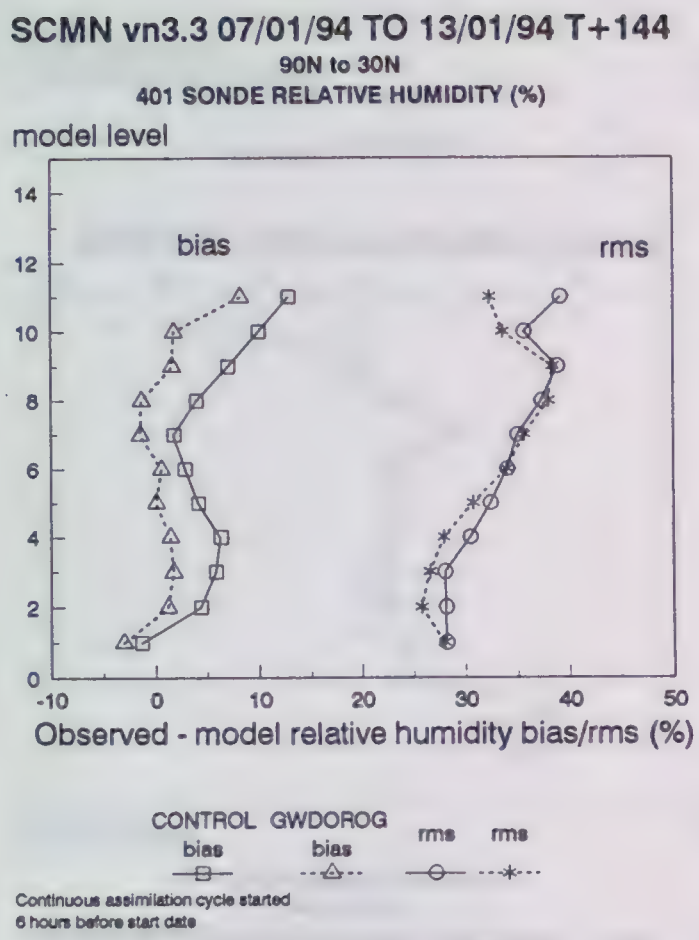

(b)

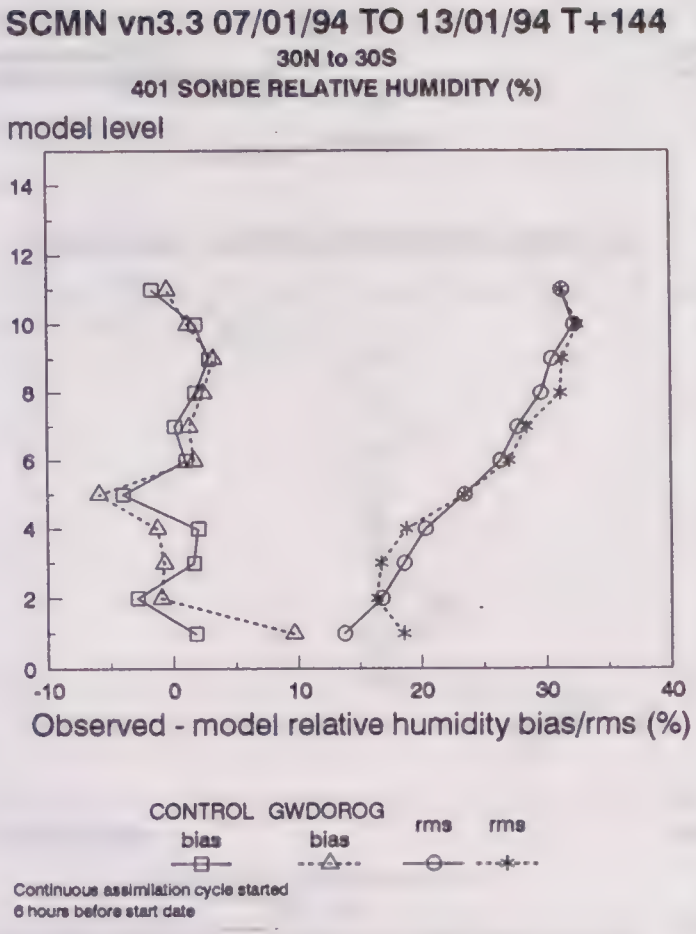

(c)

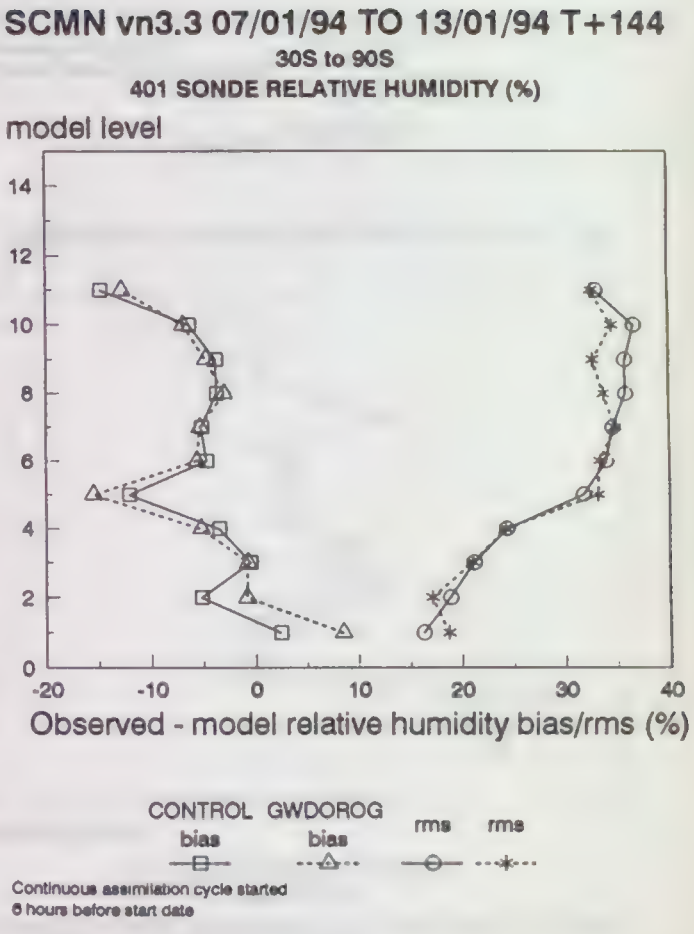

Figure 33

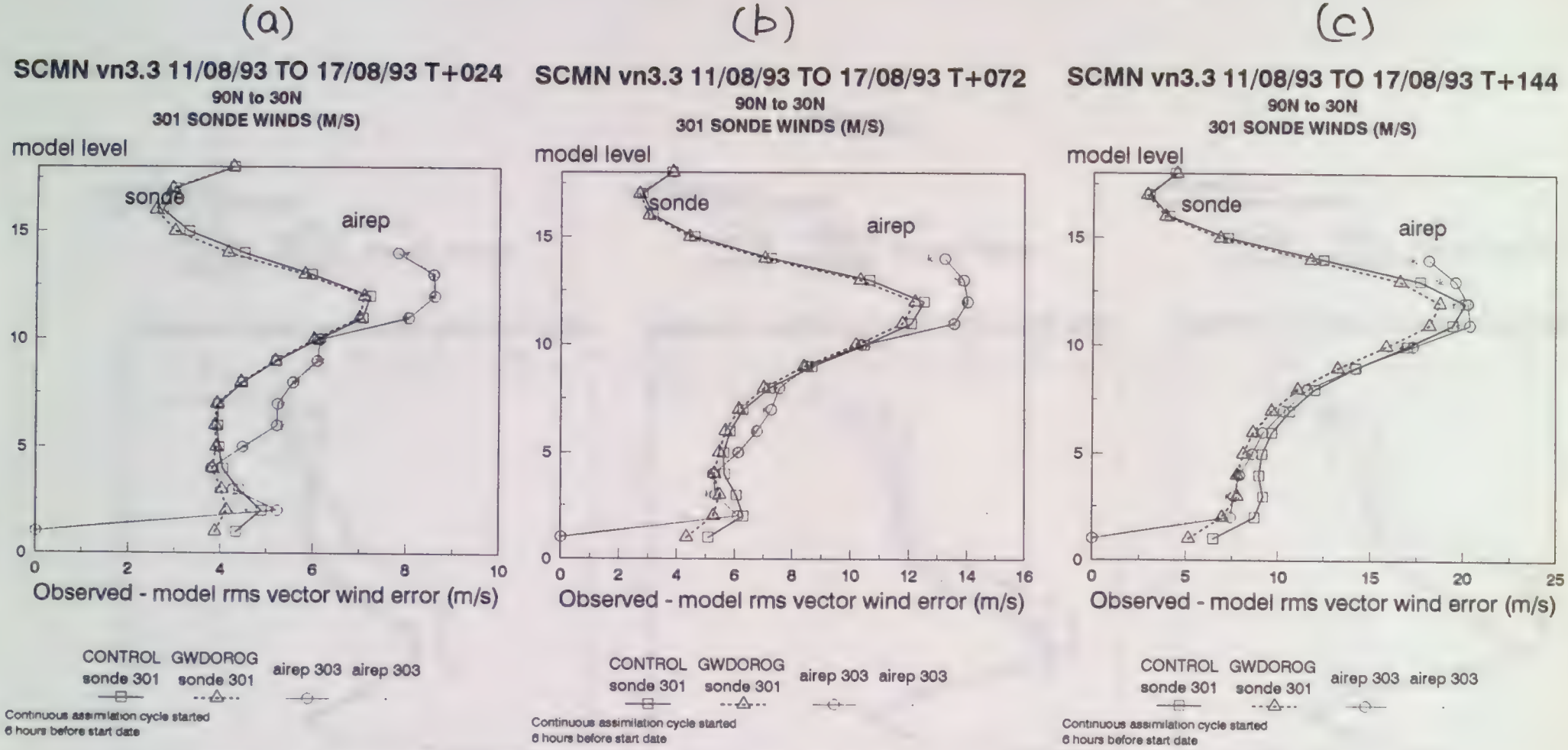
(a)
SCMN vn3.3 11/08/93 TO 17/08/93 T+024
90N to 30N
301 SONDE WINDS (M/S)
model level
sonde
airep
Observed - model rms vector wind error (m/s)
CONTROL sonde 301
GWDOROG sonde 301
airep 303
airep 303
Continuous assimilation cycle started 6 hours before start date
(b)
SCMN vn3.3 11/08/93 TO 17/08/93 T+072
90N to 30N
301 SONDE WINDS (M/S)
model level
sonde
airep
Observed - model rms vector wind error (m/s)
CONTROL sonde 301
GWDOROG sonde 301
airep 303
airep 303
Continuous assimilation cycle started 6 hours before start date
(c)
SCMN vn3.3 11/08/93 TO 17/08/93 T+144
90N to 30N
301 SONDE WINDS (M/S)
model level
sonde
airep
Observed - model rms vector wind error (m/s)
CONTROL sonde 301
GWDOROG sonde 301
airep 303
airep 303
Continuous assimilation cycle started 6 hours before start date

Figure 34

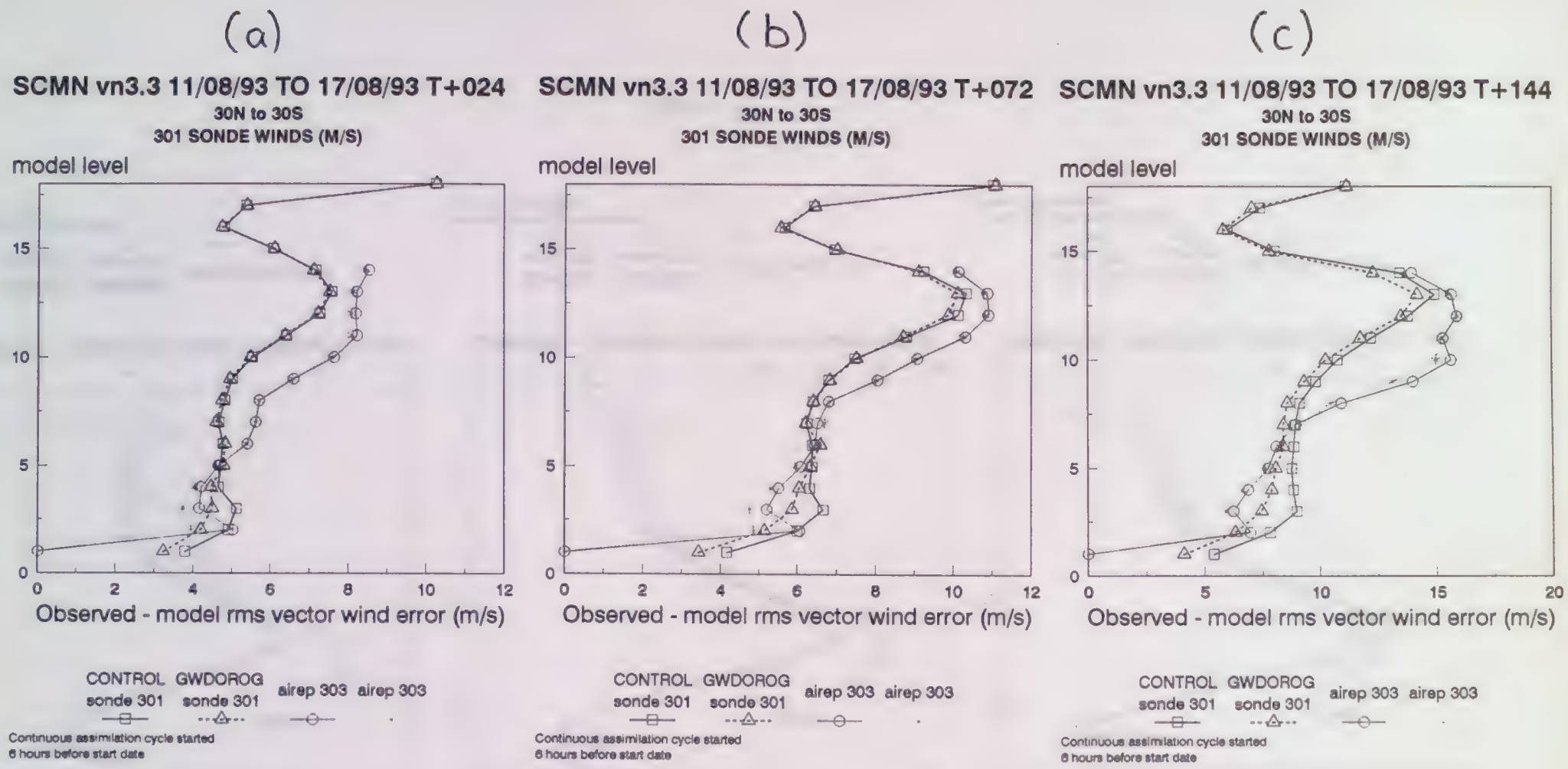
(a)
SCMN vn3.3 11/08/93 TO 17/08/93 T+024
30N to 30S
301 SONDE WINDS (M/S)
model level
Observed - model rms vector wind error (m/s)
CONTROL sonde 301
GWDOROG sonde 301
airep 303
airep 303
Continuous assimilation cycle started 6 hours before start date
(b)
SCMN vn3.3 11/08/93 TO 17/08/93 T+072
30N to 30S
301 SONDE WINDS (M/S)
model level
Observed - model rms vector wind error (m/s)
CONTROL sonde 301
GWDOROG sonde 301
airep 303
airep 303
Continuous assimilation cycle started 6 hours before start date
(c)
SCMN vn3.3 11/08/93 TO 17/08/93 T+144
30N to 30S
301 SONDE WINDS (M/S)
model level
Observed - model rms vector wind error (m/s)
CONTROL sonde 301
GWDOROG sonde 301
airep 303
airep 303
Continuous assimilation cycle started 6 hours before start date

Figure 35

(a)

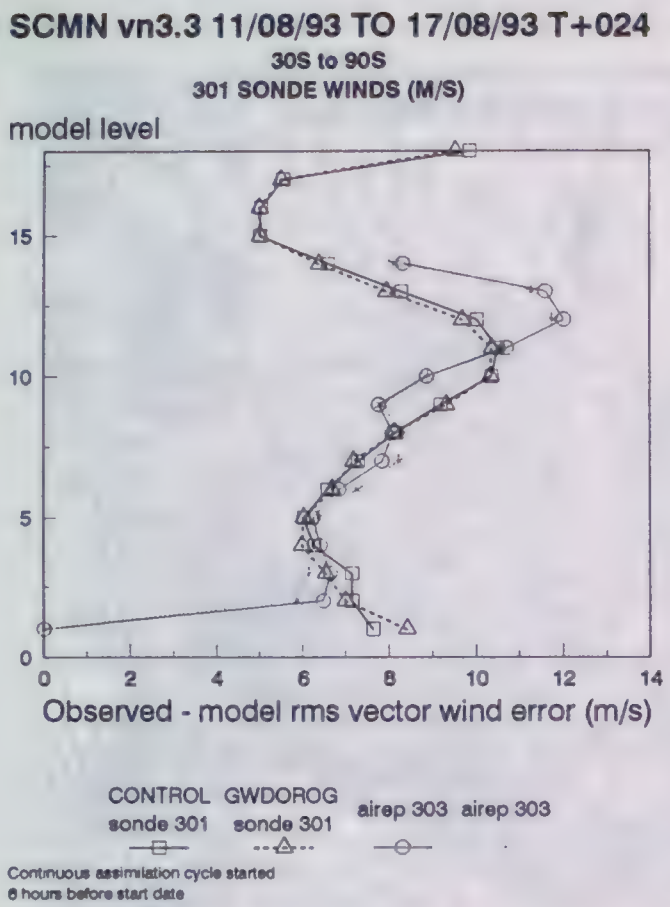

(b)

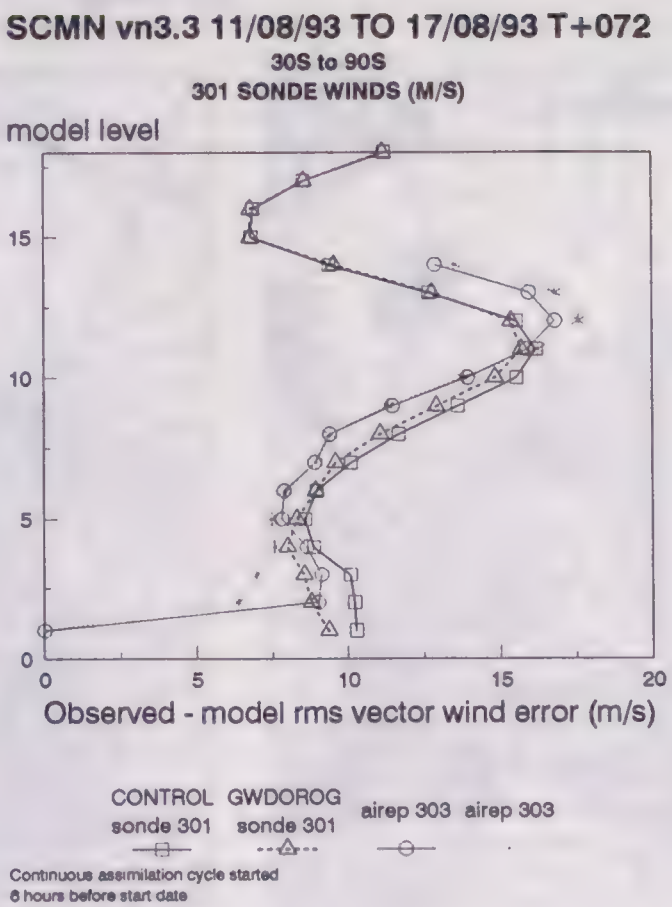

(c)

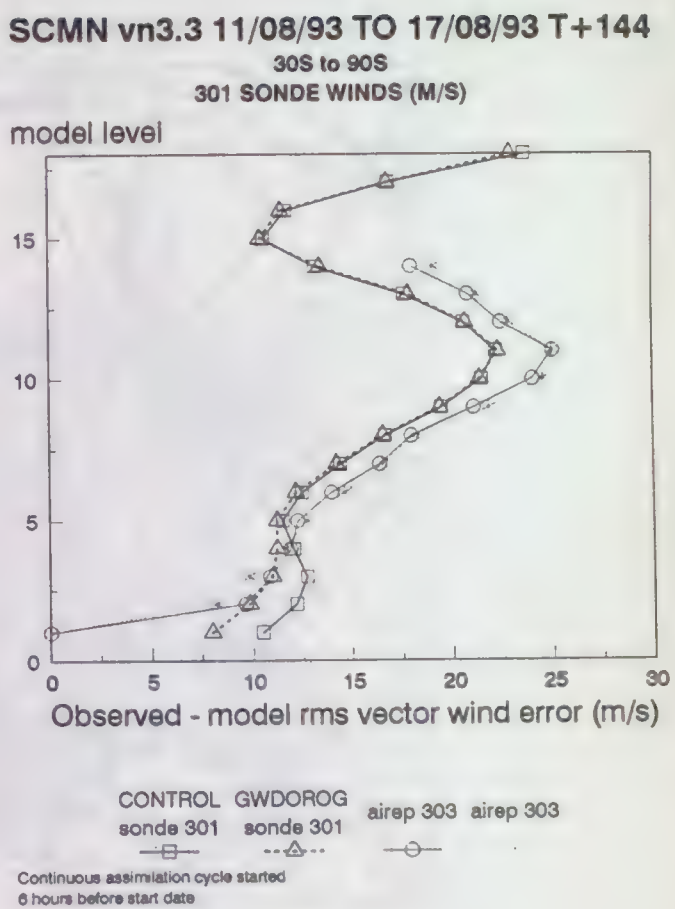

Figure 36

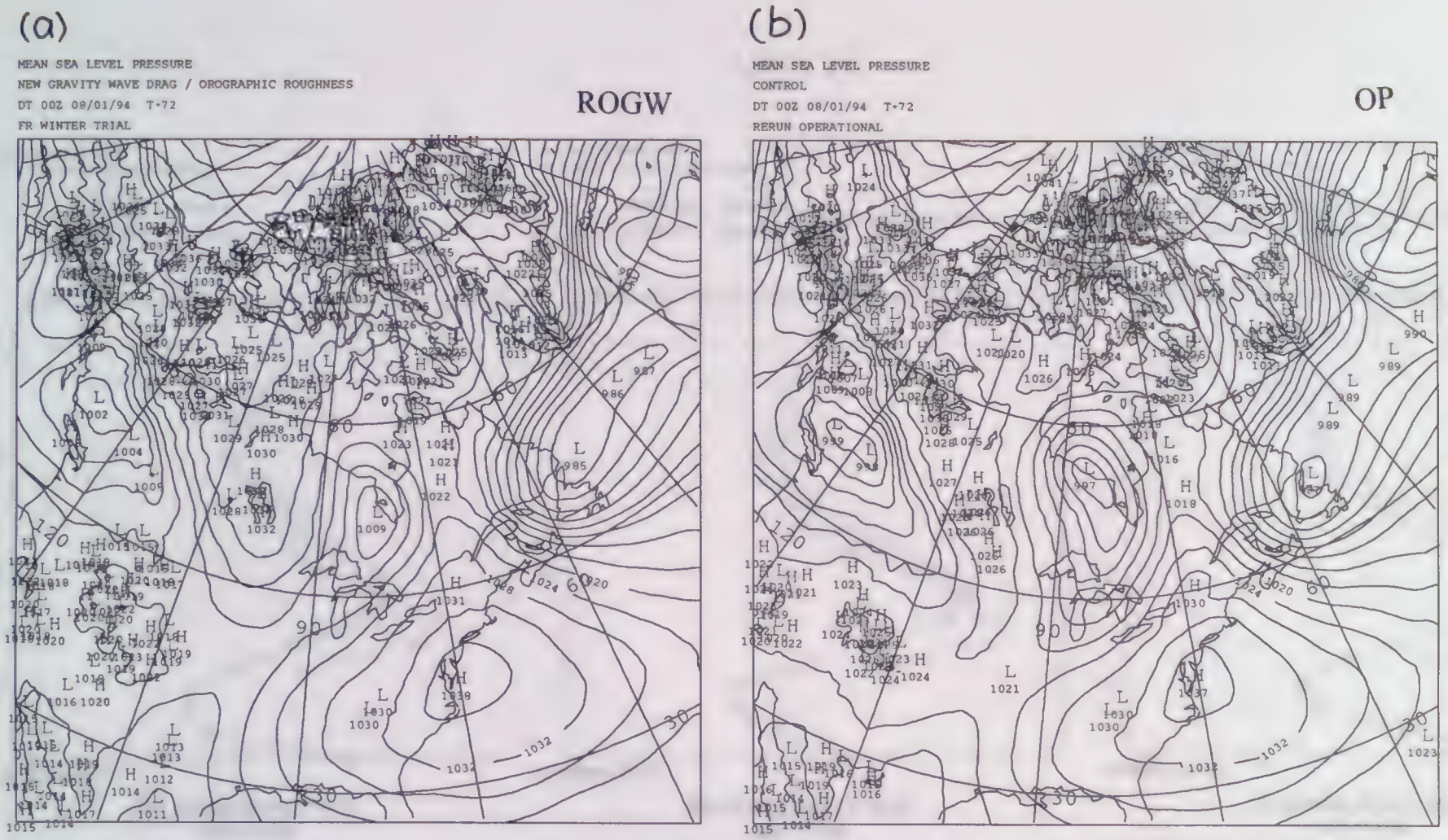
(a)
MEAN SEA LEVEL PRESSURE
NEW GRAVITY WAVE DRAG / OROGRAPHIC ROUGHNESS
DT 00Z 08/01/94 T+72
FR WINTER TRIAL
ROGW
(b)
MEAN SEA LEVEL PRESSURE
CONTROL
DT 00Z 08/01/94 T+72
RERUN OPERATIONAL
OP

Figure 37

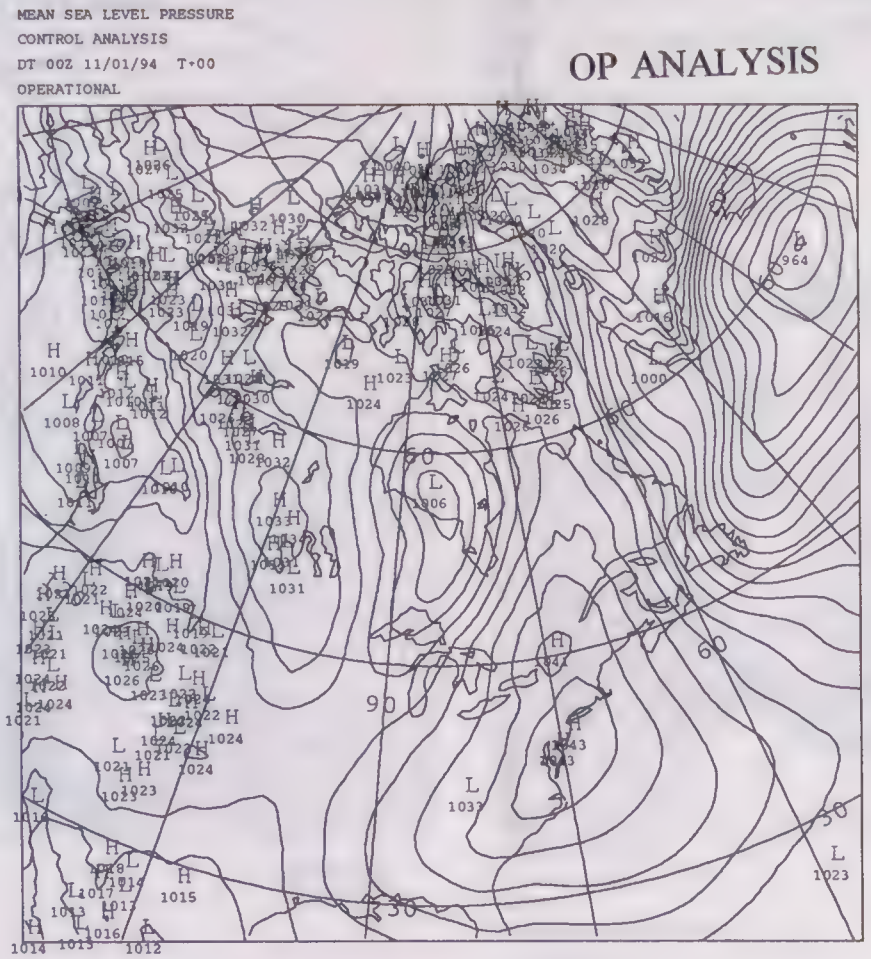
MEAN SEA LEVEL PRESSURE
CONTROL ANALYSIS
DT 00Z 11/01/94 T+00
OPERATIONAL
OP ANALYSIS

Figure 38

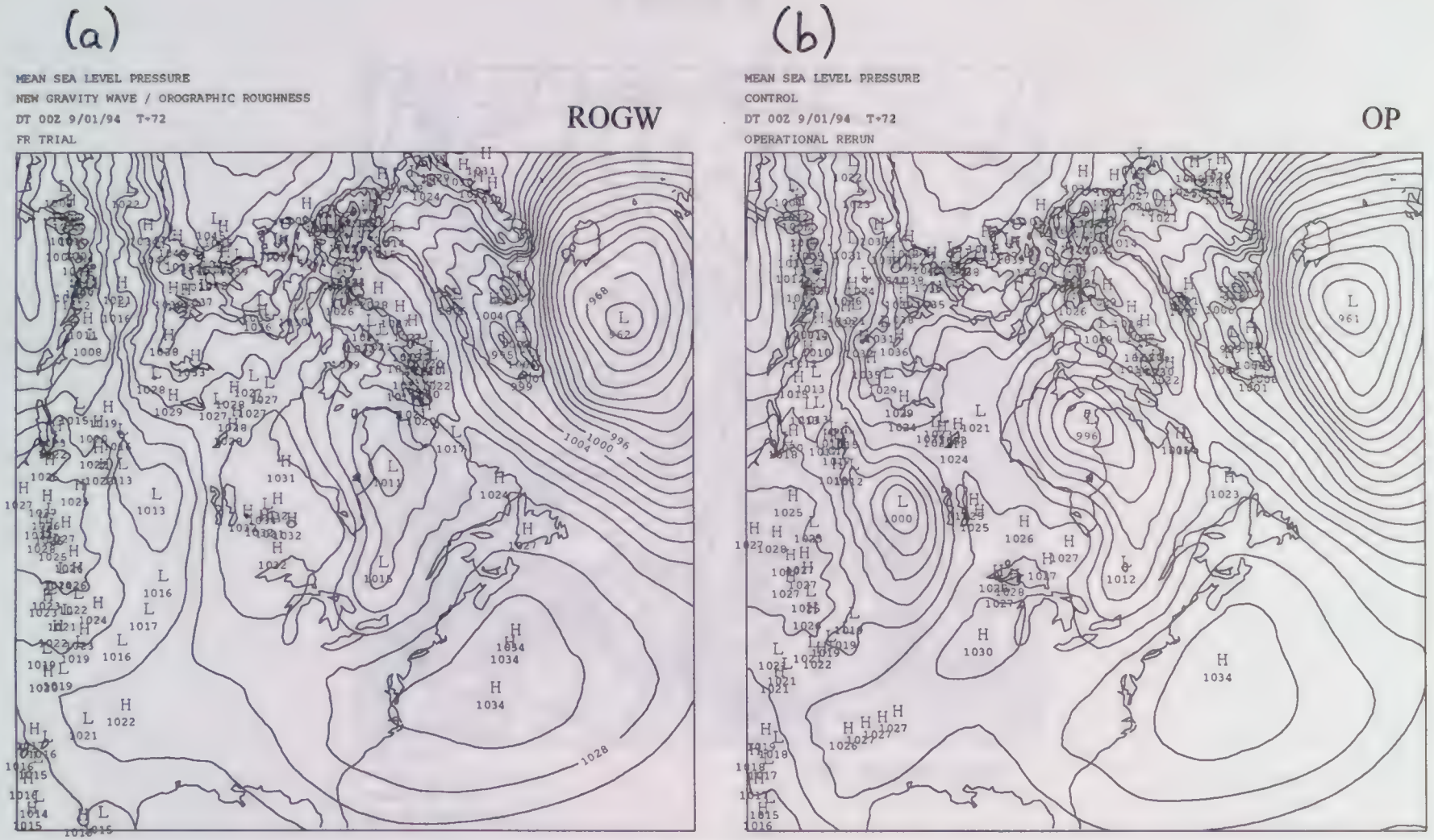
(a)
MEAN SEA LEVEL PRESSURE
NEW GRAVITY WAVE / OROGRAPHIC ROUGHNESS
DT 00Z 9/01/94 T+72
FR TRIAL
ROGW
(b)
MEAN SEA LEVEL PRESSURE
CONTROL
DT 00Z 9/01/94 T+72
OPERATIONAL RERUN
OP

Figure 39

(a)

MEAN SEA LEVEL PRESSURE
CONTROL ANALYSIS
DT 00Z 12/01/94 T+00
OPERATIONAL RERUN

OP ANALYSIS

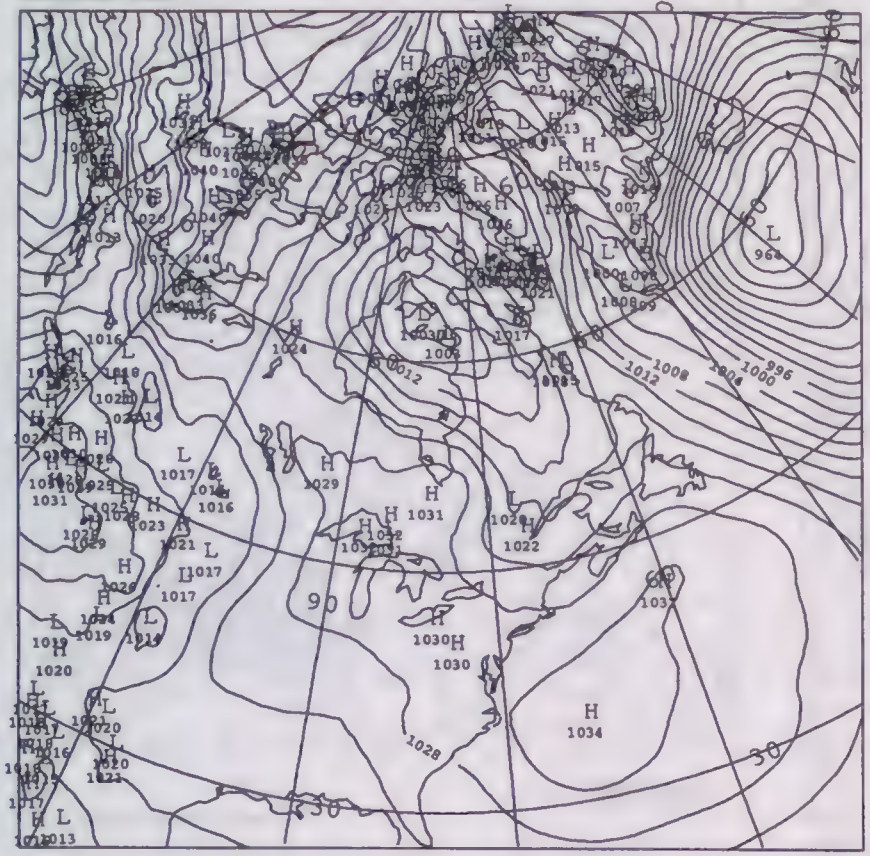

(b)

500MB HEIGHT
OPERATIONAL
ANALYSIS
DT00Z 12/01/94

OP ANALYSIS

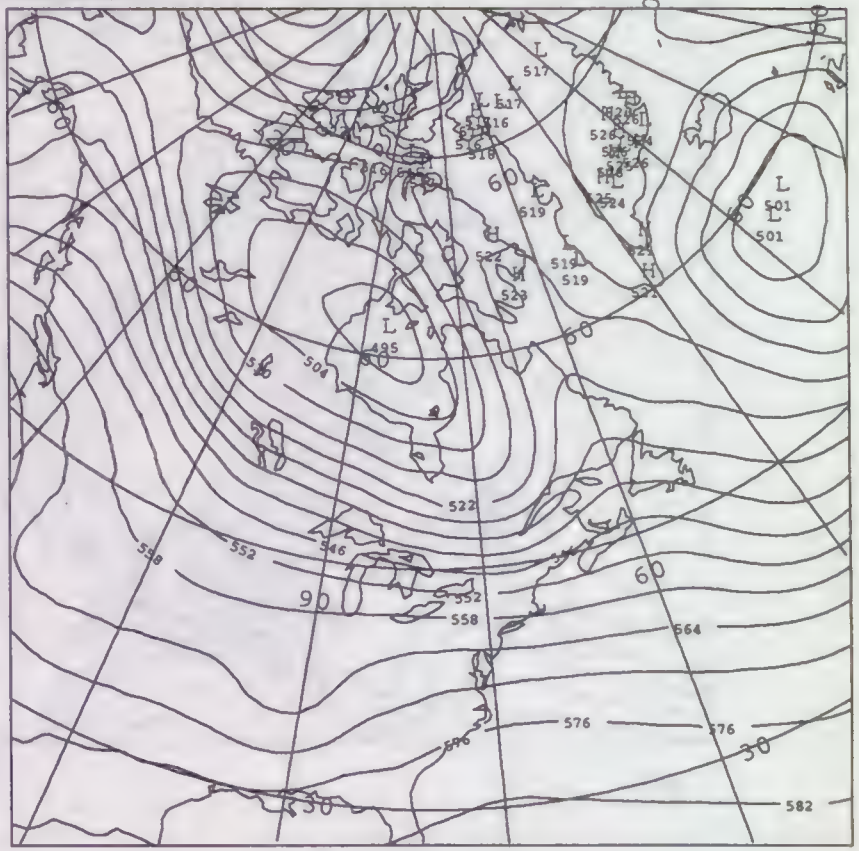

Figure 40

(a)

500hPa HEIGHT
NEW GRAVITY WAVE / OROGRAPHIC ROUGHNESS
DT 00Z 9/01/94 T+72
FR TRIAL

ROGW

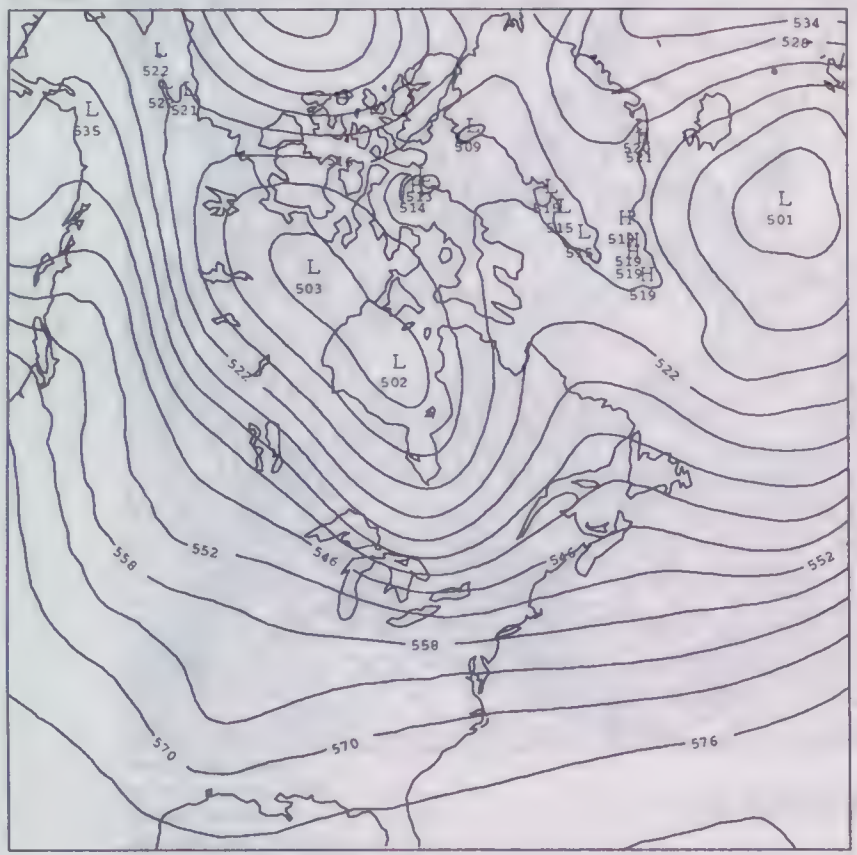

(b)

500hPa HEIGHT
CONTROL
DT 00Z 9/01/94 T+72
OPERATIONAL RERUN

OP

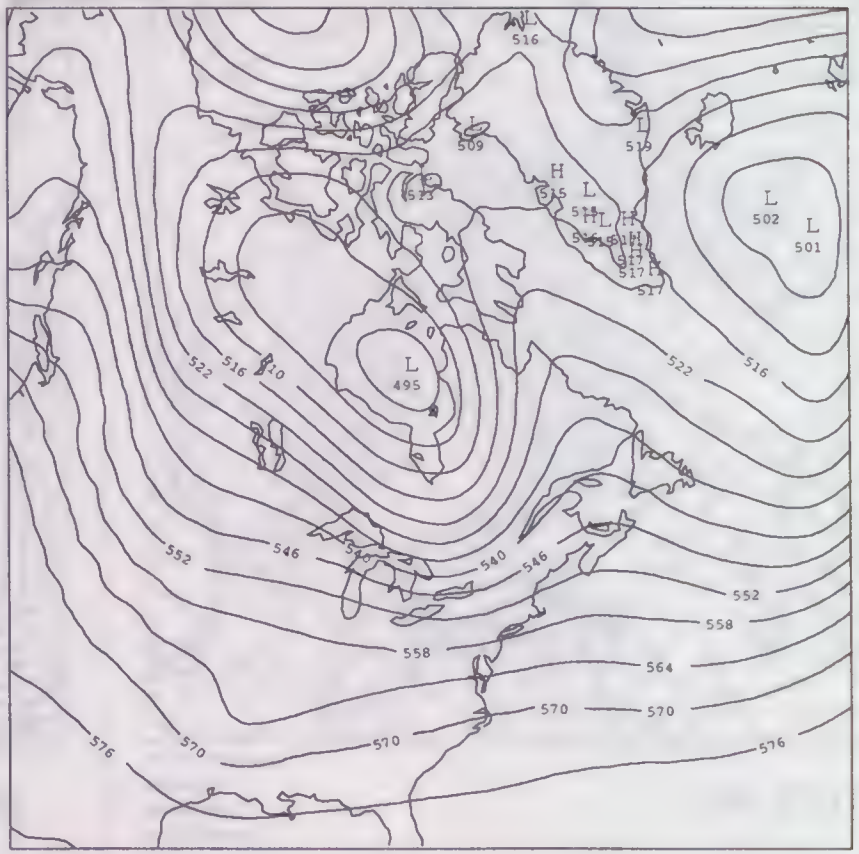

Figure 41

(a)

MEAN SEA LEVEL PRESSURE
NEW GRAVITY WAVE / OROGRAPHIC ROUGHNESS
DT 00Z 12/01/94 T+120
FR TRIAL

ROGW

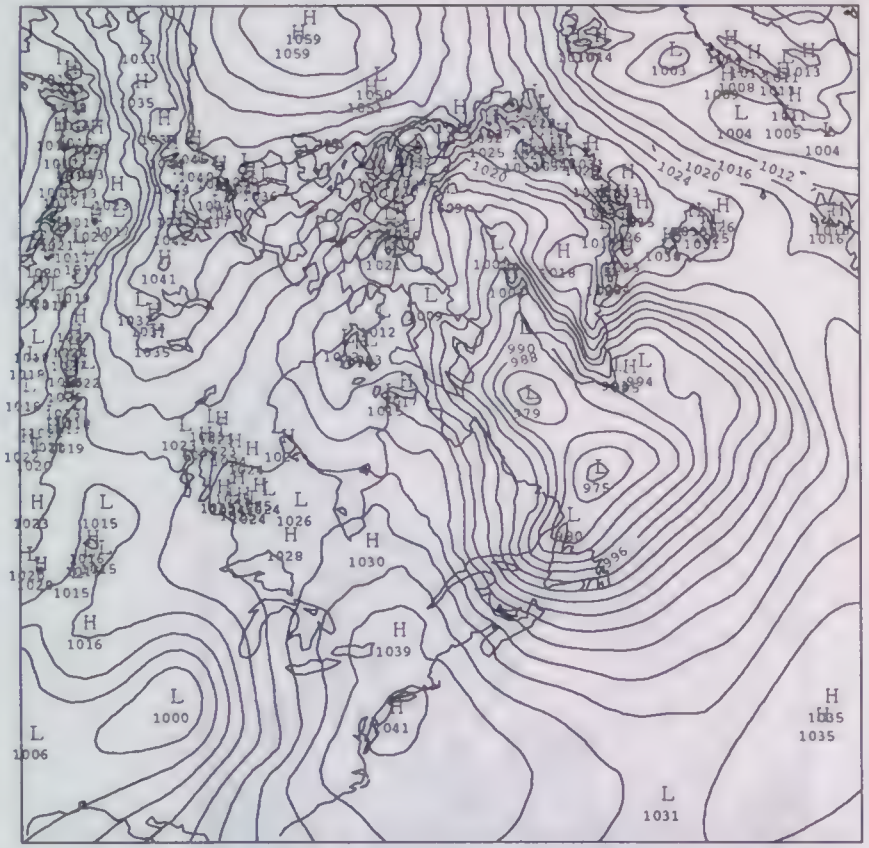

(b)

MEAN SEA LEVEL PRESSURE
CONTROL
DT 00Z 12/01/94 T+120
OPERATIONAL RERUN

OP

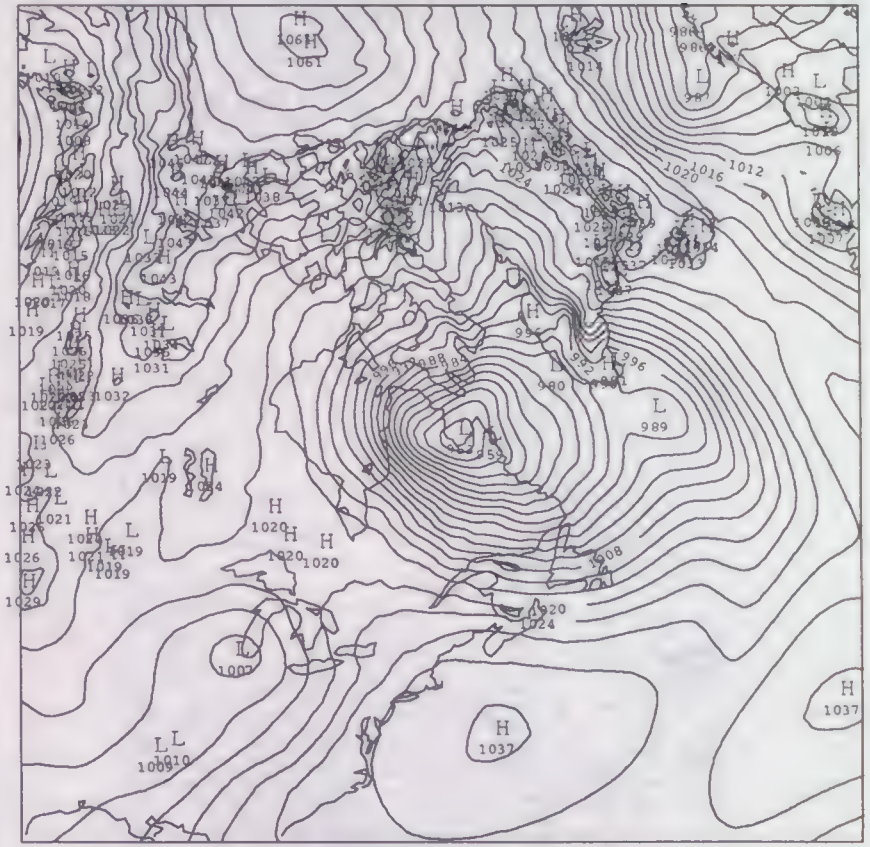

FIGURE 42

(a)

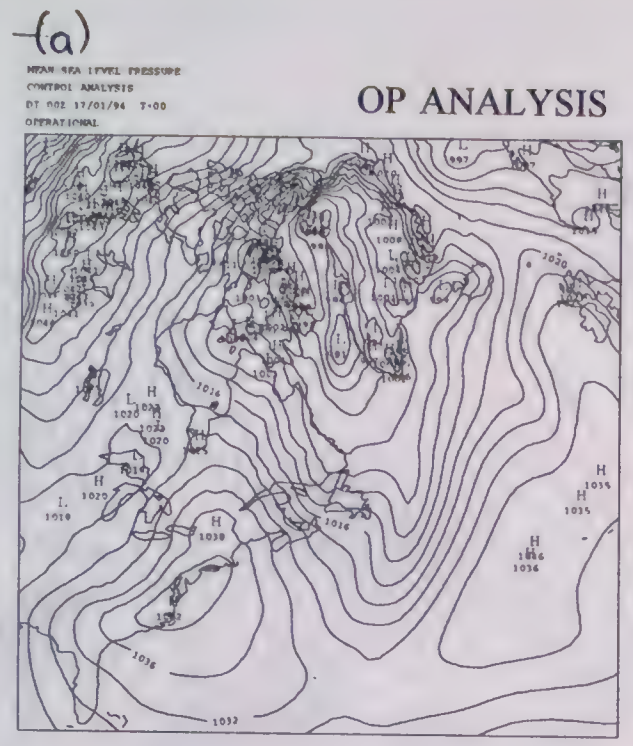

(b)

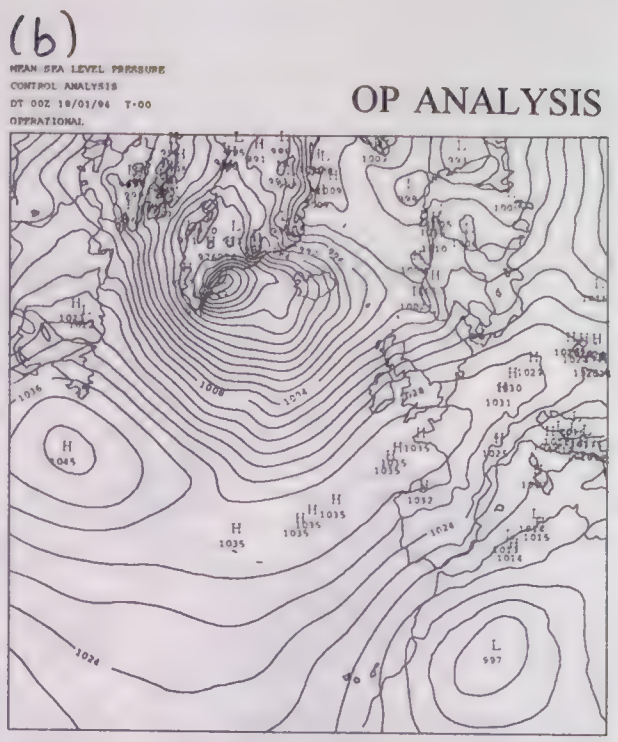

(c)

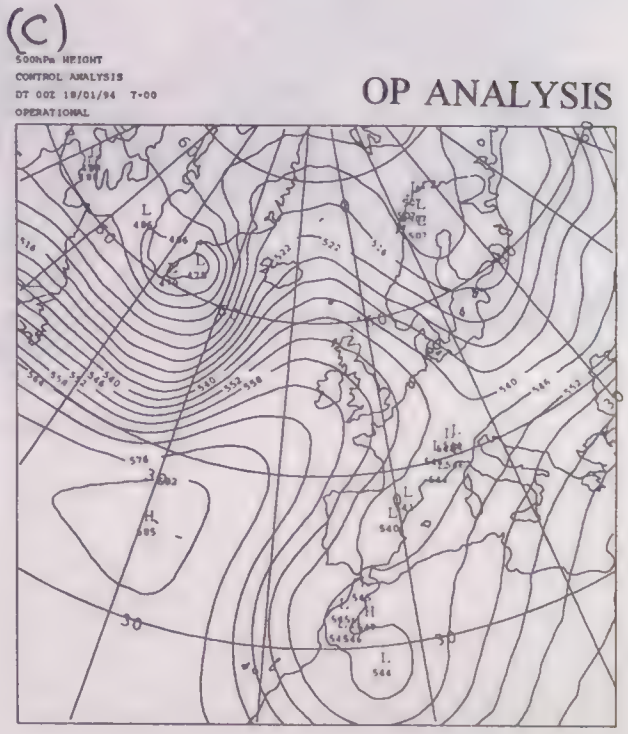

Figure 43

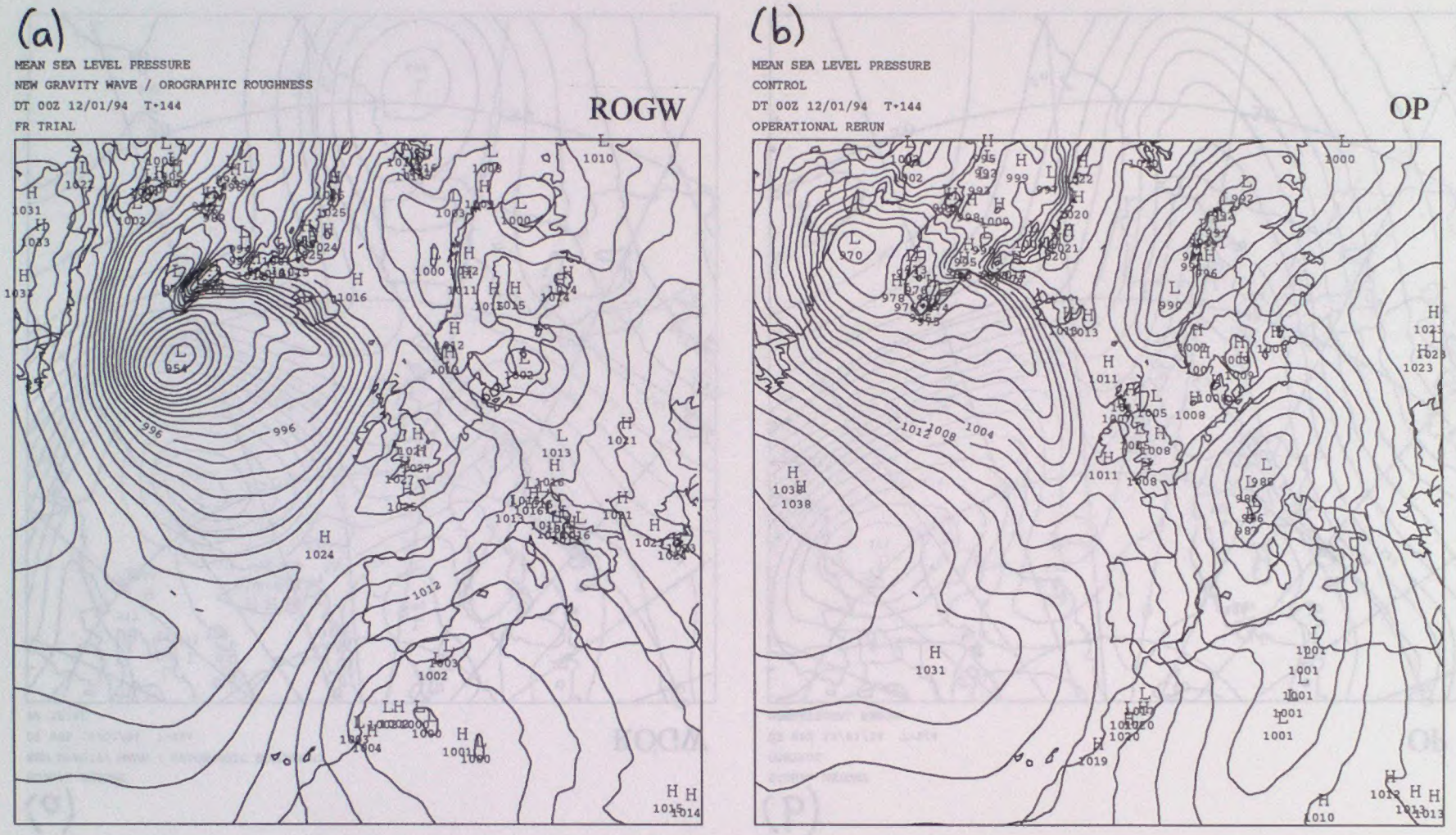
(a)
MEAN SEA LEVEL PRESSURE
NEW GRAVITY WAVE / OROGRAPHIC ROUGHNESS
DT 00Z 12/01/94 T+144
FR TRIAL
ROGW
(b)
MEAN SEA LEVEL PRESSURE
CONTROL
DT 00Z 12/01/94 T+144
OPERATIONAL RERUN
OP

Figure 44

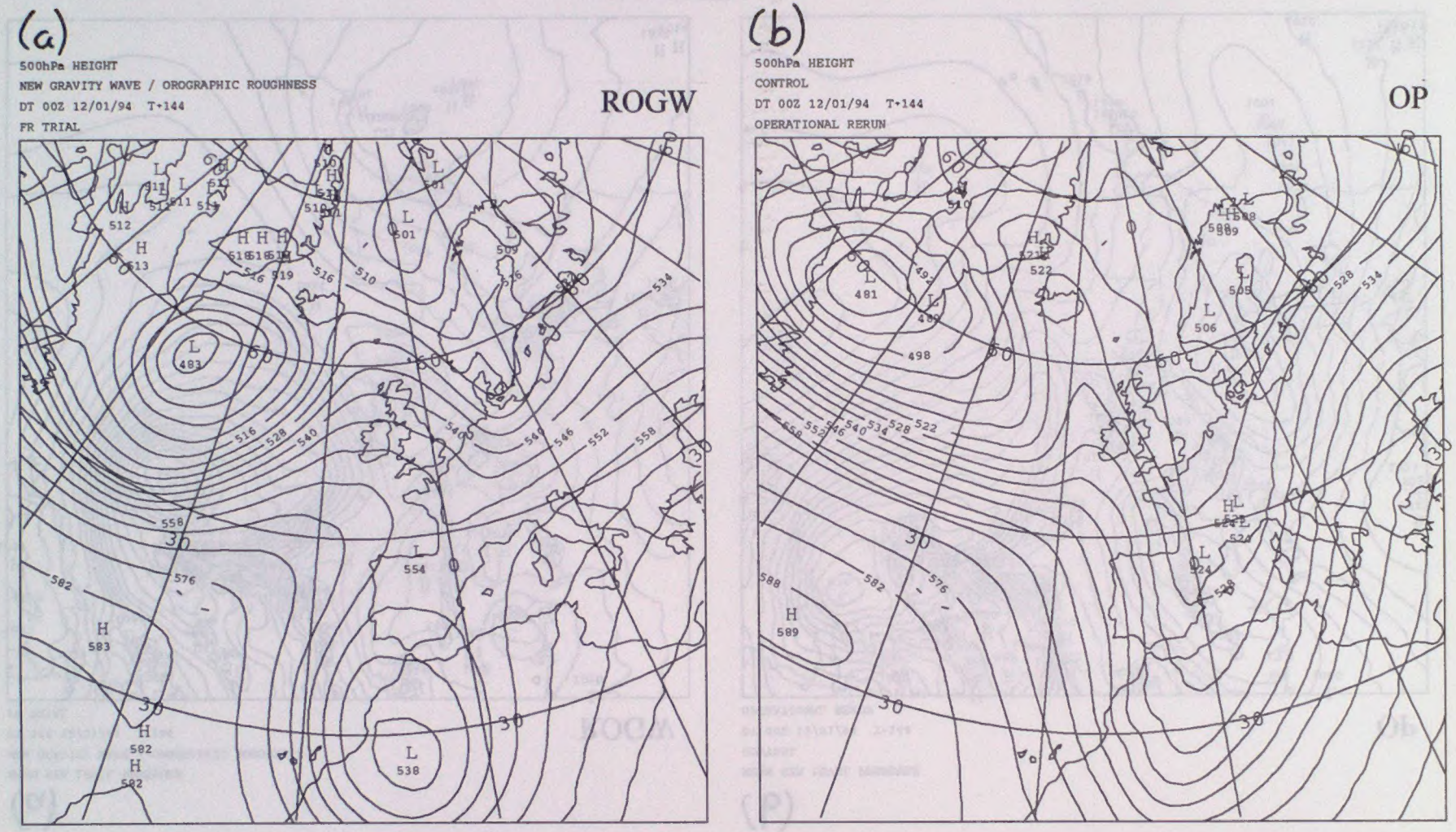
(a)
500hPa HEIGHT
NEW GRAVITY WAVE / OROGRAPHIC ROUGHNESS
DT 00Z 12/01/94 T+144
FR TRIAL
ROGW
(b)
500hPa HEIGHT
CONTROL
DT 00Z 12/01/94 T+144
OPERATIONAL RERUN
OP

Figure 45

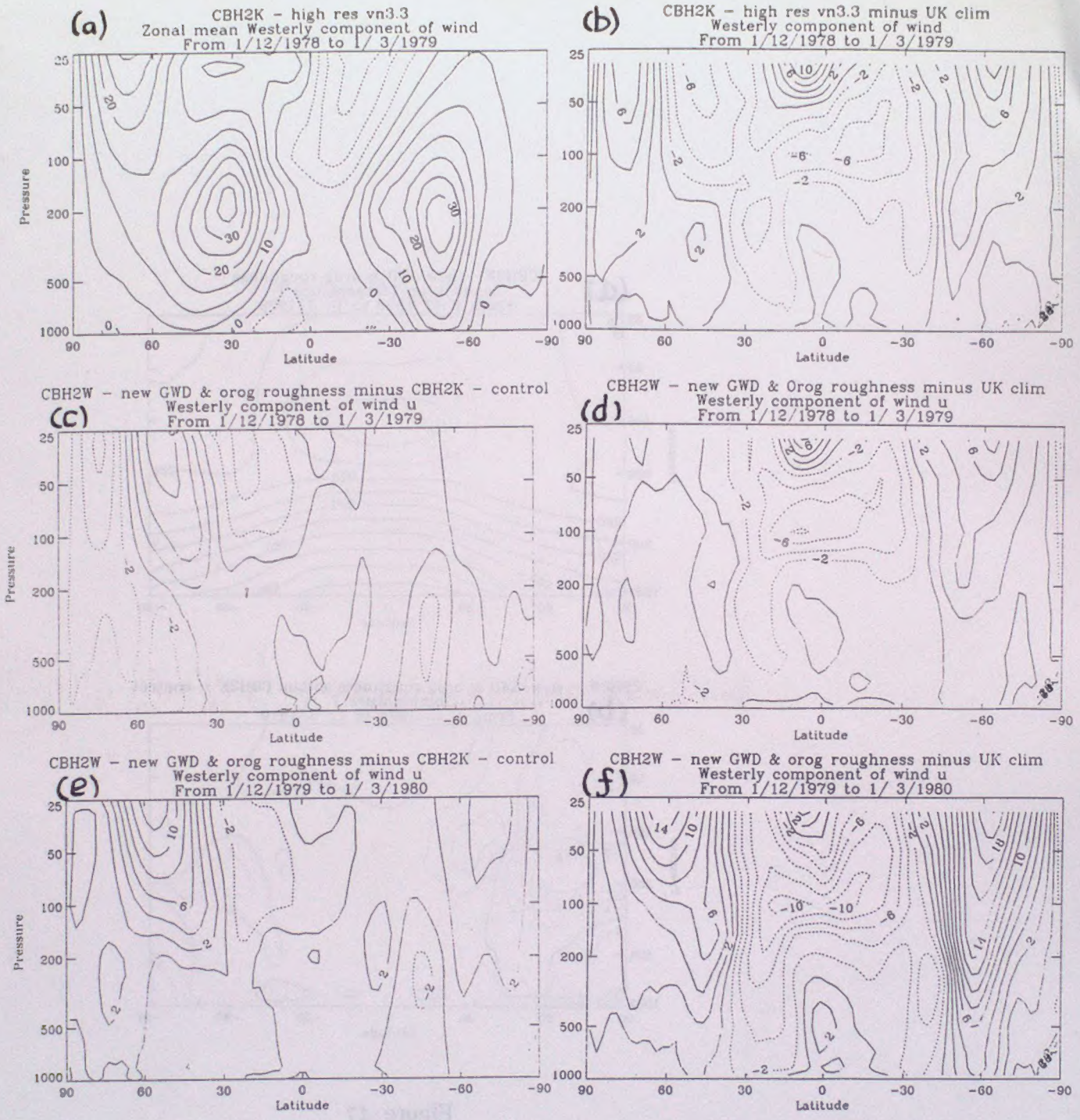
(a)
CBH2K - high res vn3.3
Zonal mean Westerly component of wind
From 1/12/1978 to 1/ 3/1979
(b)
CBH2K - high res vn3.3 minus UK clim
Westerly component of wind
From 1/12/1978 to 1/ 3/1979
CBH2W - new GWD & orog roughness minus CBH2K - control
(c)
Westerly component of wind u
From 1/12/1978 to 1/ 3/1979
CBH2W - new GWD & Orog roughness minus UK clim
(d)
Westerly component of wind u
From 1/12/1978 to 1/ 3/1979
CBH2W - new GWD & orog roughness minus CBH2K - control
(e)
Westerly component of wind u
From 1/12/1979 to 1/ 3/1980
CBH2W - new GWD & orog roughness minus UK clim
(f)
Westerly component of wind u
From 1/12/1979 to 1/ 3/1980
Pressure
Latitude
25
50
100
200
500
1000
90
60
30
0
-30
-60
-90

Figure. 46

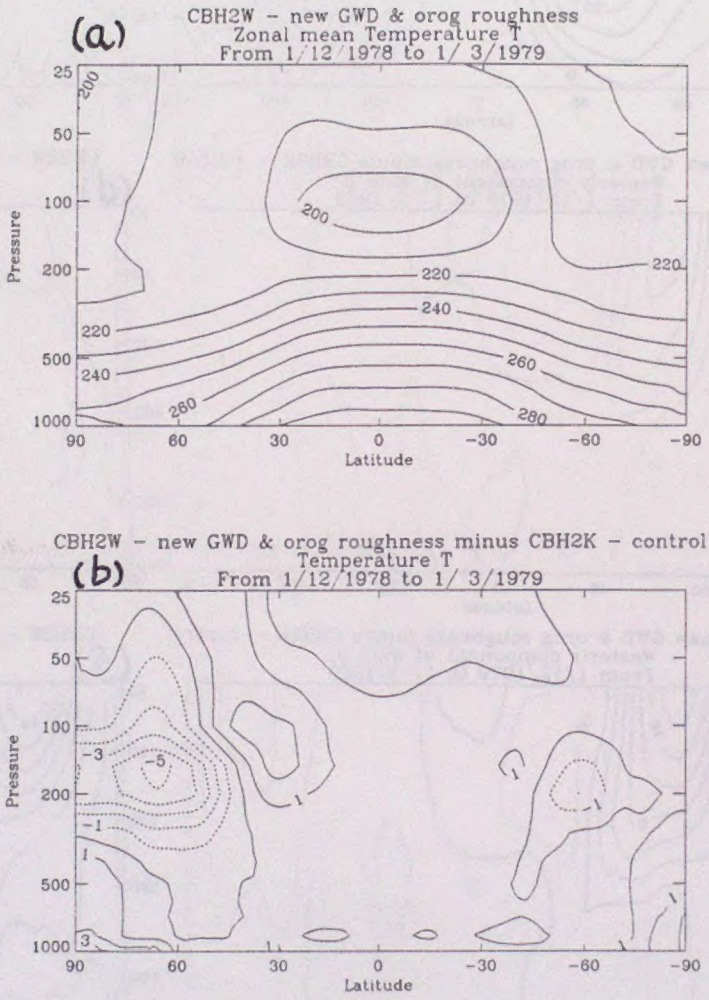
(a)
CBH2W - new GWD & orog roughness
Zonal mean Temperature T
From 1/12/1978 to 1/ 3/1979
Pressure
25
50
100
200
500
1000
200
200
220
220
240
260
280
90
60
30
0
-30
-60
-90
Latitude
CBH2W - new GWD & orog roughness minus CBH2K - control
(b)
Temperature T
From 1/12/1978 to 1/ 3/1979
Pressure
-3
-5
-1
1
3
Latitude

Figure 47